TECHNISCHE UNIVERSITÄT WIEN

DIPLOMARBEIT

The upper threshold phenomenon in a pyramidal neuron simulated with a multicompartment model

Ausgeführt am Institut für
Analysis und Scientific Computing
Technische Universität Wien

Unter der Anleitung von

ao. Univ.-Prof. Dipl.-Ing. DDDr. Frank Rattay

und

Dipl.-Ing Andreas Fellner

durch

Isabel Burian
Maurer-Lange-Gasse 9-13/7/3
1230 Wien

Wien, 9. Dezember 2017

Abstract

Neuronal stimulation with electrodes is an actively researched technology that has many therapeutic and diagnostic applications. A promising subfield is stimulation of the cerebral cortex via microelectrodes, which is used or researched as treatment for a variety of conditions such as pain and blindness. One challenge facing these practical applications is a lack of knowledge regarding the exact effects of stimulation on neurons in the tissue. This may lead to unwanted effects including failure of medical interventions and prostheses.

One of the topics that are still under dispute is the upper stimulation threshold, its causes and the conditions under which it manifests. The upper stimulation threshold is an effect in which a neuron ceases to be excited by stimulation if a certain current strength is exceeded but which is still far below an intensity that would damage the cell. Several causes have been proposed for this. One is current reversal, in which sodium ions pass the membrane in the direction opposite to what is needed for excitation. Another is anodal surround block, where parts of the cell experience a drop in membrane potential upon stimulation instead of a rise that would lead to excitation.

The aim of this work was to investigate whether an upper threshold could be found and its causes identified for different stimulation regimes in the model of a single layer 5 neocortical pyramidal cell. For comparison, several simpler models were also used, with one consisting just of a spherical soma, one with an axon attached to the soma, one with an additional single dendrite and finally a two-dimensional version of the pyramidal cell. The pyramidal neuron was chosen because it is one of the cell types targeted with cortical implants and because its dimensions and membrane properties are relatively well known. The geometry of the pyramidal cell in the model was taken from the tracing of a real cell and the original soma replaced with a special spherical version to make it suitable for close quarter stimulation.

The implementation was done with the software NEURON and is based on a multi-compartment model using Hodgkin-Huxley channel kinetics. Active channels and mechanisms known to exist in real layer 5 pyramidal cells were integrated into the model. Cathodic extracellular stimulation using a point sized current source was applied with varying intensity, duration and electrode position.

Cellular voltages and sodium currents were recorded for the different models and thresholds identified. The results confirmed the existence of an upper threshold for all models and stimulation modalities. For the model consisting only of a soma, net sodium current reversal cold be ruled out as a cause for the upper threshold at least for short stimulation durations. It was not possible to draw any other conclusion about the causes of the upper thresholds with much certainty for any model. In some cases, even strong current reversal during stimulation was not enough to prevent excitation.

Some patterns across different models could be identified. Stimulation near the dendrites was more difficult than in other regions and in the case of the three-dimensional pyramidal cell sometimes completely failed. The soma was easier to stimulate and had higher upper thresholds if other neurites were attached to it. Stimulation near the axon generally led to a large stimulation window with high upper thresholds.

These results of this thesis should shed some light on the reaction of pyramidal cells to different stimulation modalities and the question under what circumstances a failure of excitation can be expected.

Kurzfassung

Nervenstimulation mit Elektroden ist ein aktives Forschungsfeld mit vielen therapeutischen und diagnostischen Anwendungen. Ein vielversprechendes Teilgebiet ist die Stimulation der Großhirnrinde unter der Benutzung von Mikroelektroden, welche als Behandlung einer Vielfalt von Beeinträchtigungen wie Schmerzen oder Erblindung entweder erforscht oder bereits angewandt wird. Eine Herausforderung in allen diesen praktischen Anwendungen ist mangelndes Wissen über die genauen Auswirkungen der Stimulation auf Nervenzellen im Gewebe. Dies könnte zu unbeabsichtigten Effekten bis hin zu einem Versagen der klinischen Intervention oder Prothese führen.

Eines der Themen die aktuell diskutiert werden ist der Upper Stimulation Threshold, dessen Ursachen und die Bedingungen unter welchen er in Erscheinung tritt. Mit Upper Stimulation Threshold bezeichnet man einen Effekt bei welchem eine Nervenzelle ab einer gewissen Stromstärke nicht mehr anregbar ist obwohl die Stimulationsintensität immer noch weit unter jener liegt, bei welcher die Zelle beschädigt würde. Mehrere mögliche Ursachen dieses Phänomens sind unter Diskussion. Eine davon ist Current Reversal, wobei Natriumionen die Zellmembran in der Richtung passieren die gegenläufig zu jener ist welche bei einer angeregten Zelle auftritt. Eine andere mögliche Ursache ist Anodal Surround Block, bei welchem Teile der Zelle ein Absinken anstatt eines Anstiegs des Membranpotentials (welcher für die Anregung nötig wäre) durch die Stimulation erleiden.

Das Ziel dieser Arbeit war es zu klären, ob ein Upper Threshold festgestellt werden kann und was die Ursachen dafür unter verschiedenen Stimulationsgegebenheiten sind. Dies wurde anhand einer Pyramidenzelle der 5. Schicht der Großhirnrinde untersucht. Zum Vergleich wurden mehrere einfachere Modelle ebenfalls simuliert. Diese umfassen ein einfaches kugelförmiges Soma, ein kugelförmiges Soma erweitert um ein Axon, dasselbe zuzüglich eines einzigen dicken Dendriten und schließlich eine zweidimensionale Version der Pyramidenzelle. Die Pyramidenzelle wurde als Modell ausgewählt da sie einen der Zelltypen darstellt die mittels Großhirnrindenimplantats stimuliert werden und da die

Dimensionen und Membraneigenschaften einer solchen Zelle relativ gut erforscht sind. Die Geometrie der Pyramidenzelle im Modell stammt von einer vermessenen realen Zelle bei der das Soma des Originals durch ein spezielles kugelförmiges Soma ersetzt wurde um Stimulation aus kurzer Entfernung zu ermöglichen.

Die Implementierung erfolgte mittels des Programms NEURON und basiert auf einem Multi-Compartment Modell mit Hodgkin-Huxley Ionenkanalkinetik. Aktive Ionenkanäle und Mechanismen von welchen bekannt ist, dass sie in einer realen Pyramidenzelle vorkommen wurden in das Modell integriert. Die Stimulation erfolgte mittels einer punktförmigen extrazellulären Kathode und mit unterschiedlichen Intensitäten, Zeitdauern und Elektrodenpositionen.

Die dabei auftretenden Spannungen und Natriumströme wurden für die verschiedenen Modelle aufgezeichnet und die jeweiligen Thresholds identifiziert. Diese Resultate bestätigten das Auftreten eines Upper Threshold für alle Modelle und Stimulationskonfigurationen. Für das einfache Somamodell konnte ein absoluter Current Reversal als Ursache für den Upper Threshold für kurze Stimulationsdauern ausgeschlossen werden. Es war jedoch für keines der Modelle möglich andere sichere Schlüsse über die Ursachen des Upper Threshold zu ziehen. In einigen Fällen reichte selbst starker Current Reversal nicht aus um eine Anregung der Zelle zu verhindern.

Es konnten einige modellübergreifende Reaktionsmuster festgestellt werden. Die Stimulation nahe der Dendriten war schwieriger als in anderen Regionen und im Falle des dreidimensionalen Pyramidenzellmodells teilweise gar nicht möglich. Das Soma war einfacher anzuregen und hatte höhere Upper Thresholds wenn es mit anderen Neuriten verbunden war. Stimulation in der Nähe des Axons führte in der Regel zu einem breiten Stimulationsfenster mit hohen Upper Thresholds.

Die in dieser Arbeit vorgestellten Resultate sollen einen Beitrag zum besseren Verständnis der Reaktion einer Pyramidenzelle auf verschiedene Stimulationsmodalitäten liefern. Sie soll auch die Frage beantworten helfen unter welchen Umständen eine Anregung der Zelle nicht (mehr) möglich ist.

Contents

Acknowledgements

First of all, I want to thank the advisor of this thesis, Prof. Frank Rattay. It was him who introduced me to neuronal stimulation in general and the topic that grew into this work in particular. He successfully managed the balance between giving me enough guidance and support to make it easy to find a fruitful path and leaving me the space to follow and investigate things I found interesting. In our conversations, he could often easily dispell confusion and point out related topics that caused me to view things in a different light and helped me find new approaches.

I would also like to thank Dipl.-Ing. Andreas Fellner, who often took the time to meet me and have long discussions of issues that cropped up during the work. He helped me resolve problems I had with the software and shared information and insights about it with me that saved me a lot of time and allowed me to concentrate on more substantial questions. Our conversations also contributed greatly to improving and deepening my understanding of neurons and their behavior under stimulation. I am grateful for the patient and methodical way in which he questioned the model I had created and the assumptions underlying it.

Last but not least, I want to thank my family for their help and patience. I would especially like to thank my fiancé Nisan, and my mother, both of whom provided an especially large share of the support I received. Without them, I would not have finished this work.

1. Glossary

C'	Length-related membrane capacitance
C_m	Membrane capacitance
E	Equilibrium potential
F	Faraday's constant
G'	Radial (membrane) conductance in cable model
g_{pas}	Passive membrane conductance in NEURON
$\bar{g}_{\mathrm{X}}$	Maximum conductance for ion type X
h	Potassium channel inactivation factor
I	Stimulating current
m	Sodium channel activation factor
n	Potassium channel activation factor
q_{10}	Temperature sensitivity
R	Ideal gas constant; segment radius
$R_{Transfer}$	Transfer resistance between electrode and neurite
Ra	Cytoplasmic resistivity in NEURON
R'_E	Extracellular (axial) resistivity in cable model
R'_I	Intracellular (axial) resistivity in cable model
r	Distance from the electrode at which the stimulating field is measured
T	Temperature
T_{Orig}	Recording temperature for channel properties
T_{Sim}	Simulation temperature
t_{adjust}	Temperature adjustment for channel activity

t	Point in time during simulation
$U_{R'}$	Voltage source for modeling resting potential
V_e	Stimulating field
V_i	Internal potential
V_m	Membrane potential
V_X	Nernst potential for ion type X
$\bar{V}_\mathrm{e}$	Average surface potential
$[X]$	Concentration of ion X
$[X]_{in}$	Concentration of ion X inside of the cell
$[X]_{out}$	Concentration of ion X outside of the cell
$xraxial$	Resistance between two extracellular nodes in NEURON
z	Ion charge
α_x	Opening constant for gating factor x
β_x	Closing rate constant for gating factor x
Δx	Distance between nodes in the cable model
ρ_e	Resistivity of the extracellular medium
Action Potential	Self-propagating rapid rise and fall in membrane potential
AIS	Axon initial segment
Anodal surround block	Hyperpolarized areas some distance away from the electrode prevent action potential propagation
Compartment Model	Representation of a system by one or more internally homogeneous subdivisons that interact with their environment

Current reversal block	Outward flowing sodium currents prevent action potential formation
Current − distance relation	Link between electrode-neuron distance and stimulation current intensity leading to cell excitement
Hodgkin − Huxley Model	A differential equation based model to simulate action potentials
Nernst Potential	Membrane potential for a specific ion type at which electrostatic and diffusion forces balance and result in a net current of zero
Section	Part of a model neuron with uniform parameters
Segment	Subdivision of a section
Stimulation intensity	Stimulation current strength delivered by electrode
Stimulation window	All current intensites between upper and lower threshold
Strength − duration relation	Correspondence between stimulation duration and intensity needed for excitement
Threshold	Stimulation intensity at the border between intensities leading to excitation and those not leading to excitation

Variables that were just mentioned briefly in a single context are not listed.

2. Introduction

Using electric currents of the right strength, neurons can be artificially stimulated to produce an action potential that propagates along the cell. The necessary current can be introduced either intracellularly or extracellularly via electrodes.

This effect is used in neuroengineering, part of which involves electrodes creating an interface between an electronic system that produces stimuli and nerve cells in human and animal tissue. The field has generated a variety of practical applications, such as in neuroprosthetics, the discipline concerned with the augmentation or replacement of functions of the nervous system by artificial devices.

A prominent example for the successful application of neurostimulation is the cochlear implant, which restores hearing to people with hearing loss. The external part of the device records incoming sounds and converts it to electrical signals. The internal part receives them and directly stimulates the auditory nerve, thus bypassing the damaged part of the patient's auditory system.

Other applications of electrostimulation in neuroengineering include retinal implants and cortical stimulation, two active research fields which will be briefly discussed in the following section.

2.1 Retinal Implants

Retinal implants are devices aimed at restoring sight to people blinded by damage to or degeneration of retinal cells.

The retina is the innermost layer of tissue of the eyeball, coating the back part of the eye. Its main function is to convert incoming light into electrical signals to be transmitted to the brain via the optical nerve. For this purpose, the retina contains several different types of neurons whose purpose is either light detection (rod and cone cells) or the

signal integration and conduction to the optical nerve (bipolar, horizontal, amacrine and ganglion cells).

While there are different types of retinal implants, the general principle is always the same: Incoming light is detected by a photodiode array or camera (Chuang et al., 2014), processed and signals are sent to an electrode array located in the retina, with the individual electrodes stimulating nearby neurons.

Several medical conditions can impair or destroy the supporting tissue and the neurons it contains. If the damage leaves some cells (at minimum the ganglion cell layer) intact, it is in some cases possible to partially restore visual with a retinal implant. Examples for diseases that implants are tested for are retinitis pigmentosa and age-related macular degeneration (Lewis et al., 2016).

Although it is a comparatively young technology and research is still ongoing, several medical devices are in development and undergoing testing in human patients. One (Argus® II Retinal Prosthesis System by Second Sight Medical Products) was already approved for market in the European Union and the USA (Chuang et al., 2014).

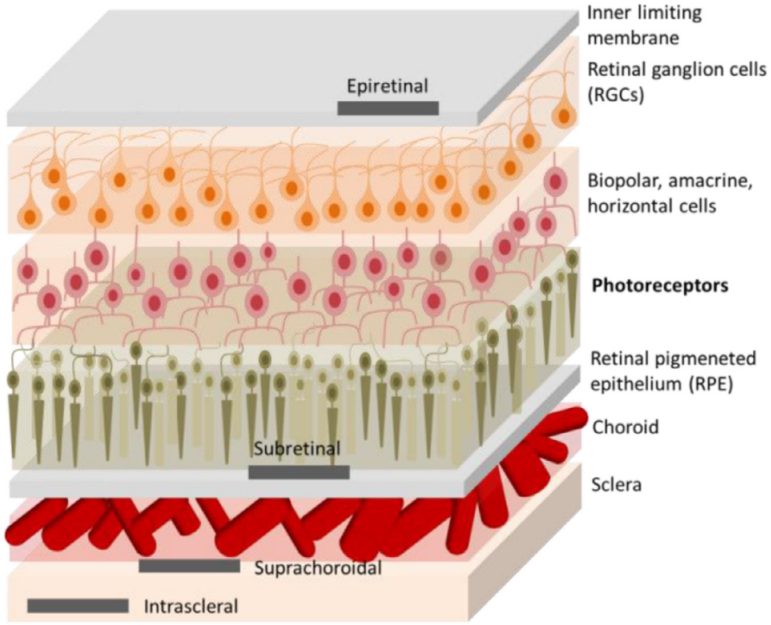

Figure 2.1: *Layers of the retina with different neuron types and possible electrode positions for visual implants. Image and part of the caption from Bareket et al. (2017).*

A common way to categorize implants is based on locations of the electrode array or of the camera. Examples for array positions are epiretinal and subretinal, with epiretinal implants being placed atop the inner retina surface and subretinal implants being located between the photoreceptor layer and the retinal pigment epithelium. Other possibilities are suprachoroidal or intrascleral implants (Bareket et al., 2017). Light detection can be handled either by a camera external to the body or an intraocular photodiode array.

Existing implants generally use between 25 and 1.500 electrodes (Werginz & Rattay, 2015). Depending on implant characteristics and patient-specific factors, the devices allow their users to recognize some patterns or the direction of movements. Most patients reacquire at least some visual sense (Chuang et al., 2014).

The small currently possible number and density of electrodes compared to visual neurons is a limiting factor for visual acuity (usually up to 100 electrodes and roughly 100 million rod and cone (Curcio et al., 1990) or ca 1 million ganglion cells (Watson, 2014), with individual variation). Another issue is that stimulation intensity needs to be high enough to trigger an action potential in desired cells, but low enough to avoid undesired effects such as inhibition of action potentials by overstimulation (Boinagrov et al., 2014), stimulation of non-targeted cells (Rattay & Resatz, 2004) or in the worst case, damage to the tissue (Eiber et al., 2013). Given the electrode density necessary for better acuity and the intrinsic variability of human tissue, this is a challenging task.

2.2 Cortical Stimulation

Cortical stimulation involves artificially induced changes of neural activity in the brain cortex either indirectly (eg transcranial electric or magnetic fields) or directly (eg by using microelectrodes). The following discussion will be limited to stimulation by electrodes.

The cerebral cortex is the largest area of the mammalian brain. It forms the outer layer of the cerebrum and in many animals and especially humans it is folded to allow it to take up a larger part of cranial space. It has various functions, including processing of sensory data, control of voluntary movements as well as consciousness and memory and attention,

to name a few. It shows spatial differentiation in two ways: between regions on the surface and within such a region, between points further or closer to its surface. The first kind of differentiation allows different cognitive functions to be mapped to different areas on the cerebral cortex surface. The depth differentiation means that it consists of several layers (numbered I to VI going from the outer to the inner part). They are characterized by the presence of different neurons and neuronal structures, although there is some overlap.

Given the broad spectrum of its functions as well its relative accessibility as the outer cerebral layer, many applications of electrical cortex stimulation have been explored and are currently used in research and for clinical treatment.

One widely used technique is cortical stimulation mapping. Electrical current is applied to a site on the exposed cortex, inhibiting the regular neuronal activity at the location. This results in either preventing or causing an action in the animal or patient if the site corresponding to that function is stimulated. If done systematically, regions of the brain corresponding to different functions can be mapped out. Apart from research, this method can be used for treatment, eg to determine which part of the brain can be cut during surgery without risking major impairment or to find the inition point of seizures in epileptic patients (Noachtar & Rémi, 2009).

Intracranial cortex stimulation via implanted electrodes or electrode arrays is being investigated or in use for epilepsy, pain, depression, tinnitus, Parkinson's disease and others (Johnson et al., 2013). For Parkinson's disease and pain, clinical trials indicate that while the results are mixed, most patients experience improvement (Cioni, 2007; Rasche & Tronnier, 2016; Fontaine et al., 2009). Research with the goal of directly stimulating the visual cortex in blind patients with electrode arrays is ongoing (Lewis et al., 2015).

One challenge for cortical stimulation, be it for mapping or treatment, is that the precise mechanisms and effects of stimulation are still poorly understood or subject to individual variation in patients (Johnson et al., 2013). This may lead to unwanted effects or misinterpretation of data in the case of mapping (Borchers et al., 2012).

2.3 Utah Electrode

An electrode type commonly used for both neuronal stimulation and recording is the Utah electrode. It is an array of microelectrode needles produced with different specifications, mostly with an area of 0.5-4 mm^2 and about 100 individual electrodes (Normann & Fernandez, 2016). The bulk consists of silicon and the recording/stimulating tips of the needles are made of platinum, iridium alloys or similar materials.

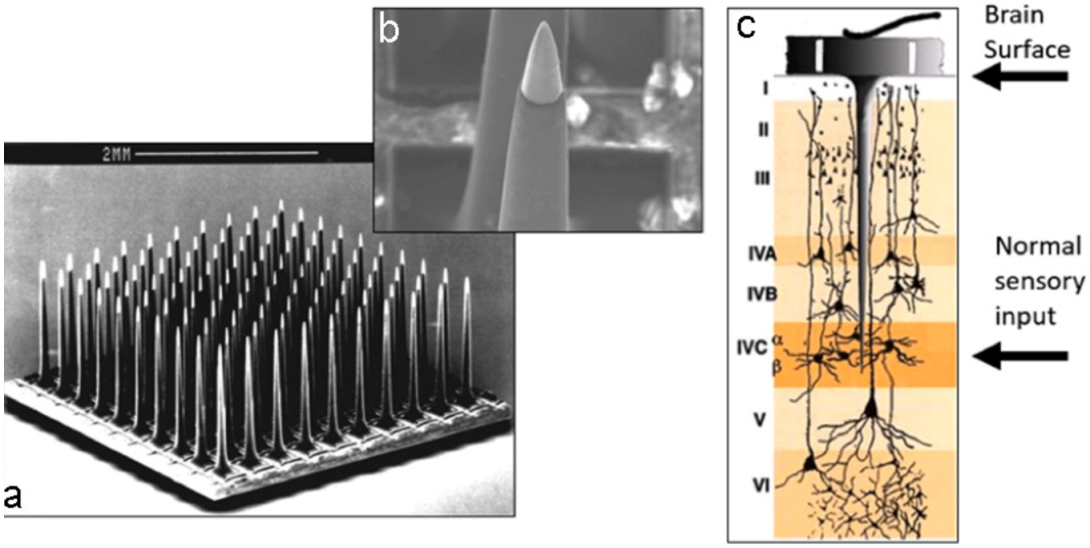

Figure 2.2: *a) Microscopic image of a Utah electrode, b) Close-up of the tip, c) Layers of the visual cortex with Utah electrode pin, it reaches down to the fourth layer, which is the first one to receive visual input from the eyes. From "Introduction to Visual Prostheses" by Norman and Fernandez (n.d.)*[1].

The small exposed area of the tips make Utah electrodes nearly point shaped sources for electric current. The individual needles are relatively long (1.5 mm), slender as well as strong and flexible. This makes the Utah array a good candidate for visual cortex stimulation, which needs electrodes that take up little volume in the cortex while still having sufficient penetration. Due to the high number and density of the needles, it achieves stable anchorage while still being able to accomodate movement of the cortex (Normann et al., 1999).

[1]The abbreviation n.d. in this context means that the source could not be dated.

Current clinical uses for Utah Electrodes include recording motor commands in the central nervous system and inducing somatosensory percepts in the peripheral nervous system. There is ongoing research into a potential use in cortical visual implants (Normann & Fernandez, 2016).

3. Neuron Properties

Neurons share many of the structures and properties of other animal cells, such as a nucleus or organelles. In the following sections, those that are important for modeling electrical stimulation on the level of a single neuron will be discussed.

3.1 Interior and Exterior

3.1.1 Cell Membrane

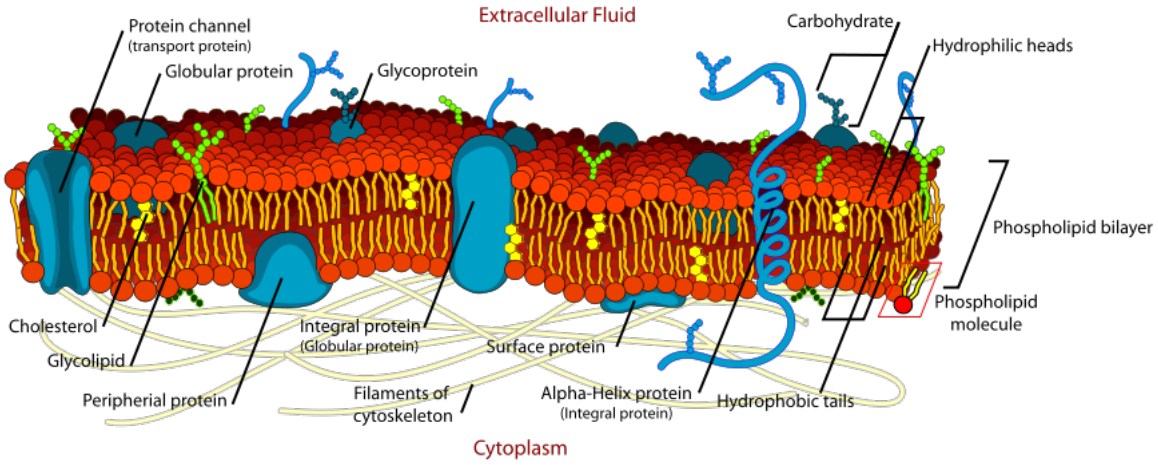

Figure 3.1: *Schematics of the cell membrane double layer separating the cytoplasm and extracellular medium. Different types of proteins are embedded, including a channel protein to the far left. Image by Ruiz (n.d.) published on Wikipedia .*

In animal cells, the cell border is formed by the cell membrane, which is 5-8 nm thick. It is a self-assembling structure formed by amphiphilic lipid molecules. It is energetically favorable for the hydrophobic fatty acid tails of the lipid molecules to be in contact with one another and not the aqueous medium inside and outside of the cell. The hydrophilic head groups prefer contact with water. This allows for the formation of a double layer, with the tail groups in the middle and head groups facing the aqueous medium on either side of the cell membrane. Embedded in the cell membrane are a variety of proteins with many different functions.

Electric Properties

The cell membrane plays a prominent role in the electric behavior of a neuron. Due to its nonpolar inner layer, it acts as a barrier to ions and electric current, which causes its high resistivity relative to the extracellular medium and the cytoplasm. This resistance allows the generation of a membrane voltage, which is defined by the difference between the potential on the cellular side of the membrane and the potential just on the outside. Since the membrane forms a thin dielectric between two conductive media it also has a relatively high capacitance. While the membrane resistance of a neuron can vary a lot, the capacitance is rather constant at around $1\mu F/cm^2$ (Rattay, 1990).

Some membrane proteins are ion channels and selectively allow for the passage of ions through the membrane. Several channel types can be distinguished based on the circumstances under which they are permeable to ions. Those used in this thesis fall into three general categories:

- **Voltage-gated channels** cause the initiation and propagation of action potentials. Some channels of this type also support the return to a negative membrane voltage afterwards.
- **Passive channels** are always open for ions to cross the membrane.
- **Ligand-gated channels** vary their permeability to ions in response to certain chemicals.

A specific channel is typically only permeable to one kind of ion. Channel types are not generally evenly distributed over all cells or even in different membrane regions in the same cell. This influences the electrical properties of neurons and their behavior when stimulated. An impotant part of the function of ion channels is to permit the generation of the resting potential (about -70 mV) or of action potentials. The resting potential is the membrane voltage a cell assumes if it is not exposed to stimulation.

3.1.2 Cytoplasm

The Cytoplasm is the substance making up the cell's interior. It includes organelles as well as macro- and micromolecules suspended in an aqueous solution. In this thesis, this inner structure is disregarded and a constant intracellular resistivity is assumed in the whole neuron. It contains a mix of ions, which can cross the cell membrane dependend on the channels and their state.

3.1.3 Extracellular Medium

The extracellular medium comprises the substance outside of the cell. It is an aqueous solution with suspended molecules of varying size (importantly including ions in different concentrations than in the cytoplasm). Its resistivity influences the stimulating field felt by the neuron if an extracellular electrode is present.

3.2 Action Potentials

Action potentials are defined by membrane potential quickly rising and then dropping again in excited regions of neurons. This induces the same state in adjacent regions and causes a nervous impulse to propagate along the cell. Different neurons and even different regions within one neuron have different spiking characteristics such as threshold voltage and spike frequency.

Responsible for the generation and propagation of action potentials are voltage-gated ion channels, such as those for sodium and potassium.

3.2.1 Equilibrium Potential

An important quantity in this context is the equilibrium potential defined by the Nernst equation. It accounts for the concentration and charge of ions of one type on each side of the membrane and the resulting electrochemical potential and is defined by

$$E = \frac{RT}{zF} \ln \frac{[\mathrm{X}_{in}]}{[\mathrm{X}_{out}]} \tag{3.1}$$

E is the equilibrium potential, R is the ideal gas constant, T is the temperature in Kelvin, F is the Faraday constant, z is the ion charge and $[X_{in}]$ and $[X_{out}]$ are the ion concentrations on each side of the membrane.

The equilibrium potential of each ion type is the transmembrane voltage at which the entropic force from the concentration gradient and the electrostatic force from the ion's electric charge balance so there is no net ion movement across a permeable membrane.

The Nernst potential is different for different ion types. There are several physiologically important ones. The most relevant ones for this thesis are those of sodium (60 mV) and potassium (-90 mV). Note that these values are the standard values used in the simulations and according to equation (3.1), they depend on the ratio of intra- and extracellular ion concentrations. The respective Nernst potentials result in a net electrochemical driving force inwards for the sodium and weaker outward driving force for potassium at the resting potential of the cell.

Together with mechanisms that provide active ion transport against the electrochemical gradient, the contributions of the individual equilibrium potentials are responsible for the membrane potential and generation of action potentials.

If the membrane is permeable to multiple types of ions, the membrane potential will be somewhere between the respective equilibrium potentials. For neurons in the resting state, it is around -70 mV and mostly determined by potassium and sodium, with potassium playing the dominant role due to the higher permeability of the cell membrane to this ion (Purves et al., 2004).

The Goldman-Hodgkin-Katz equation formulates the membrane potential arising from the presence of multiple ion types with individual membrane permeances. After equilibrating to this potential, there is no net ion flux across the membrane as long as the cell is not otherwise perturbed (Kaniusas, 2012).

$$V_m = \frac{RT}{F} \ln \left(\frac{P_{\mathrm{K}^+}[\mathrm{K}^+]_{\mathrm{out}} + P_{\mathrm{Na}^+}[\mathrm{Na}^+]_{\mathrm{out}} + P_{\mathrm{Cl}^-}[\mathrm{Cl}^-]_{\mathrm{in}}}{P_{\mathrm{K}^+}[\mathrm{K}^+]_{\mathrm{in}} + P_{\mathrm{Na}^+}[\mathrm{Na}^+]_{\mathrm{in}} + P_{\mathrm{Cl}^-}[\mathrm{Cl}^-]_{\mathrm{out}}} \right) \tag{3.2}$$

The structure is similar to that of the Nernst equation, with the ion types potassium ($[\mathrm{K}^+]$), sodium ($[\mathrm{Na}^+]$) and chlorine ($[\mathrm{Cl}^-]$). $[\mathrm{P}_X]$ is the membrane permeability for ion type X.

3.2.2 Phases of an Action Potential

Starting out at the resting potential, the generation of an action potential proceeds in several steps.

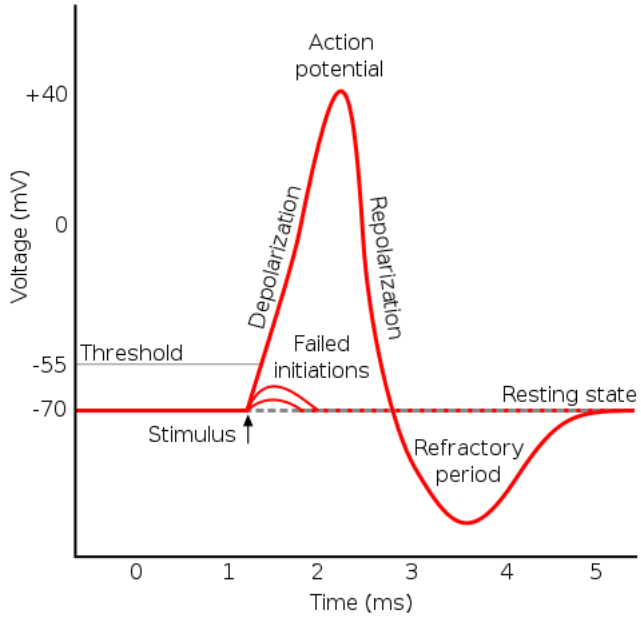

Figure 3.2: *The membrane voltage charted over time in a specific place in the neuron during an action potential. The different phases of the action potential are indicated. Also visible in this image are the voltage charts of two failed initiations by stimuli below the threshold. Image published on Wikipedia (*Action Potential*, n.d.).*

Depolarization Phase

The first phase is initiated by a depolarizing stimulus. If the membrane potential goes above a certain threshold (usually above -50 or -55 mV) (Seifter et al., 2005), voltage-gated sodium channels start to open. Since the sodium equilibrium potential is positive,

this leads to an influx of sodium ions into the cell and a further increase of the membrane potential, which leads to an opening of more sodium channels in a self-reinforcing reaction.

Repolarization Phase

This process peaks a bit below the sodium equilibrium potential when all channels are opened. The high potential triggers the inactivation of the channels, which become impermeable to ions. The membrane is now once again more permeable to potassium ions than to sodium ions, which drives the potential downwards. This process is accelerated by voltage-gated potassium channels, which open at high membrane potentials. This continues until the membrane potential is somewhat below the resting potential, a phenomenon called afterhyperpolarization. The phenomenon of hyperpolarization does not only occur at the end of action potentials, it can appear under other circumstances as well, some of which will be discussed later.

Refractory Period

Afterhyperpolarization is the cause for the relative refractory period, in which a stronger stimulus is required to elicit an action potential. The shorter absolute refractory period is due to the inactivated sodium channels, which cannot be opened at all until the inactivation period has expired. This stops an action potential from propagating in the direction it came from.

Return to the Resting Potential

After closing of the voltage-gated potassium channels, the membrane potential slowly assumes the resting potential again.

This model for the generation of action potentials is simplified, real neurons possess more than two channel types, with different characteristics or altogether different ion types.

The depolarizing stimulus can occur naturally, caused by other cells via synapses or by sensory input. Synapses are contact areas between two neurons, where the action potential in one cell can influence the second cell. This occurs either via chemical or electrical means. In chemical synapses, a change in the membrane potential (usually due to an

action potential) in the first neuron causes it to release neurotransmitters into the narrow gap between the cells. Receptors in the postsynaptic membrane of the second cell can detect this and trigger further intracellular processes which under the right circumstances result in an action potential in the second cell. Electrical synapses consist of channels spanning the membranes of both cells, allowing charges to be transmitted directly from one cell into the other.

Additionally, action potentials can be induced artificially via stimulation by intracellular or extracellular electrodes.

3.3 Layer 5 Neocortical Pyramidal Cells

The neocortex is the largest part of the cerebral cortex. It is comprised of six layers, going from superficial to deep, each of which is distinguishable by its characteristic structure and cell population.

Among other cells, the layer V contains neocortical large pyramidal neurons, whose cell body is situated in that layer but whose axons run down into the subcortical areas and whose dendrites reach up into the superficial layers. Pyramidal neurons are one of the more abundant and well-studied neuron types (Spruston, 2008). This and the fact that they can be excited (deliberately or inadvertently) by cortical stimulation makes them an interesting and useful model for this thesis.

With their branched processes, layer 5 pyramidal neuron reach into different layers and via synaptic contact receive input from cells in these layers. The function of the pyramidal neuron is to accept the stimuli from one or more other neurons, and if the cumulative incoming signals exceed a certain threshold, to generate an action potential. The action potential then travels down the cell and is passed on to other neurons via synapses at the end of the axon.

Pyramidal neurons can be roughly structurally divided into the soma, the dendrites and the axon.

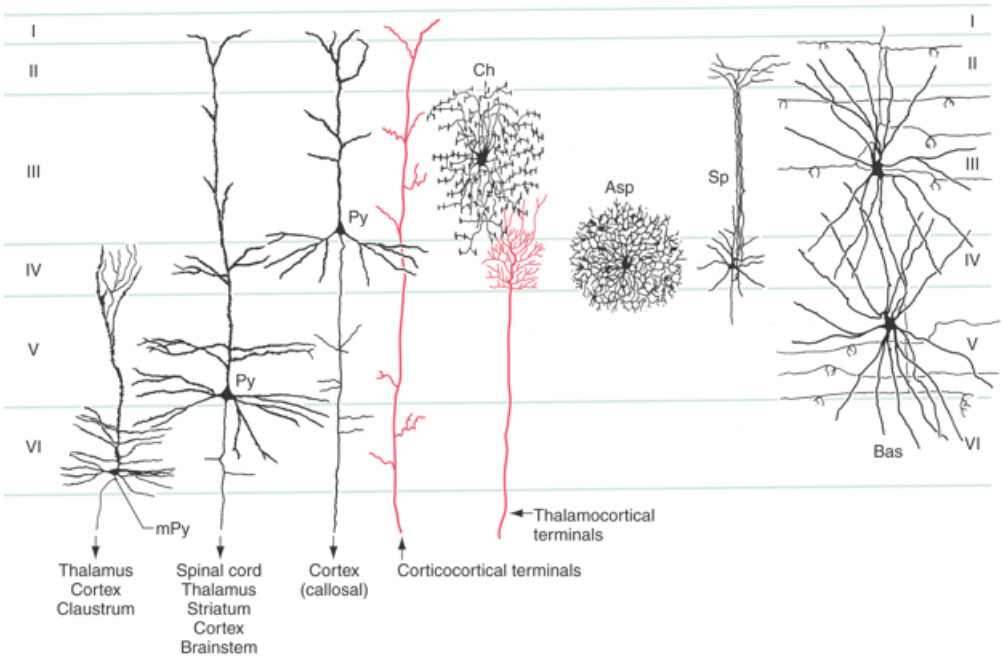

Figure 3.3: *Morphology of cell types present in the cortex. The vertical division to the left indicates the cortical layer, the total thickness of all layers in the human cerebral cortex is between 1 and 4.5 mm (Fischl & Dale, 2000). The second neuron from the left is a layer V pyramidal cell, a type which will be investigated in this thesis. Its soma is the roughly triangular structure next to the letters "Py", the axon is the thin neurite extending straight down, the apical dendrite is the long multibranched neurite reaching towards layer I. The other, shorter neurites are the basal dendrites. Note the "rough" texture of the dendrites, whose appearance is due to the presence of dendritic spines. Image by Lynch (n.d.).*

3.3.1 Soma

Pyramidal neurons derive their name from their characteristic cone-shaped soma, which is tapered in the direction of the apical dendrite (see Figure 3.3). Like in other neurons, it contains the cell's organelles including the nucleus and is thus responsible for its metabolism. In order to accomodate all of the necessary structures, the soma has a larger diameter than any of the other parts of the neuron (ca 20 μm in our case, but sometimes more or less).The axon and dendrites are all connected to the soma.

3.3.2 Dendrites

Two groups of dendrites can be distinguished in pyramidal neurons: the larger apical dendrite and several (in our model nine) smaller dendrites.

The apical dendrite is a slender structure that arises from the "tip" of the somatic cone and stretches with a length between 100 μm and over 1 mm relatively straight into the direction of cortical layer I. With increasing distance from the soma, it becomes more and more branched, structurally resembling the tree after which it is named.

Basal dendrites are smaller, less branched dendrites that connect to the base of the soma and extend in different directions away from the soma, causing the latter to seem surrounded by a small halo of dendrites.

Dendrites are responsible for receiving input from other cells and integrating multiple synaptic inputs from other neurons it to produce an output in the form of an action potential. A structural feature aiding this are dendritic spines, wich are small (ca 1-3 μm long) appendages of various shapes covering dendrites. They are postsynaptic connection sites facilitating communication with other neurons, although their full function is not completely understood (Spruston, 2008).

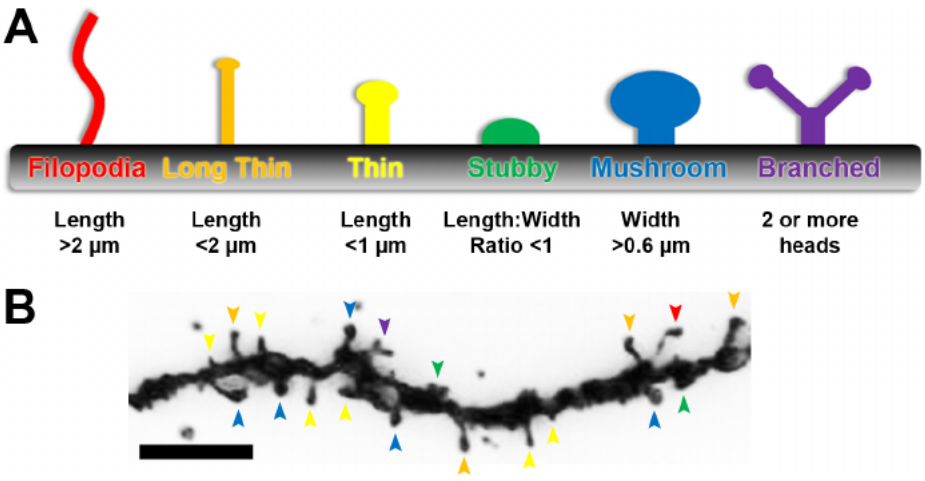

Figure 3.4: *A) Different types of dendritic spines commonly found in the cortex. B) An example for a dendrite segment with several kinds of spines as indicated by the coloured arrows. The dendrite is from a mouse Layer II/III neocortical pyramidal neuron. The scale bar has a length of 5 µm. Image and some of the caption by Risher et al. (2014).*

3.3.3 Axon

The axon emerges from the base of the pyramidal cell, running towards the higher cortical layers and thus in roughly the opposite direction as the apical dendrite. Its function is

to transmit signals in the direction away from the soma to other neurons. It can have collaterals (branches).

Joining the soma to the axon is the hillock, which is an element about 10 μm long and roughly the shape of a cone frustrum that is connected to the soma on the broader end and to the axon on the tapered end. The neuronal section closest to the hillock is the axon initial segment. Like the hillock it has a high density of sodium channels, which is important for its ability to initiate action potentials (Hu et al., 2009).

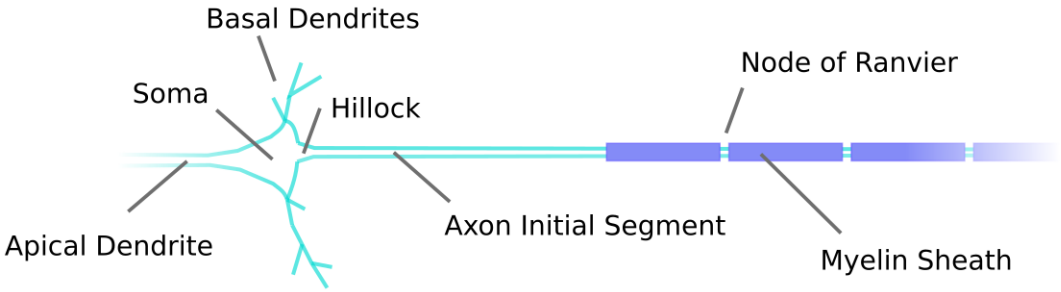

Figure 3.5: *Schematic drawing of the central part of a myelinated pyramidal neuron. The axon begins at the hillock, which is followed by the axon initial segment. At a distance of about 150 μm from the soma, the myelinated axon starts. The myelinated sections have a length of about 100 μm each and are separated by unmyelinated nodes of Ranvier with a length of about 1 μm each. For clarity's sake, the structures in the image are not to scale and most of the axon and apical dendrite is left out.*

Following the initial section is the myelinated section which covers most of the axon until it branches and terminates in synaptic connections at the distal end.

The myelinated sections are created by oligodendrocytes that wrap around sections of the axon several times. This forms layers of myelin (a fatty white substance) which changes the electrical properties of the affected sections. If N layers of myelin are present, the affected section has N times the resistance of an exposed membrane. Conversely, the capacitance is inversely proportional to the distance between the cytoplasm and the extracellular medium. This means that the capacity of the myelinated parts is reduced to $\frac{1}{N}$ times the capacity of an unmyelinated membrane.

The increased resistivity reduces the loss of signal amplitude of the action potential over distance. The decrease of capacity reduces the time it takes to charge the capacitor, which increases the signal velocity. The latter phenomenon is known as "saltatory conduction".

N is not infinite, so the signal still decays over distance. For this reason, the myelinated sections are interrupted by nodes of Ranvier, which are short (1 μm) exposed membrane sections with a high ion channel density. The nodes provide a boost to the signal between each myelinated segment. The signal propagation speed in the myelinated part of the axon is therefore higher than it would otherwise be.

4. Previous Research

As mentioned in the previous chapters, a challenge to targeted neurostimulation in general and extracellular stimulation specifically is that some of the effects of stimulating nervous cells are still not fully understood. This is not only true for entire tissues with their complex interdependent network of neurons and other cells and variation between patients, but also for individually analyzed and modeled neurons.

4.1 Modes of Stimulation

Stimulation in neuroengineering is often achieved by introducing a voltage or an electric current via electrodes. It is generally accepted that an action potential can only arise in a cell if the stimulation current and thus the stimulation intensity is above a certain strength. Two general electrode locations can be distinguished:

Intracellular Stimulation

For intracellular stimulation, an anode is placed within the cell. The applied current introduces positive charge into the cell interior, which causes the membrane voltage to rise. If the intensity and duration is sufficient, enough voltage-gated sodium channels can open to trigger an action potential.

4.1.1 Extracellular Stimulation

For extracellular stimulation, one (or sometimes a group of) active electrodes is positioned outside of the cell. As described by the ohmic law, current together with the resistivity of the extracellular medium leads to a gradient of the electric potential. Thus, different parts of the neuron are exposed to different field intensities, depending on their locations relative to the electrode(s). If this extracellular field changes the membrane voltage by the right amount in a region of the neuron, an action potential can form.

This is the preferred setup for neuroprosthetics, since placing electrodes directly into the target cells is either not possible or not desired. Issues with this kind of stimulation are the higher current needed as well as cell and electrode geometry (including present non-targeted neurons) causing more complicated activation patterns not seen in intracellular stimulation. The distance of the active electrode to excitable parts of the cell is now an important factor for stimulation, in addition to stimulation intensity and duration. In a single electrode setup, it is possible to use either cathodic (negative) or anodic (positive) current. For most purposes, cathodic stimulation is better suited for extracellular stimulation (Rattay, 1999).

Stimulating Field

In this thesis, the stimulating electrode (a cathode unless mentioned otherwise) is a point-shaped current source. The anode is assumed to be infinitely far away and so does not itself influence the stimulating electric field. The extracellular medium is modeled as having a purely ohmic resistance and no capacitance or inductivity. This leads to a spherically symmetric extracellular potential with magnitude proportional to the inverse of the distance from the electrode, which is given for a point at a distance r in from the electrode by the equation

$$V_e = \frac{I\rho_e 10^4}{4\pi r} \tag{4.1}$$

With the units used in the simulation, I is the electrode current in mA, ρ_e is the resistivity of the extracellular medium in $\Omega\ cm$ and the unit of r is μm. Since V_e is given in mV, the right side has to be multiplied with a factor of 10^4 to reconcile the units.

Regardless of electrode placement inside or outside of the cell, stimulation can be achieved with a single (long or short) pulse or several, depending on the task. If the aim is to find the lowest current a cell will respond to, a long stimulus is necessary. If the voltage-over-time course of an action potential needs to be analyzed, the stimulation time should be as short as possible to minimize the distortion of the voltage curve by stimulation artifacts.

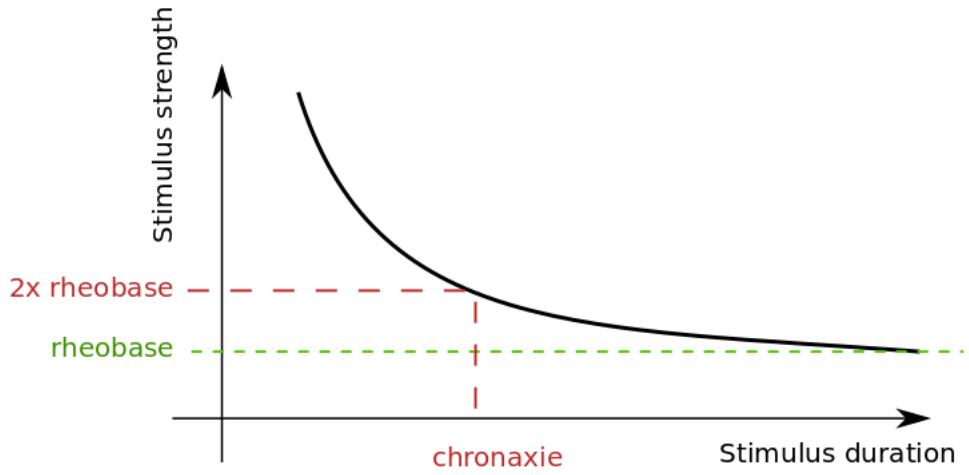

Figure 4.1: *A typical strength-duration curve with the corresponding rheobase and chronaxie. Image from Wikipedia (*Chronaxie*, n.d.).*

Several concepts are important for understanding the response of a neuron to stimulation:

- The **stimulation threshold** is the minimum stimulus intensity capable of evoking an action potential in a neuron. (There can also be an upper threshold, which is central to this thesis and will be discussed later but is not what is meant by the word "threshold" in the following few paragraphs.)

- The **strength-duration relationship** results from the fact that the stimulation threshold does not only depend on the intensity, but also on the duration of the stimulus. These two factors do not contribute independently from each other, but there is an inverse relationship between them. The shorter the stimulating pulse is, the higher the intensity has to be to trigger an action potential and conversely, a lower intensity requires a greater amount of stimulation time. This can be visualized as a curve of stimulation intensity over time (see figure 4.1). While the intensity falls with stimulation duration, it never reaches zero and instead converges towards a value called "rheobase".

- The **rheobase** is the stimulation intensity required to trigger an action potential if the stimulus duration is infinitely long. As such, it is the lowest possible intensity to be able to excite the cell for the given electrode/cell configuration.

- The **chronaxie** is the stimulus duration necessary to cause an action potential if the intensity has twice the value of the rheobase.

- The **current-distance relationship** is important for extracellular stimulation and describes the connection between the distance of the electrode from the targeted neuron or neurite and the minimum current needed to reach the stimulation threshold. This quantity is somewhat fuzzier than the strength-duration relationship because it can to a large part depend on the electrode and neurite geometry and their orientation relative to each other.

It is not surprising that extracellular stimulation is somewhat harder to model than intracellular stimulation. While intracellular stimulation also depends on neurite geometry (e.g. the area of the membrane can influence the threshold), the problem is far more pronounced for electrodes placed outside of the cell. In the following, some simple configurations that occur in our simulation will be briefly described.

Cylindrical Neurite

A very common way to model a neurite exposed to an extracellular stimulus is to regard it as a long, relatively thin cylindrical structure, with an electrode placed somewhere along its length at a distance. If a point electrode is used, the spherically symmetric field will result in a stronger electrical field in the region closest to the electrode, which gets weaker as one moves along the neurite axis in both directions away from the point nearest to the electrode. This also means that the potential gradient over the the neurite's surface is higher near the electrode (see figure 4.2).

The intensity of the extracellular field along the axis of such a neurite axis can be seen in image B of figure 4.3. When the stimulation is turned on, the potential inside of the cell becomes imbalanced, which causes electrical currents in the cytoplasm. Limiting these currents is the cytoplasm's resistivity. Due to the small diameter of the neurite, charge equalization over the length will take a relatively long time time. The equalization in radial direction is much faster in comparison. Another factor influencing the intracellular field are ions that leak through the membrane.

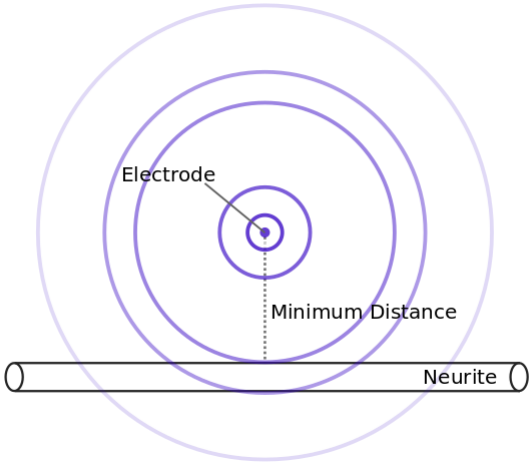

Figure 4.2: *A point shaped current source surrounded by concentric equipotential circles in fading blue. A nearby cylindrical neurite is exposed to the stimulating field. In the region closest to the electrode the potential gradient along the membrane can be large, especially in the radial direction. If the neurite is thick near the electrode, there might be a noticeable potential difference between the side near the electrode compared to the far side.*

The effect of the stimulus on the membrane potential depends on whether the stimulating electrode is a cathode or an anode. If it is an anode, the region near the electrode becomes hyperpolarized and regions further away depolarized, if it is a cathode the opposite is the case (Rattay, 1986, 1990).

Spherical Neurite

An important difference between the spherical and the cylindrical model is the greater symmetry and larger diameter of the sphere. If the sphere is located in the electric field of a point source, the field difference beween the point closest and the point farthest from the electrode will be large. Due to the symmetry of the sphere, charges can easily travel within the cytoplasm. Any potential difference in the cytoplasm (whether introduced by an external field or by an influx of ions) can therefore quickly be equilibrated. If there is a potential gradient over the outside of the sphere due to the stimulating electrode, the membrane potential (which is the difference between the external and internal potential) will therefore vary strongly over the surface and a polarization of the sphere can be observed.

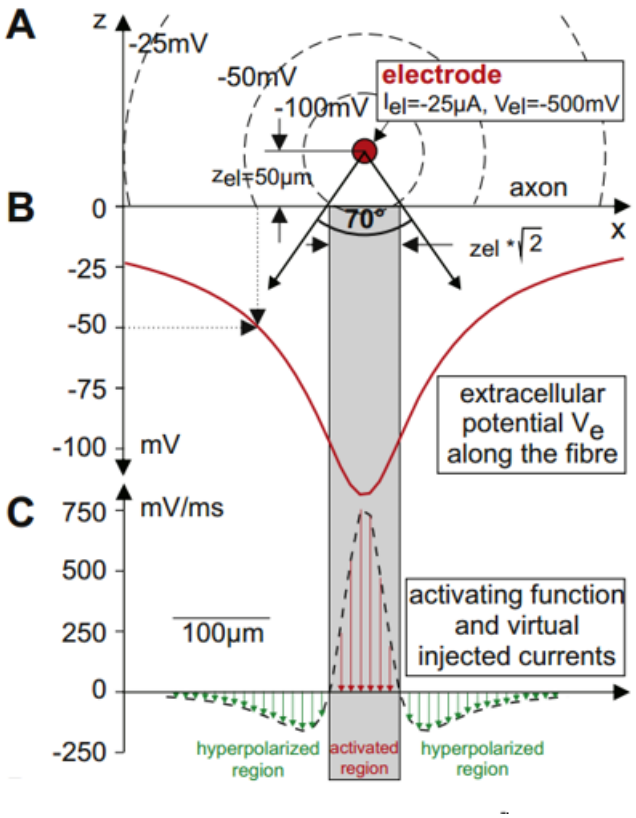

Figure 4.3: *A) Cathodic extracellular stimulation of an axon. The activated region is within 70 degrees to the axon position closest to the electrode. B) The extracellular potential along the axon. C) Values of the activating function along the fiber. The activating function can under some circumstances be used to estimate hyperpolarized or depolarized regions on the membrane. Positive values indicate membrane depolarization and negative values hyperpolarization. Image and some captions from Rattay et al. (2012).*

The depolarized pole will be close to and the hyperpolarized pole far from the electrode in case of cathodic stimulation, in anodic stimulation it is the other way around. In between these two extremes, there will be an unpolarized line separating them. Since the potential gradient is higher in regions closer to the electrode, this line will not be exactly on the equator of the sphere but shifted in the direction of the electrode. The shift also depends on the distance of the electrode from the soma and the soma's diameter (Fellner, 2017).

The polarization makes it more difficult to induce an action potential in a sphere than in the cylindrical neurite. If an action potential can be induced, it starts out in the depolarized part as is usual. Due to the fast equibrilation, there is very little delay

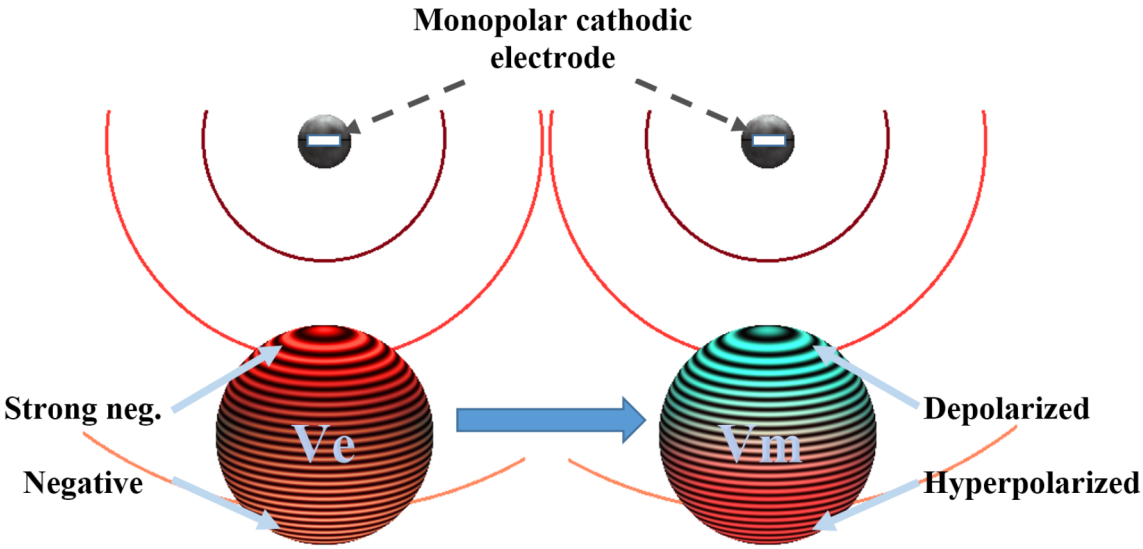

Figure 4.4: *Cathodic stimulation of a spherical neurite. On the left, the potential gradient of the external field is indicated. Pictured on the right side is the resulting membrane potential. The blue region indicates the depolarized and the red region the hyperpolarized pole. Note the unpolarized border between the poles, which is closer to the electrode than the equator. Image from Fellner (2017).*

between the initiation and the excitation of the entire sphere. This means that the whole sphere triggers almost as a unit, in contrast to a long cylinder where an action potential is initiated in one site and then travels along the neurite.

In the model of this thesis, the soma is assumed to be spherical and the rest of the neurites almost cylindrical. Since the simulation program and general modelling approach used in this work was developed for cylindrical neurites, some adjustments have to be made. More will be said about this in the next chapter.

4.2 Block Phenomena

4.2.1 Upper Threshold Phenomenon

In 2010, Boinagrov et al. described the upper threshold phenomenon, which predicts that no action potential will be produced if the stimulus is not only too weak as is generally accepted, but also if it is too strong (Boinagrov et al., 2010). In another paper from 2012, Boinagrov et al attributed this phenomenon to sodium current reversal, which can occur

in neurons with a membrane potential above the Nernst potential for sodium (such as in strong stimulation). This causes the flux of the sodium ions to reverse, with the ions flowing out of the cell instead of in. Since the formation of an action potential is caused by a sodium ion inflow, the current reversal should result in a block. The upper and lower thresholds were reported to also depend on stimulation time, with both thresholds lowering for longer stimulation durations (Boinagrov et al., 2012).

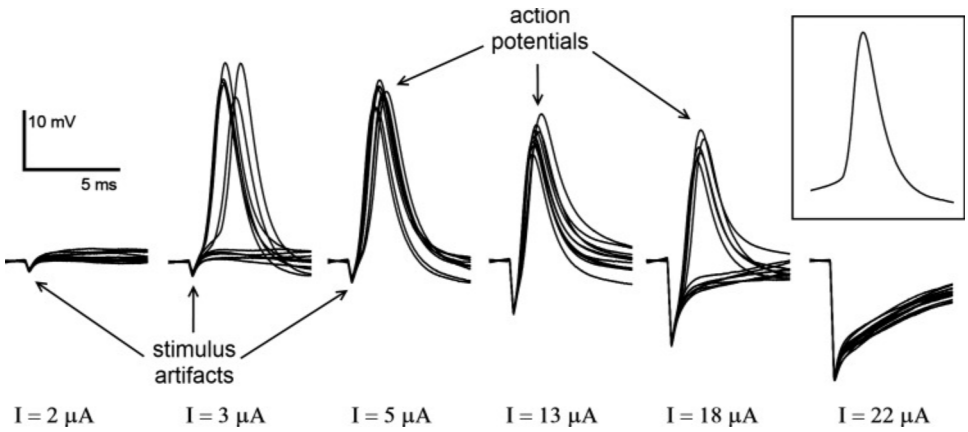

Figure 4.5: *In vitro recordings of retinal cells using the patch clamp technique in the soma with varying extracellular current strength and a duration of 0.2 ms. It is clear that a block occurred at higher voltages. The rectangle to the upper right contains a spontaneous action potential for comparison. Figures and parts of the caption by Boinagrov et al. (2012).*

In addition to simulations with a spherical neuron model, the authors demonstrated their discovery in vitro in rat retinal ganglion cells. They first proved the existence of an upper threshold by subjecting cells to increasing stimuli and observing the failure to form an action potential above a certain threshold. In the next step, they tested whether sodium current reversal was responsible by placing the cells in a low sodium medium. They predicted that this would decrease the upper threshold because the reduced sodium ion concentration gradient would shift the reversal potential towards a lower value. The results of their experiment confirmed this prediction.

Simulation with Additional Neurites

The soma-near region of the axon has a high sodium channel density which means that action potentials are usually initiated in this spot rather than in the soma. This means

that a model comprised solely of a spherical soma only yields an incomplete picture of the block related dynamics in a ganglion cell.

Rattay expanded the simulation in Boinagrovs spherical cell model by using a compartment model including an axon and a dendrite (Rattay, 2014). As predicted by Boinagrov et al., the spherical soma reacted with a block above certain current thresholds. At the same intensities, a one-sided action potential starting in the axon and propagating away from the soma was still observed.

A stimulating electrode was placed in a way that it was both near the soma and the high-sodium density region (sodium band) of the axon, and recordings were taken in the soma and at a distant axon site. The stimulation current was set to different intensities and the latencies of the arrival of the action potential recorded for both sites and each stimulus. While the latency decreased with increasing current for the distant axon, the relationship for the soma was U-shaped. At first, the latency decreased as in the distant axon site, but above a certain voltage there was an increase again, culmulating in a complete block in the soma at the upper threshold.

Rattay attributed this to an increasing hyperpolarization in the soma, which if weak enough (at lower stimulation intensities) can still be overcome by an arriving action potential. If it is strong , it causes a complete block, meaning that the action potential is now incapable from propagating into the soma.

The same study also mentions the position of the electrode relative to the axon as an important parameter. If it is shifted away from the soma in direction of the axon, the block vanishes. Other factors that strongly influence the existence and value of the upper threshold are the axonal pathway curvature and electrode position relative to the axonal region with high sodium channel density.

4.2.2 Anodal Surround Block

Rattay proposed as an alternative explanation for the results in his paper and that of Boinagrov et al. a well-known phenomenon called anodal surround block. Extracellu-

lar stimulation by a sufficiently small cathode produces membrane depolarization in the neuronal region closest to the electrode, but hyperpolarisation to both sides (see figure 4.3). The hyperpolarized regions will be located at an angle of 70 degrees if the center of the depolarized region is at zero degrees (Rattay, 1990). This leads to an inhibition of action potential propagation if the stimulation intensity is much greater than the lower excitation threshold. (Barriga-Rivera et al., 2017).

The cause for this phenomenon is ultimately Kirchhoff's current law, which states that the sum of all currents crossing a closed surface must be zero. Since this holds for a neuron's surface as well, the depolarizing current near the electrode must be compensated by an opposing current elsewhere. Since there is no electrode inside of the neuron, that current has to pass through the membrane somewhere. These regions turn out to be adjacent to the depolarized section and experience hyperpolarization. They also cover a much larger area than the depolarized section, which is why the hyperpolarization intensity is lower than that of the depolarization (see figure 4.3). When the stimulus is small, the weak hyperpolarisation can be overcome by an action potential generated at the depolarized site, if it is larger the action potential cannot propagate through these regions anymore (Ranck, 1975).

Boinagrov and Palanker (2014) replied to Rattay. They stated that the anodal surround block and the sodium current reversal phenomena could be distinguished since in the case of the surround block, the action potential is initiated at one site but may be stopped from propagating further. In the sodium current reversal phenomenon, no action potential arises in the first place.

The upper threshold phenomenon assumed to be of practical importance in neuroprosthetics such as retinal implants (Barriga-Rivera et al., 2017) and in cortical stimulation. It is often assumed that neurons in a tissue will be excited if they lie within a spherical volume surrounding the electrode (which is assumed to be a point source) and not be excited if they lie outside. Based on this assumption, in neurostimulation and especially prosthetics, many electrodes lie in a close range and current is often set to be far above the stimulation threshold in order to ensure effectivity (Boinagrov et al., 2012).

The existence of an upper threshold complicates this by implying that neurons that are close enough to the electrode to experience stimulation above the upper threshold will not generate action potentials. Therefore, the stimulation will only affect neurons in a spherical shell centered on the electrode and not those inside and outside of the shell. Implants designed without taking this into account may perform worse or even fail. Specifically in retinal implants, electrodes that lie close together to ensure higher resolution may cause overlapping electrical fields. Together they may surpass the upper threshold even if individual electrodes by themselves would not (Barriga-Rivera et al., 2017). Conversely, if properly understood, the block phenomena could be used to strategically deactivate neurons.

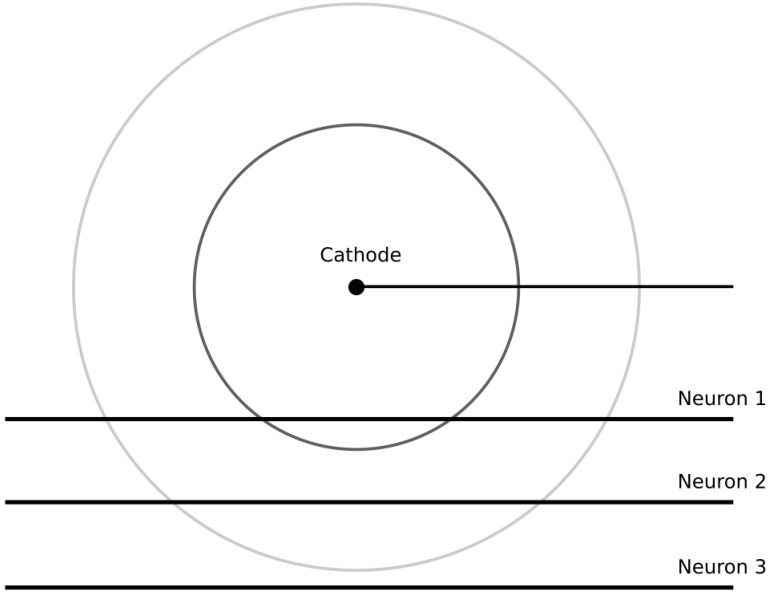

Figure 4.6: *Three neurons in a spherically symmetric field by a nearly point-shaped electrode. Two equipotential rings (spheres in three dimensions) indicate the borders for lower and upper stimulation threshold. Neuron 3 is completely outside of the ring-shaped area (or volume in three dimensions) where the field is high enough to elicit an action potential. Neuron 2 passes through that field and can be stimulated. A region of Neuron 1 close to the electrode is exposed to a field that is strong enough to elicit a block. This may mean that an action potential is not initiated in this region, but it can also stop an action potential originating elsewhere in the affected cell from passing through the hyperpolarized parts.*

Another phenomenon explained by hyperpolarization of some regions in the cell membrane is the chronaxie discrepancy between intracellular and extracellular stimulation in the

same cell. The hyperpolarization of some parts of the cell and depolarization of others in extracellular stimulation if the electrode is close enough to the neuron can account for the shorter chronaxie in extracellular stimulation, as demonstrated by Rattay, Paredes and Leao (Rattay et al., 2012). A pyramidal cell quite similar to the one used in this work concerning both morphometry and channel density was used in their investigation.

In their paper, the stimulating electrode was positioned relatively close to the cell (ca 50 μm) in order to trigger the effect. This means that the diameter of larger parts of the cell, especially the soma, is in the same order of magnitude as the distance to the electrode. The result is that the difference of the extracellular electric field between the part of the soma closer to the electrode to the furthest part is likely to be significant and has to be accounted for. This can be achieved by dividing the compartment into suitable segments, each of which only experiences a negligible potential gradient over its surface.

As part of his thesis (Fellner, 2017), Andreas Fellner used a method to subdivide a spherical soma model into segments of the right dimension and orientation to avoid strong electrial gradients over the surface of any one segment. He implemented it in a simplified model of a retinal ganglion cell consisting of a soma, a cylindrical dendrite and an axon. Since the electrode could be moved to different positions, the soma had to be implemented so it could be rotated to be well-aligned with the electrode for all positions. His experiments used two different channel configurations, one with channel distributions and kinetics from the tiger-salamander retinal ganglion cell as described by Fohlmeister and Miller (Fohlmeister & Miller, 1997) and for comparison one with the channels found in the original model[1] by Hodgkin and Huxley (Hodgkin & Huxley, 1952).

A big part of Fellner's thesis was to analyze the possible contribution of the sodium current reversal or the anodal surround block to the upper threshold phenomenon. As

[1]This influential model, invented by Hodgkin and Huxley in 1952, is the basis for many simulations in neuroscience. Originally invented as a way to mathematically describe the formation and propagation of action potentials in a squid giant axon with a sodium and a potassium channel, an expanded upon version of it is now used for different neuron types in different species. Both the Fohlmeister-Miller model and the one used in this thesis are such implementations. This and the fact that the software NEURON used in Fellner's work (and also in this thesis) natively allows the original Hodgkin-Huxley channels to be easily implemented make it a good comparison model. It will be described in detail in a later chapter.

was expected, he could establish a distance-dependend stimulation window in his model. He also analyzed the sodium ion currents and their direction (ie into or out of the cell) during stimulation. He predicted that if a current reversal occurred in the soma due to high stimulation intensities, an action potential should not be able to form.

To test this, he exposed a cell with a spherical soma to different stimulation intensities. The soma in his model did experience sodium current reversal in some of its surface if the stimulus was sufficiently strong. Fellner compared the upper thresholds for action potential generation with the stimulation intensities where the current reversal started to occur. It turned out that sodium current reversal was sometimes observed even below the upper threshold, ie even though the current was reversed in some regions of the soma, an action potential was still able to form.

Further investigation revealed that while current reversal only in some areas wasn't enough to induce a block, the net sodium current over the whole somatic membrane was important. In the Hodgkin-Huxley model simulation, the current reversal for the whole membrane occurred only above the stimulation threshold. Surprisingly, in the Fohlmeister-Miller model, the limit for the sodium outflow was markedly different. It was inside the stimulation window, meaning that an action potential seemed to form even though there was a net sodium outflow over the whole somatic membrane. The upper threshold and the outflow limit were very close together. It is sometimes challenging to judge from a voltage chart whether an spike in the voltage chart represents a successful initiation of an action potential, especially at the stimulation thresholds. Therefore, one possible explanation for the outflow limit and upper threshold discrepancy for the Fohlmeister-Miller model could be that spikes at the upper limit where errorneously identified as action potentials. This would mean that the upper threshold was assumed to be higher than it was and that the actual upper threshold is either at the same intensity or below that of the sodium current reversal threshold.

Fellner then simulated the soma together with the axon, with different stimulation strengths and an electrode placement that produced a comparable field in different sections. As a result, he observed blocks both in just the soma or in the soma and the axon, depend-

ing on the parameters of the stimulation. Since the reasons for the somatic block were not completely clear, no definite conclusion was possible about the contributions of the sodium current reversal or the anodal surround block to the observed thresholds.

4.2.3 Collision Block

Immediately after an action potential has passed through an area in a neurite, the refractory period stops that region from becoming excited anew in a very short time. While a strong enough stimulus could overcome the afterhyperpolarization, the absolute refractory period caused by the inactivation of the voltage-gated sodium channels cannot be lifted by any stimulus intensity.

It is sometimes possible to elicit more than one action potentials in different places in the same cell. If this happens at the right time, they propagate towards one another along the cell and eventually meet. This can result in annihilation of both action potentials, as was experimentally confirmed by Tasaki (1949) and agrees with the Hodgkin-Huxley model (Budvytyte et al., 2015; Hodgkin & Huxley, 1952). This effect is used in the study of nerve fibers (Lipski, 1981).

4.3 Aim of this Thesis

The goal of the work here presented was to investigate block phenomena in a layer 5 pyramidal neuron model. Up until now, the debate over the cause of the upper threshold involved mostly models using retinal ganglion cells. When a pyramidal neuron was used, things other than the exact behavior of the soma were investigated. The realism of the interaction between each part of the simulated soma and the stimulated field where therefore not prioritized.

Several issues are of interest and will be analyzed:

- The effect of parameters like stimulation strength, intensity and electrode position on the generation and propagation of action potentials in different parts of the neuron.

- The presence or absence of an upper stimulation threshold.
- Whether the upper threshold phenomenon is due caused by sodium current reversal, anodal surround block or both.
- Whether the main (pyramidal cell) model differs from other, simpler models.

5. Methods

In neuron modelling, several approaches are possible, each with their advantages and drawbacks.

5.1 Biological and Computational Models

Neurons can be investigated either in vivo (in a living animal) or vitro (as explanted cells) or by using computational models.

A major advantage of in vivo and vitro experiments is that they are intrinsically physiologically accurate, possessing properties and behaviors that would be difficult to incorporate into a computer simulation. This is either because those properties are not known, not well enough understood or too difficult or computationally expensive to properly represent. Disadvantages are the large expenses a laboratory working with or extracting cells from tissue requires. This includes the fact that each individual neuron or tissue has a limited time of use, which also negatively impacts replicability. Another problem is the large and hard to control amount of parameters and their interactions that is intrinsic to work with biological cells and makes gaining and interpreting data challenging (Blackwell, 2014).

Since the development of the Hodgkin-Huxley Model (Hodgkin & Huxley, 1952) for the squid neuron, many mathematical models and techniques have been developed to allow the simulation of the behavior of neurons and the generation of action potentials. Nevertheless, it is advantageous to later validate the results of a simulation with experiments on real neurons.

An advantage of in silico models can be the higher comparability of results, especially those reached with similar modelling techniques. Other advantages include low cost in some approaches and the comparatively manageable amount of parameters. Especially

the easy control over individual model parameters and the precision possible in tracking neuronal excitation make this an attractive approach which was taken in this thesis.

5.2 The Model

5.2.1 Overview

The implementation of the model was done in NEURON, a widely used computational neuroscience software package created by Hines (1993). It was complemented by a supplemental package by Carnevale, which introduces the ability to process extracellular stimulation needed in the model (Carnevale, 2005).

The tracing of the main pyramidal neuron model used in this thesis is taken from the layer 5 rat pyramidal neocortical neuron used by Mainen et al. (1995) in their paper "A model of spike initiation in neocortical pyramidal neurons". It was modified by exchanging the soma in the original model with a soma similar to the one used in Fellner's thesis to account for the non-negligible physical dimensions of the soma (Fellner, 2017).

The ion channels in the model by Mainen were replaced with the channels presented in the paper "Distinct contributions of Nav1.6 and Nav1.2 in action potential initiation and backpropagation" by Hu et al. (2009). This modification was done to account for recently mapped channel types and their spatial distributions that were not known at the time Mainen et al. published their model.

5.2.2 Simulation Methods

The software Package NEURON enables the creation of model neurons (or networks of neurons) and the simulation of action potentials. In the following, an overview of the conceptual and mathematical framework used by NEURON will be provided.

In NEURON, the smallest unit to represent either a very simple individual cell or parts of neurons in more complex models is the section. A section is usually of cylindrical shape (but sometimes, as in our model, it can consist of one or even several connected cone frustra). Each section has uniform membrane properties. The mantle represents the cell

membrane and defines its area (which is needed in the model's calculations). The ends can either be free or connected to other sections (often more than one to create branching neurites) to form a more complex shape. Although it is somewhat less common, it can make sense to connect the ends of some sections to the middle of another section, which was also done in this work. The segments in the model were treated as compartments in contact with their environment.

Compartment Modelling

Compartment modelling is a way to discretize a system by dividing it up into one or more parts (compartments) that interact in a defined way with their environment (such as other compartments). The individual compartments are assumed to be internally homogeneous. Examples for interactions between compartments or with their environment can be material exchange (such as ions passing through a membrane or between two sections) or exchange of energy (e.g. the capacitive behavior of the cell membrane). By defining and solving the equations for these exchanges, the behavior of the whole system (such as a neuron consisting of compartments) can be modeled.

Cable theory and Electrical Properties of the Neuron

Cable theory was initially developed in order to calculate signal propagation in undersea cables and was later adapted to model action potentials in neurons. The basic assumption in cable theory is that the cable (or neurite) consists of a simple cylinder divided into subsections (compartments), which is described with equivalent circuits. The interior of the cable is assumed to have a uniform axial resistance, the border to the outside is considered to have both a capacitance and an ohmic resistance.

The interior of the neuron or neuron part is approximated by a chain of nodes connected via resistors. These resistances are the resistivitiy of the cytoplasm, called R'_I in the diagram times the distance Δx between two adjacent nodes. The interface between the interior and exterior of the cell is modeled by a capacitance and resistor in parallel extending to the outside of the cell. As mentioned before, the capacitance $C' \cdot \Delta x$ arises from the lipid bilayer acting as a thin dielectric and is proportional to the membrane area.

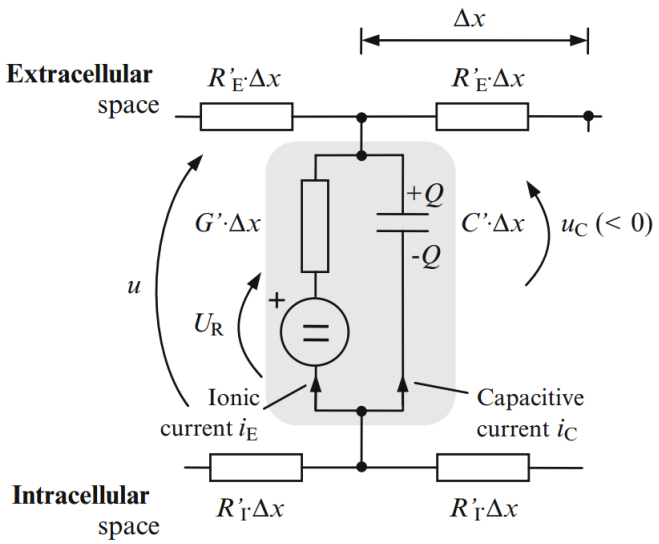

Figure 5.1: *Equivalent circuit for the interactions of a cable compartment with its environment. The node in the middle of the cable represents the compartment, the electrical circuit elements determine its interactions with its environment. Image and part of the caption by Kaniusas (2012).*

The radial resistance is given as its inverse, a conductance G', which is due to ions being able to move through channels in the membrane.

R'_E is the extracellular resistivity, which is much smaller than the intracellular resistivity R'_I. This is caused by the increased mobility of extracellular ions and the small cross-section of the area inside of the membrane (Kaniusas, 2012). A neuron also possesses a nonzero resting potential, which can be modeled with a voltage source U'_R in series with the passive conductance.

NEURON uses the geometric centers of the specified sections (or segments) as nodes. The resistance between the nodes is derived from cytoplasm resistance, which is assumed to have the same value everywhere in the cell and no capacitance. The value for the cytoplasmic resistivity Ra in this model is 150 Ω *cm*.

The Passive Mechanism

NEURON supports a mechanism for nonspecific current through the membrane. The passive mechanism covers the electric properties in the membrane not counting specific ion channels. In the main model used in this thesis, the conductance g_{pas} is 0.05 mS/cm^2 for all sections except for the nodes with a $g_{pas,node}$ of 20 mS/cm^2. Unlike in the specific ion channels described later, the conductance of the passive layer does not change with parameters such as membrane voltage or ion concentration. The specific capacitances of the unmyelinated and myelinated sections are 0.5 and 0.02 $\mu F/cm^2$, respectively. This passive model can describe the membrane in the subthreshold case, in some models it is also used to simulate the behavior of dendrites.

To model more than passive behavior, e.g. to enable action potentials, this passive cable model is added upon by the ion transport mechanisms required by the individual simulation.

5.2.3 Ion Channels and Transport

Apart from the contributions from the lipid bilayer, the membrane's electric properties are determined by ion transport through the membrane, either through passive diffusion or through active transport in channels. In the model in this thesis, Hodgkin and Huxley (1952) type channel kinetics are used for both passive and active ion currents.

The Hodgkin-Huxley Model

In 1952, Alan Lloyd Hodgkin and Andrew Fielding Huxley came up with a mathematical model for the formation and propagation action potentials in a giant squid axon. It has been expanded and modified to suit different neuron types in many species and as such remains popular in many simulations. Like the passive cable model, it simulates the functions of the membrane with an equivalent circuit.

In Hodgkin-Huxley kinetics, the current of channels into or out of the cell are assumed to be ohmic, i.e. proportional to the channel conductance and the transmembrane voltage (Destexhe & Huguenard, 2007). Other important parameters are channel activation and

deactivation rate constants, which are defined by differential equations that account for the time and voltage dependent permeability of the channels to ions, among other factors. Individual channels proteins are not considered by the model, the aggregate conductance of all channels of a specific type per unit area is used instead.

The model consists of several differential equations. The total current per area through the membrane is stated by the original model as follows

$$I = C_m \frac{\mathrm{d}V_m}{\mathrm{d}t} + \bar{g}_{\mathrm{K}} n^4 (V_m - V_K) + \bar{g}_{\mathrm{Na}} m^3 h (V_m - V_{Na}) + \bar{g}_l (V_m - V_l) \tag{5.1}$$

It expresses the total current I per membrane area in terms of the membrane voltage V_m, the membrane capacitance per unit area C_m, the individual maximum conductances $\bar{g}_K$ and $\bar{g}_{Na}$ of the ions K and Na per unit area and the differences between the membrane voltage and the Nernst potentials V_K and V_{Na} of each ion. The leak currents are also accounted for, with their own maximum conductances $\bar{g}_l$ and equilibrium voltage V_l . Additionally, the channel conductivities depend on dimensionless factors n, m, h; with n being associated with potassium channel activation, m with sodium channel activation and h with sodium channel inactivation.

The factors n, m, h follow the equations

$$\frac{dn}{dt} = \alpha_n(V_m)(1-n) - \beta_n(V_m)n \tag{5.2}$$

$$\frac{dm}{dt} = \alpha_m(V_m)(1-m) - \beta_m(V_m)m \tag{5.3}$$

$$\frac{dh}{dt} = \alpha_h(V_m)(1-h) - \beta_h(V_m)h \tag{5.4}$$

The individual α_x and β_x, with x standing for n, m or h are the rate constants governing the equations. For the original Hodgkin-Huxley equations they are

$$\alpha_n(V_m) = \frac{0.01(10 - V_m)}{\exp\left(\frac{10-V_m}{10}\right) - 1} \qquad \beta_n(V_m) = 0.125 \exp\left(\frac{-V_m}{80}\right) \tag{5.5}$$

$$\alpha_m(V_m) = \frac{0.1(25 - V_m)}{\exp\left(\frac{25-V_m}{10}\right) - 1} \qquad \beta_m(V_m) = 4 \exp\left(\frac{-V_m}{18}\right) \tag{5.6}$$

$$\alpha_h(V_m) = 0.07 \exp\left(\frac{-V_m}{20}\right) \qquad \beta_h(V_m) = \frac{1}{\exp\left(\frac{30-V_m}{10}\right) + 1} \tag{5.7}$$

While the last equations are only strictly applicable in the original Hodgkin-Huxley channels, some more recent channels (e.g. sodium channels used in this thesis) have comparable rate constant equations. The Hodgkin-Huxley model serves as the basis, with some channels added and the parameters in the equations fitted to align with experimental values by the respective authors of the mechanisms.

Temperature Adjustment

A further adaptation is the introduction of a temperature adjustment variable that accounts for changes in channel behavior due to different model temperatures. The measurements to determine channel properties are often done in vitro and at ambient temperature, so the measured values may not fit well with channel behavior at body temperature. In this simulation, 37° C was used and the correction was

$$t_{adjust} = q_{10}^{\frac{T_{Sim} - T_{Orig}}{10}} \tag{5.8}$$

With t_{adjust} being the temperature correction factor, q_{10} being the temperature sensitivity, which is 2.3 for almost all channels in the model, T_{Sim} (37° C) being the temperature the channels are simulated at and T_{Orig} (23° C) being the temperature the channels were originally recorded at. The unit for all temperatures in the model is Celsius. The internal calcium concentration mechanism and the leakage channel are the only two in our model that are not corrected for temperature. In order to integrate this temperature adjustment

into the model, t_{adjust} is multiplied with the maximum conductance $\bar{g}_X$ for ion channel X.[1]

In addition to the passive mechanism described before, the model in this thesis uses six different ion channels with two sodium, three potassium and one calcium channel.

Sodium channels

The sodium channels in this model are voltage-gated and as discussed are the channels usually responsible for the first phase of the action potential. They differ from one another in their biophysical properties such as their activation threshold and also their location in the cell (Rush et al., 2005). The contribution of the sodium channels to the current across the membrane is analogous to the original Hodgkin-Huxley equation

$$g_{\mathrm{Na}} = t_{adjust}\ \bar{g}_{\mathrm{Na}}\ m^3 h (V_m - V_{Na}) \tag{5.9}$$

with g_{Na} being the total conductivity of the channel in S/cm^2. The activation and deactivation constants m and h are given by equations (5.2) and (5.4).

The sodium channel mechanisms in this simulation were authored by Zach Mainen, with the kinetics fit to data from Huguenard et al. (1988) and Hamill et al. (1991), with some adjustments. Hu et al. (2009) added an input voltage shift to each of the channel types in order to account for differences in threshold values.

- **$\mathbf{Na_v1.2}$** is one of a group of related voltage-gated sodium channels and is primarily found in unmyelinated axons and dendrites (Shah et al., 2001). It is characterized by a high threshold and in the model used here is present throughout the neuron with the exception of the nodes of Ranvier. It contributes to the action potential backpropagation to the soma (Hu et al., 2009).

[1] Adjusting the temperature this way ignores its influence on the gating variables and thus may not be very accurate (Rattay et al., 2003). This will be looked into in our experiments.

- **$\mathbf{Na_v1.6}$** belongs to the same channel subfamily as $Na_v1.2$. $Na_v1.6$ are low threshold voltage gated channels present in the axon initial segment and the nodes of Ranvier. They are largely responsible for the action potential initiation in the axon initial segment (Hu et al., 2009).

Potassium channels

The potassium channels present in this simulation are somewhat more diverse than the sodium channels. Apart from the voltage-gated channel, there is one muscarinic channel and one calcium-activated potassium channel. They regulate the inward potassium flow and the current contribution by each is given by

$$g_{\mathrm{K}} = t_{adjust}\ \bar{g}_{\mathrm{K}}\ n^4(V_m - V_K) \tag{5.10}$$

with g_{K} being the total conductivity of the channel in S/cm^2. The activation constant n is given by equation (5.2).

- The $\mathbf{K_v}$ voltage-gated potassium channel is ubiquitous in animal cells and plays an important role in action potential propagation. As mentioned before, it opens at high membrane potentials in order to allow an inflow of potassium ions. There are many subtypes, but the distinction is not important for this model so they are all subsumed into one generic channel. In our model it can be found in all sections of the cell except for the myelinated axon and the nodes. The mechanism was written by Mainen based on kinetics by Huguenard et al. (1988) and Hamill et al. (1991).
- The $\mathbf{K_M}$ muscarinic channels are regulated by a signal cascade connected to a G-protein-coupled receptor in the cell membrane. K_M is slow and non-inactivating. In our simplified model, its kinetics are analogous to the previously mentioned voltage-gated channel, leaving ligand interactions out. It functions as a small current counteracting stimuli and so slightly inhibits spiking (Koch & Segev, 2003). The soma and dendrites are the only locations this channel is found in our model. It was created by Mainen.

- The $\mathbf{K_{Ca}}$ calcium dependent potassium channel used in this model opens following an increase in calcium ions in the cell interior. This leads to an efflux of potassium ions from the cell, causing the membrane potential to drop. This notably happens after an action potential involving calcium ions, where the phenomenon contributes to afterhyperpolarisation. It is present in the soma and dendrites.

  The kinetics of this channel are somewhat different from the other two potassium channels. The rate constant for the activation is given by the equation $\alpha = a_{max}\ [\mathrm{Ca}^{2+}]_{\mathrm{in}}$ and the inactivation rate by $\beta = b_{max}$, with $a_{max} = 0.01/ms$ being the maximum activation rate, $[\mathrm{Ca}^{2+}]_{\mathrm{in}}$ being the calcium ion concentration inside of the cell in mM and $b_{max} = 0.02/ms$ being the maximum inactivation rate. The author of the mechanism is again Mainen, who based the mechanisms on the work of Reuveni et al. (1993).

Calcium Mechanisms

Two types of Ca^{2+} mechanism are used in this simulation. One is a high-voltage activated channel and the other one is a mechanism covering both passive inflow and an active pump transporting calcium out of the cell.

- $\mathbf{Ca_v}$ is a high-voltage-gated calcium channel activates at a high membrane potential. Due to the high concentration gradient of calcium from the outside to the inside of the cell, calcium ions enter the cell following activation. The total conductivity g_{Ca} of the channel is given by

$$g_{\mathrm{Ca}} = t_{adjust}\ \bar{g}_{\mathrm{Ca}}\ m_{\mathrm{Ca}}^2\ h_{\mathrm{Ca}}(V_m - V_{\mathrm{Ca}}) \tag{5.11}$$

  with the calcium activation and deactivation constants m_{Ca} and h_{Ca} respectively. The equations determining these constants are analogous to those for sodium ions in equations (5.2) and (5.4). Like the sodium channels, they show inactivation following opening. In this model they can be found in the soma and dendrites. The channel dynamics were fitted by Mainen based on the model by Reuveni et al. (1993).

- **$\mathbf{Ca_{cm}}$**, an internal calcium concentration mechanism covers the transfer of calcium ions from the inside to the outside of the cell, as well as a calcium current into it. The latter is simplified by only considering the ions in thin shell beneath the membrane and not in the entire cytoplasm. The kinetics for the influx of calcium are given by the differential equation

$$[\dot{\mathrm{Ca}}^{2+}]_{\mathrm{in}} = \frac{-1000\ I_{\mathrm{Ca}}}{2Fd} \tag{5.12}$$

$F = 96485.3329\ sA/mol$ is the Faraday constant, $d = 0.1\ \mu m$ is the depth of the shell and I_{Ca} is the calcium transmembrane current in mA.

The kinetics for the calcium ion ATPase pump that moves calcium to the outside is

$$[\dot{\mathrm{Ca}}^{2+}]_{\mathrm{in}} = \frac{-K_{\mathrm{T}}\ [\mathrm{Ca}^{2+}]_{\mathrm{in}}}{[\mathrm{Ca}^{2+}]_{\mathrm{in}} + K_{\mathrm{d}}} \tag{5.13}$$

with $K_{\mathrm{T}} = 10^{-4}\ mM/ms$ and $10^{-4}\ mM$. The mechanism can be found in the soma in our model. It is not strictly speaking a channel, but rather a mechanism to determine the calcium ion concentration inside of the cell. Alain Destexhe created it for NEURON based on the mechanism described in Destexhe et al. (1993).

5.2.4 Extracellular Stimulation

The model as discussed up to now lacks the ability to handle extracellular processes. Since this thesis involves stimulation from the outside of the neuron, it is necessary to add a framework that can deal with this.

As mentioned in the previous chapter, the stimulating electrode is assumed to be a point source imparting cathodic current in a homogeneous medium with ohmic resistance. In this model, the extracellular resistivity ρ_e is 300 $\Omega\ cm$ and was set to be the same as in the model by Rattay et al. (2012).

NEURON's Extracellular Mechanism

The extracellular mechanism in NEURON builds on the Hodgkin-Huxley type cable model by adding an extra layer to the circuit (by default it is two layers, but only one is needed in this model).

As described in the previous sections, the inside of the cell is connected to the outside via Hodgkin-Huxley-type dynamics. The equivalent circuit is now expanded by extra elements on the outside of the cell (see figure 5.2). Several new parameters are introduced by this mechanism. These include, in the nomenclature NEURON uses, $xraxial$, which is the resistance between two nodes at the outside of the cell and the radial conductances and capacitances xr and xc, respectively. The potentials these nodes are on is $vext$. In our case V_e is the extracellular potential imposed by the stimulating electrode.

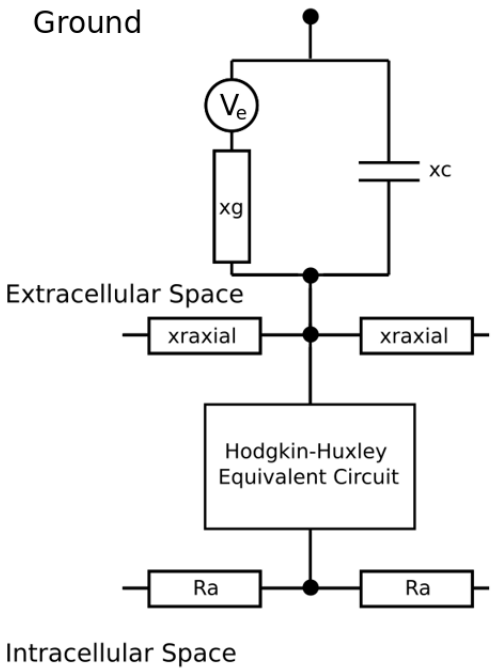

Figure 5.2: *Circuit diagram of the extracellular mechanism with one layer as needed for our model. The membrane mechanisms are omitted for clarity. The stimulating field V_e is pictured as a voltage source.*

The xtra Mechanism

One way to introduce extracellular stimulation to a NEURON model is the "extracellular stim and rec" package created by Carnevale (2005). The following assumptions underlie this mechanism:

- The extracellular medium has no capacitance or inductivity.
- The currents generated by the cell's activity don't influence the stimulating field.
- The distance between the segments and the electrode are large compared to the segment's size.

The package calculates the geometric centers of each segment. Based on these coordinates, it determines the distance of each segment from the stimulating electrode (which is simple in our case as it is a point source). With the assumption of the extracellular medium having uniform resistivity, the transfer resistance R_{transfer} in $M\Omega$ between the electrodes and the segment's location can be calculated with

$$R_{\text{transfer}} = 0.01\rho_e \; r \tag{5.14}$$

and r being the segment-electrode distance in μm.

Note that the accuracy of this approach relies on the difference between the segment's center and its immediate exterior being small compared to its distance to the electrode.

The resistance between two segment exteriors $xraxial$ is set to "infinite" (in reality to a value high enough to have an equivalent effect). This causes V_e for each segment to be isolated from V_e of its neighbors. The values for xc and xr are set to zero. Therefore, V_e is considered to be directly connected to the segment's membrane. The equation determining V_e for each section is as mentioned in chapter 4:

$$V_e = \frac{I\rho_e}{4\pi r}$$

5.3 The Activating Function

As briefly mentioned in chapter 4, under some circumstances the depolarization or hyperpolarization of the membrane under extracellular stimulation can be estimated using the activating function. It was first developed by Rattay (1986) based on a myelinated neuron model by McNeal (1976) and has since been adapted to different applications.

The model describes a neurite divided into cylindrical compartments, which are exposed to an external stimulus. The activating function is then for compartment n

$$f_n = \left(\frac{V_{e,n-1} - V_{e,n}}{R_{n-1}/2 + R_n/2} + \frac{V_{e,n+1} - V_{e,n}}{R_{n+1}/2 + R_n/2} + ... \right) / C_m \tag{5.15}$$

with the membrane capacity C_m and $V_{e,n}$ being the external voltage at the outside of compartment n. R_n is the axial resistance of compartment n.

The dimension of f_n can be V/s or mV/ms. As mentioned, if the activating function is positive, it indicates depolarization, if it is negative it indicates hyperpolarization. If a neuron is stimulated from its resting state, the activating function f_n is equal to the slope of the membrane voltage V_n.

5.4 Model Anatomy

5.4.1 Handling of Coordinates

NEURON allows for more than one way to define the physical dimensions of the neuron in question. One possibility is to define the length and diameter of a section and, if applicable, also the number of segments it is to be divided into. If the neuron consists of more than one section, those segments will be joined together according to the instructions

provided in the model. This simple model works well if the exact position and orientation of the sections don't influence the behavior of the neuron.

Another possibility, which is used in this thesis, is to specify the sections via their location in a three-dimensional coordinate system. For each section, at least two sets of coordinates are needed, one for its beginning and one for its end. If it consists of n segments, n coordinates can be used, each coordinate defining either the ends of the section or the position of inner segments. These coordinates do not need to all be on a straight line, which allows for curved sections.

Independently of which of the two methods was used, the neurite needs to be subdivided into several sections if it is either branching or if the parts have different biophysical properties. Examples for the latter are channel densities or membrane resistivity.

Each set of coordinates can also have its own diameter. By specifying different diameters for the beginning and the end of each section or segment, it can be created as a truncated cone instead of a cylinder. This influences the model insofar as it changes the membrane area. In our case, the three-dimensional coordinates are appropriate. There are two reasons for this. Firstly, the traced dendrites of the model are given as lists of coordinates and diameters. Secondly, in order to be able to use extracellular stimulation, the distance between the electrode and the respective section or segment needs to be known in order to calculate the local intensity.

5.4.2 Soma

In our model the soma is approximated by a spherical section with a rather large diameter compared to the other sections.

Implementation

In the original traced neuron by Mainen et al., the soma had a length of 25.79 μm and a diameter that tapered towards both ends, with a maximum roughly in the middle with about 24 μm. Its total area was 1230.27 μm^2. The distance between the stimulation

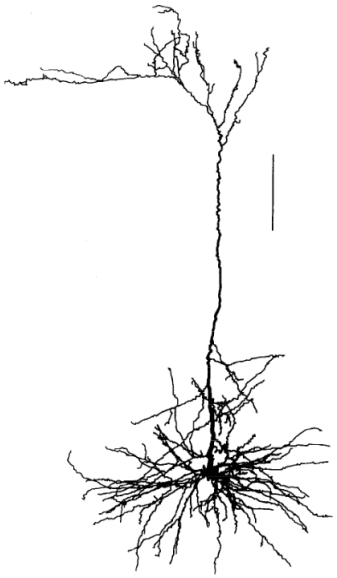

Figure 5.3: *The neuron tracing created by D. K. Smetters and S. Nelson, which was adapted by Mainen et al. (1995) and is the basis for the model in this work. The scale bar to the right has a length of 100 μm. Not pictured is the linear axon which is added in both the model by Mainen and in the model in this thesis. Image from Mainen et al. (1995).*

electrode and the soma (sometimes as little as 10 μm) is thus in the same order of magnitude as the soma's dimensions.

This causes problems with the extracellular mechanisms as implemented in the simulation. Since the xtra mechanism calculates the stimulating electric field for the coordinates of the segment's center, the segment's surface needs to be on the same isopotential surface or close. If this is not the case, the calculated stimulation field will not be representative of the field that is actually present on the surface. Due to its large diameter, the soma cannot easily be subdivided into suitably small segments like more slender sections can.

This is especially problematic since one of the tasks is to investigate upper threshold phenomenon in the soma, which depend sensitively on such potential differences. For some models it would be sufficient that the average field on the membrane is close to or the same as the one calculated in the mechanism. In our case however, the effect is caused by the gradient of the stimulating potential over the section. It is therefore important

that the potential on each point on the membrane doesn't deviate too far from the one in the center of the respective segment (see figure 5.4).

As previously mentioned, Fellner (2017) used a way to orient and divide up the soma that solves this problem. NEURON allows for the soma section to be separated into segments, with the planes dividing it being perpendicular to its main axis. These segments can be made almost arbitrarily thin but there is still the problem of their diameter being non-negligible. This issue can be mitigated by orienting the section in a way that the direction of the biggest decay of the electric field is in the direction of the soma axis. In other words, the axis of the soma needs to point in the direction of the stimulating electrode.

The individual segments are frustra of different diameters that are stacked on top of each other to form a roughtly spherical shape (a schematic image of this can be seen in 5.4, the model as used in this thesis has more segments). The point at the center of each segment (i.e. the point for which the segment's stimulating field will be calculated) lies on the section axis.

The frustra are rotationally symmetric around the soma axis. Since the latter is pointed directly at the electrode, the field on the individual frustra is also rotationally symmetric, meaning that at each height along the axis, the segment border at that height feels the same stimulating field. If the soma is divided up into sufficiently thin slices (a bit less than 1 μm in our model), the field at any point on the segments surface will be roughly the same.

Most of the distance between the segment center and surface points is in a direction perpendicular to the direction of the largest field decay. Thus, the model ensures that the field calculated for the segment center is representative of the actual stimulating field on any point on the segment's membrane.

This simulation requires stimulation from different positions. The ability to realign the soma axis in whatever direction the electrode is currently pointing is therefore part of the

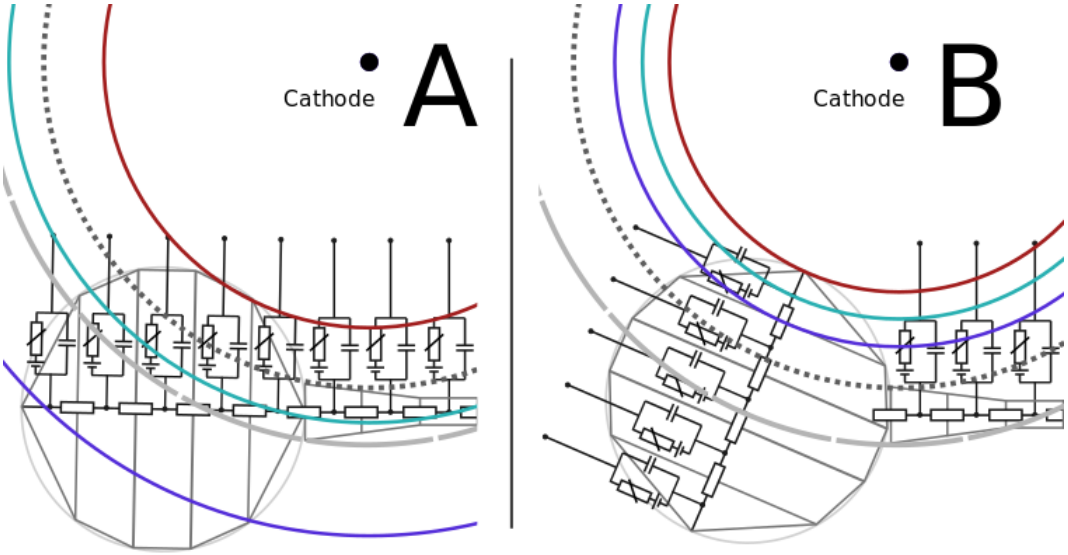

Figure 5.4: *Sketch of a soma and an axon with hillock in a spherical electric field. Both neurites are divided up into segments along the main axes of each section, with circuit elements sketched to indicate the interactions of these compartments with their environment. A) While the soma has been divided up into segments, it is not aligned with the electrode. For the segment closest to the axon, the equipotential lines of the stimulating field are drawn for the point closest (red) and the point farthest (dark blue) from the electrode. The equipotential line at the segment center, for which the stimulating field is calculated by the xtra mechanism is drawn in green. The extracellular potential can be expected to be very different in each of these points. For comparison, the dotted curve is the equipotential circle for the hillock point closest to the electrode, the dashed one is the equipotential circle for the hillock point farthest from the electrode. Even though it is the thickest part of the axon, the potential deviation between those points (and the center of that segment) is much smaller than in the soma segments. B) Here the soma axis points towards the electrode. Again, the red circle is the equipotential line of the point closest, dark blue the equipotential line of the point farthest from the electrode. They are now much closer to each other and the green equipotential line for the segment center, meaning that the potential difference within the segment is now much smaller.*

model. For simplicity's sake, the soma's center was decided to be at the zero position of the three dimensional coordinate system and to rotate around this point to accommodate the electrode's current location.

Since the original soma in the model by Mainen was of irregular shape, it had to be adapted. An important parameter is the soma's area, since the membrane's resistance and

capacitance as well as the conductivity for different ions are calculated from it. Therefore, the area from the model was kept and the spherical soma's diameter (or, translated to NEURON's terms, the section length) calculated from this using the relation $A_S = \pi d_S^2$ between a sphere's diameter d_S and its surface area A_S.

The resulting section has a length of 19.78 μm (after rounding) and consists of 21 segments. Its maximum diameter is 9.89 μm at the section center, decreasing as dictated by the dimensions of the frustra towards each end. The diameter at the very ends should be zero according to this model, but in practice that turns out to be problematic. If the diameter is zero, then the resistance between this end and any section that happens to be connected to it would be infinite, resulting in action potentials not propagating past this junction. This can be resolved without perturbing the rest of the model too much by setting it to a very small nonzero value, such as 0.1 μm, as was done in our model.

The task of positioning the soma correctly relative to the electrode was accomplished by establishing the unit vector pointing from the zero point to the electrode's position. Then the soma's 3D points along the vector were defined so the section had the appropriate length, was centered at the zero point and had the correct number of evenly spaced segments. The discretization of the soma reduced the total surface area somewhat. The area as implemented is ca 1223.78 μm^2 and so about 0.5 % smaller than the area would be if it was a perfect sphere of the same length (1230.27 μm^2). A difference this small should change neither the capacitance nor the membrane conductivity enough to matter.

5.4.3 Dendrites

The dimensions and shapes of the individual dendrites are the same as in the Mainen model. Since the original soma was not centered at the zero point, the dendrites have to be shifted. The dendrite positions relative to each other were also slightly altered, since they now have to accomodate a different soma shape than in the original model. In order to accomplish this task, several steps are necessary.

As the apical dendrite is the most prominent one, it was chosen to serve as a point of reference. The first task was to determine at which 3D point its base should contact

the soma. In nature the apical dendrite emerges from the soma more or less in a radial direction away from the central point of the soma. In order to reproduce this in the model, the first two 3D points of the section connected to the soma were used to establish the direction the dendrite was pointing in. The new point where the apical dendrite emerges from the soma was chosen by taking in account the following two constraints:

- It must be located on the soma surface, i.e. it needs to be at a distance the length of the soma‘s diameter from the coordinate system’s origin.
- The dendrite needs to project from the soma at a 90 degree angle to the surface. This was accomplished by taking the direction of the first dendrite segment and lining it up so it points at the soma‘s center.

After the new first 3D point of the apical dendrite was established this way, the rest of it was shifted so the dendrite retained its shape. The basal dendrites were then moved to retain their distance and orientation relative to the apical dendrite.

While this is sufficient for the apical dendrite, the basal dendrite‘s base points are now closer to the soma, but due to the different shape of the old soma they are still not in contact with the new soma‘s surface. The relatively small remaining corrections were done by conceptually drawing a line between the soma‘s center and the base poins of the individual dendrites. The base points are then moved along this line until they contact the soma‘s surface (see figure 5.5).

As mentioned, this alters the structure somewhat in that the dendrites are now in different positions relative to each other and they also emerge from the soma at somewhat different angles than before. This should not detract from the realism of the simulation too much because dendrite positions and even their number are quite variable in nature. Additionally, their behavior is not expected to have a large influence over the outcomes of the simulation.

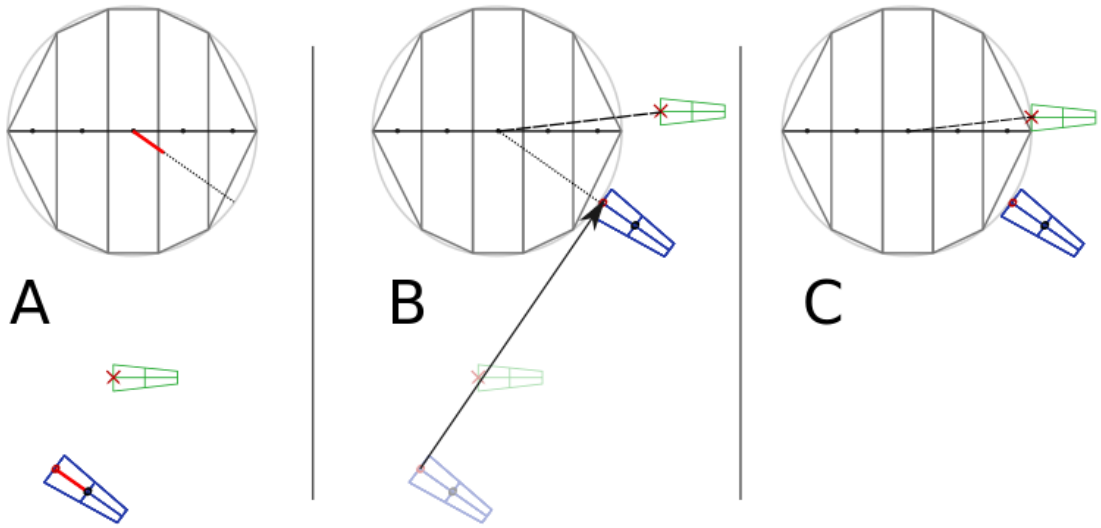

Figure 5.5: *Adjustment of the dendrites to fit the new soma. A) While the dendrites are in their original position according to the model by Mainen, they don't line up with the newly created spherical soma. The first two segments of two dendrites along wth their axes are pictured. The apical dendrite is dark blue and the basal dendrite is green. The axis of the apical dendrite's initial segment (pictured as a red line) is determined by the first two 3D coordinates of the dendrite. This is then used to find the position on the soma's surface that the dendrite needs to emerge from by drawing line parallel to it from the soma's center. B) In the next step, the apical dendrite is moved so it contacts the spherical surface at the point where the radial line determined n the last step intersects it. All other dendrites are moved by the same amount. C) To move the apical dendrites to the soma, a line is drawn from their first 3D point to the soma's center and the dendrites pulled in or pushed out along that line until their base is flush with the sphere's surface.*

Since the soma is not perfectly spherical, its borders will in general not line up perfectly with the dendrite‘s (or axon‘s) base 3D coordinate. As the gap is very small (less than a micrometer in the extreme case) this is not a problem.

It was mentioned in the second chapter that dendrites in the pyramidal cell have small protrusions called spines. Since the model in this thesis consists of a single neuron, the postsynaptic functions of the spines need not be modeled but the additional surface area provided by the spines was accounted for by adding extra area to the dendrites.

5.4.4 Axon

While the model by Mainen does come with the 3D data of the traced axon, the authors themselves discard it in favor of a straight axon. The model in this thesis makes the same choice, since the block effect in the axon is geometry dependent and any shape other than a straight one would needlessly complicate the interpretation of the results.

The hillock has a length of 10 μm and starts out at the soma with a diameter of 4 μm and tapers to 1 μm at the distal end. It is a single section consisting of ten segments. The axon initial segment in this model is 150 μm long, with a diameter of 1 μm and 150 segments.

Following this are are five alternating sections of myelinated axon and nodes of Ranvier, starting with a myelinated section at the end of the axon initial segment. The myelinated sections have a length of 100 μm each and a diameter of 2 μm with no further subdivision into segments (this helps keeping the computational cost low, there is little electrical activity in the myelinated regions themselves). The nodes have a length and diameter of 1 μm and also contain no further subdivisions. The myelinated sections are simulated by setting a very low channel density and membrane capacity (see table 2).

Since the original axon was only defined in terms of length and diameter, it needed to be converted to 3D coordinates in order to function properly with the extracellular mechanism. The first step was to pick a direction for the axon to point in, since this is not specified in the model. Given a real pyramidal cell‘s structure, it should point roughly in the opposite direction of the apical dendrite. Since the dendrite points almost in the same direction as one of the axes in the coordinate system, the negative axis direction was chosen for the axon in order to simplify things. The 3D points for each section were then calculated based on the geometric data listed above.

Hillock Dimensions and Electric Field

The hillock‘s diameter at the base is 4 μm, which is relatively large and may be enough to ensure that the stimulating field at the center of the segment is not representative of the field at its borders. Since the hillock has a higher sodium channel density than the soma,

the error caused by this may have a bigger impact on the accuracy of the simulation than it would have in non-axonal regions.

If it can be established that the potential difference is not very pronounced even in the worst case, it can be assumed to not cause trouble in more usual cases either. The maximum deviation of the membrane's potential from the potential in the segment center can be expected if the electrode is in the plane of the first segment's base. This is the place where the hillock has the largest diameter. If the electrode is in that plane, the potential difference between the closest and furthest membrane points will be maximized.

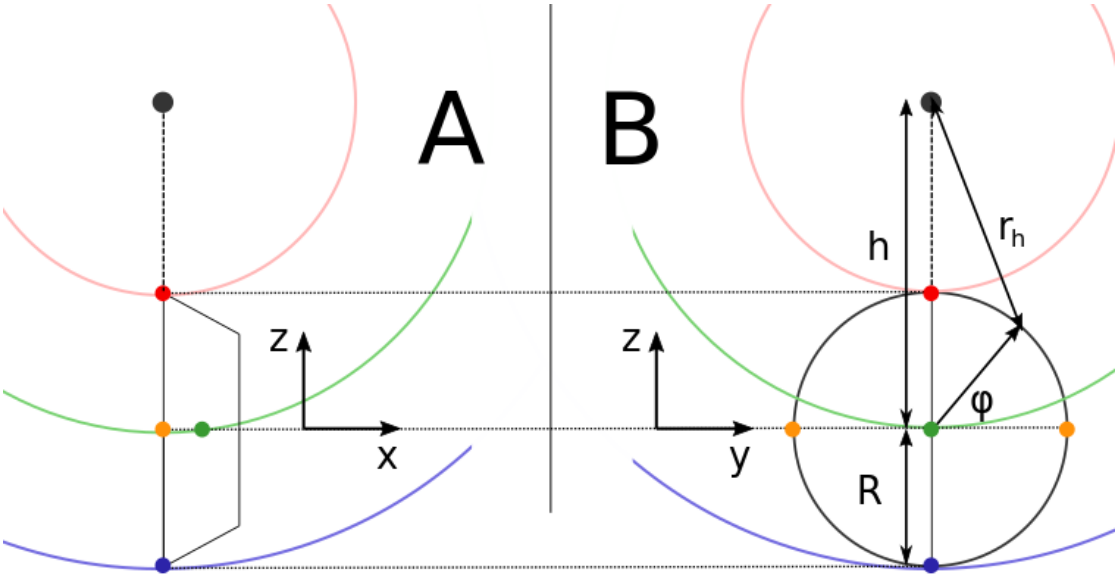

Figure 5.6: *The cone stump forming the first segment of the hillock in an electric field of an electrode (dark grey circle). A) Seen from the side. The red dot is the point on the segment closest to the electrode, the blue dot is the point furthest from it. The green point is the segment center for which the electric field is calculated by the xtra mechanism. The concentric circles are the equipotential lines for the respective points of the same color. B) The plane of the cone stump base with the quantities used to calculate the average membrane potential.*

The electrode is also assumed to be very near to the segment, at just 14.89 μm distance, which is the closest the electrode will get during the experiments. To simplify the calculation, it will not be performed for the whole membrane of the segment, but just in two dimensions for the plane of its base. The membrane is therefore reduced from the mantle of a truncated cone to the circumference of a circle with a radius of 2 μm. The potential

on this circle will deviate the most from the calculated potential so its result can serve as an upper bound for the possible error of other parts of the membrane. The extracellular potential is analogous to 4.1 and clarified in image 5.6:

$$V_e = \frac{I\rho_e 10^4}{4\pi\sqrt{x_m^2 + y_m^2 + (z_m - h)^2}} \tag{5.16}$$

I is the electrode current in mA; ρ_e is the extracellular resistivity in $\Omega\ cm$; x_m, y_m, and z_m are the coordinates at which the potential is to be measured in μm and h is the distance of the electrode from the origin in μm (it is positioned on the z-axis). 10^4 is a correction to reconcile the units on the right side of the equation with those of V_e (mV).

Potential Differences between Selected Points

Of special interest were the points on the membrane closest to (12 o'clock, red in figure 5.6) and furthest from the electrode (6 o'clock, blue), as well as the points at 3 and 9 o'clock (which have the same potential, orange). Their potential was compared to that of the segment center (green), which was -119.99 mV at a stimulation strength of -0.01 mA. As expected, the 12 o'clock point deviated the furthest from the center potential with 133.44 mV (11 % difference). On the 6 o'clock point, the potential was with -109.06 mV about 9 % weaker. The 3 o'clock point hardly deviated with 119.42 mV and less than a percent difference. The absolute values were rounded to the nearest hundreth, the percentage values to the nearest integer.

Average Extracellular Potential

In order to get a representative picture, it is interesting to calculate the average potential on the circle forming the segment border in the base plane. It can be found by integrating the potential function over the circle's boundary and dividing the result by the circumference. For this purpose, it is sensible to switch to polar coordinates. The circumference of the circle is given by $C = 2\pi R$, with R being the radius in μm. With the transformation to polar coordinates and the angle φ in radian measured from the y-axis (as in figure 5.6)

$$y = R\ sin(\varphi) \qquad\qquad z = R\ \cos(\varphi) \tag{5.17}$$

The distance vector $\vec{\mathbf{r}}_{\mathrm{h}}$ of a point located at angle φ on the circle's boundary to the electrode is

$$\vec{\mathbf{r}}_{\mathrm{h}} = \begin{pmatrix} R\ sin(\varphi) \\ R\ \cos(\varphi) - h \end{pmatrix} \tag{5.18}$$

and has a length of

$$|\vec{\mathbf{r}}_{\mathrm{h}}| = \sqrt{R^2 + h^2 - 2Rhsin(\varphi)} \tag{5.19}$$

The average potential $\bar{V}_{\mathrm{e}}$ is then given by

$$\bar{V}_{\mathrm{e}} = \frac{1}{2\pi R} \int_0^{2\pi} \frac{I\rho_e\ 10^4 R}{4\pi\sqrt{R^2 + h^2 - 2Rhsin(\varphi)}} d\varphi \tag{5.20}$$

If the stimulation current is again 0.01 mA, V_{e} is -120.33 when rounded to the next hundreth. This deviates from the segment center potential by about 0.3 %, rounded to the next tenth, which is a negligible difference.

5.4.5 Neurite-Soma Connections

After constructing the soma and neurites, some thought has to be put into connecting them. Generally, sections in NEURON begin at the arc position 0 and end at the position 1. Other positions in between can be accessed via the associated numbers, too (the middle point on the arc would be 0.5). This can for example be used to position electrodes for

internal stimulation or to set a point where another section branches off. If the sections are declared using 3D points, the first 3D point specified defines arc position zero.

When a connection between two sections is declared, one of the two is always the parent. Several child sections can branch off of the same parent, but every child only ever has one parent.

The first question is exactly which position on the soma axis the neurites should be connected to. To simplify things, all of the dendrites are connected to the center of the soma.

The justification for this lies in the soma‘s geometry. As a sphere, it is symmetric and compact, which means that internal potential gradient can relatively easily be equibrilated. Thus, the potential difference between two points within the soma is not that large. The dendrites can therefore all be connected at the 0.5 point of the soma for the sake of simplicity without sacrificing too much precision. Since the axon has a much larger influence on the bioelectric behavior of the system, a more finely grained approach was chosen.

The desired outcome was for the axon to be connected to whichever segment its first 3D point is currently in contact with. The segment borders in the 3D model are made up by planes perpendicular to the soma axis. The point on the axis that the axon should be connected to is therefore defined by a line that emerges at a 90 degree angle from the soma‘s axis and contains the first 3D point of the axon. In other words, the axon‘s first set of coordinates needs to be projected onto the soma‘s axis.

In order to do that, the unit vector in direction of the current electrode position was calculated. The inner product between this vector and the vector to the first 3D point of the axon was formed. This results in a number between – 9.89 (if the first axon point happens to be right on to the 0 end of the soma) and 9.89 (if it happens to be next to the 1 point).

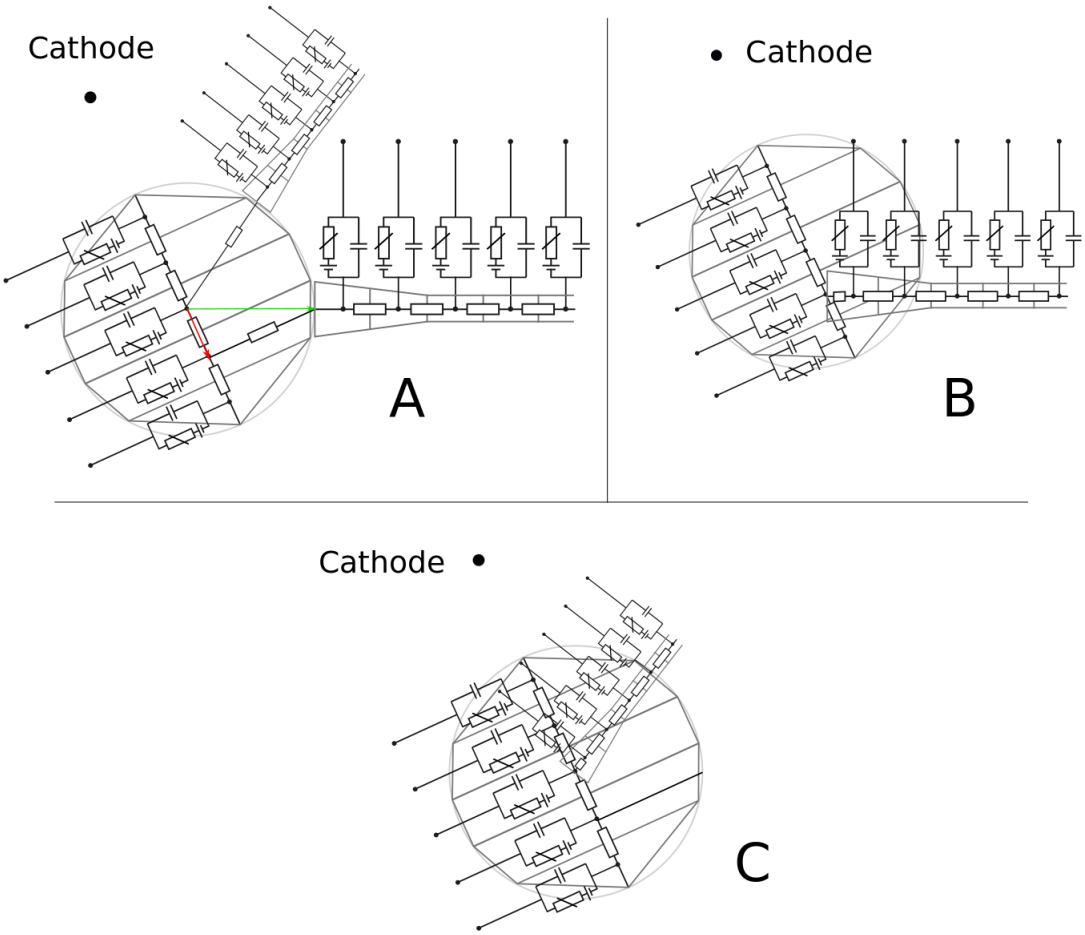

Figure 5.7: *Connecting neurites to the soma. A) Pictured are a schematic view of the soma, the axon (protruding towards the east) and a dendrite, with the latter two beginning at the soma's edge. This is the desired configuration for the extracellular mechanism. The dendrite is connected to the center, calculating the soma's connecting point involves projecting the position vector (green) of its first 3D coordinate onto the soma's axis, resulting in the red vector. B) Connecting the sections in NEURON results in the axon's base being located at the position on the soma's axis it is connected to. C) The same is true for the dendrites, all of which now start at the soma's 0.5 arc position (which is also the origin of the coordinate system).*

Since the arc length of a section in NEURON is defined by numbers between 0 and 1 instead of - 9.89 and + 9.89, our result has to be converted to this format. This was accomplished by adding 9.89 to it and dividing it by the soma‘s length (19.78 μm). This is finally the arc position on the soma‘s axis that the beginning of the axon should be connected to.

When NEURON joins two sections, it spatially moves the connecting end of the child‘s section to whichever point on the axis of the parent‘s section it is attached to. This holds true even if the child had previously been defined by different 3D points. As an example: if one of the dendrites in the model gets connected to the 0.5 arc position of the soma (which is at the 0 point in the coordinate system), the first point of the dendrite would now likewise be at the 0 position and its other points be shifted accordingly. This does not change the dendrites total dimensions or subdivision into segments.

Usually, this would be fine, in the model in this thesis however there is a snag. The soma is a section with a large diameter, meaning that the points at a given segment‘s surface are sometimes at a relatively large distance from the segment‘s axis. If a dendrite or the axon happens to be connected to this segment, its position would be shifted by this distance. Without correction, the extracellular and xtra mechanisms would use these coordinates to determine the stimulating field. In an extreme case (the neurite is connected to the middle part of the soma), there would be nearly a 10 μm discrepancy between the two positions, which is inacceptably large.

As Fellner established in his thesis, this means a way must be found to hand the spatial coordinates determined by the user to the mechanisms governing the extracellular interactions and to use another set for the neurite connections. In this model, that was accomplished by making sure the program follows three steps in sequence:

- Generate the true 3D coordinates for each section as discussed.
- Pass those coordinates to the parts of the program that handle the extracellular stimulation, followed by the calculation of the extracellular resistances for each segment.
- Only then trigger the shift of the child section‘s coordinates according to their new connections.

5.5 Electrophysiological Property Overview

Different regions in the neuron have different types and densities of channels as well as other characteristics. The following table gives a summary of the relevant mechanisms and distributions.

Property and (Unit)	Soma	Axon	Dendrites	Nodes	Myelinated
Passive Conductance g_{pas} ($\frac{mS}{cm^2}$)	0.05	0.05	0.05	20	0.05
Membrane Specific Capacitance C_{m} ($\frac{\mu F}{cm^2}$)	0.5	0.5	0.5	0.5	0.02
Cytoplasmic Resistivity Ra ($\Omega\ cm$)	150	150	150	150	150
Sodium Reversal Potential V_{Na} (mV)	60	60	60	60	60
$Na_v1.2$ Conductance ($\frac{S}{cm^2}$)	80	1000	80	-	20
$Na_v1.6$ Conductance ($\frac{S}{cm^2}$)	-	3000	-	1500	-
Potassium Reversal Potential V_K (mV)	-90	-90	-90	-90	-90
K_v Conductance ($\frac{S}{cm^2}$)	20	1000	10	-	-
K_m Conductance ($\frac{S}{cm^2}$)	0.3	-	0.3	-	-
K_{Ca} Conductance ($\frac{S}{cm^2}$)	3	-	3	-	-
Calcium Reversal Potential V_{Ca} (mV)	140	140	140	140	140
Ca_v Conductance ($\frac{S}{cm^2}$)	0.3	-	0.3	-	-

Table 2: Values for electrophysiological properties of the neuron. Not listed is the extracellular resistivity, which has the value 300 $\Omega\ cm$.

5.6 Hypotheses and Predictions

The previous parts of the thesis gave an outline of the problem and the methods chosen to investigate it. Based on this, some predictions can be made about the behavior of the model under different circumstances. This helps in finding the right questions to ask for creating a proper understanding of the system and also in identifying causes in case the outcome deviates from expectations. It also documents the knowledge before the experiment and allows it to be contrastable with the results.

During the application of a cathodic pulse, the soma is expected to display a depolarized pole near the electrode and a hyperpolarized pole on the far side. Sodium currents in any significant intensity should only occur on the depolarized side during stimulation, since the channels on the other side remain deactivated. If current reversal occurs with rising stimulation intensities, the segment closest to the electrode should be the first one to experience it, followed by the more distant depolarized ones in turn.

It is necessary for the formation of an action potential that enough sodium channels are permeable, i.e. neither deactivated nor inactivated. They are deactivated if the membrane potential is too low and inactivated shortly after activation or for a very high membrane voltage. In addition, the membrane potential must be favorable, i.e. not high enough not to trigger current reversal.

As elaborated on in earlier chapters, the slender sections should react to extracellular stimulation with a depolarized region near the electrode and hyperpolarized regions a bit further away. This heuristic is expected to work reasonably well for straight neurites, but for curved ones (i.e. dendrites) the behavior is hard to predict and expected to deviate from this.

Due to its geometry, the soma should be harder to stimulate than an individual dendrite, which in turn should be less excitable than the initial segment of the axon due to different ion channels. When these regions are connected to each other, it is not clear exactly what will happen due to their interference with each other. Especially the soma should have

a high influence at least on the near sections of the connected neurites and cause their potential to be closer to its own.

When only an axon is connected to the soma, the lower threshold for this system will likely be lower than it would be with just the soma. If the electrode is equidistant from both, the stimulation is more likely to be initiated in the more sensitive axon rather than the soma. Even if the axon is excited, the action potential might not necessarily spread to the soma. There are several possible reasons for this.

- Sodium current reversal and hyperpolarization of the soma in its wake.
- Inactivation of sodium channels due to high membrane voltages or previous activation.
- Anodal surround block in the axon, especially if the electrode is positioned in such a way that the hyperpolarized region starts near enough to the soma that it is not clear that the action potential stopped before it even reaches the soma. It should be possible to catch this by observing how far from the electrode the hyperpolarization usually starts and see if this is a possible cause.
- A lack of action potential backpropagation that is not due to any of the previously mentioned block causes. Hu et al. (2009) mention that sometimes the action potential does not make the jump from the axon to the soma during intracellular stimulation, which is something that cannot be explained by either surround block or current reversal. Since theirs is the model the ion channels were taken from, this might be a concern here, too. According to the paper, the effect depended strongly on the membrane potential in the soma as well as the density of $Na_v1.2$ channels in the axon initial segment. The higher the value of both of them, the likelier was the backpropagation. This effect will have to be investigated as a cause for a lack of propagation, which can be done by applying intracellular stimulation to the axon.

The influence of the dendrites on excitement of the neuron is somewhat harder to guess and likely geometry dependent. They might induce or help the formation of an action

potential, but they might also act inhibiting because ion buildups that might otherwise contribute to action potentials in the soma might escape into them. When the electrode is near the soma, thin distal dendrites might be close to it and therefore make a large contribution to action potential formation. The excitability of the cell could thus be rather unpredictable even for comparable electrode distances to the main neurites (soma, axon, apical dendrite).

It is not clear whether an action potential can be invoked at all for any individual experimental geometry. If stimulation is possible, there will probably be an upper current threshold as well beyond which the cell or part of the cell can no longer be excited. As with the lower threshold, this limit will likely depend on the stimulation intensity and duration.

The exact reason for the block are probably different for different places in the neuron. As mentioned, a surround block should be recognizable by an excitable region in between hyperpolarized ones that prevent the action potential from traveling and is the likely cause of blocks in slender neurites. In the case of sodium current reversal, no action potential should be able to arise in the first place and the membrane potential should be at or at least close to the Nernst potential for sodium. If it is above, the current should reverse, if it is slightly below, too little current might flow inward to allow excitation.

6. Results

6.1 Soma

The full pyramidal neuron is very complex due to its shape and region-dependent biomechanical properties. There are many factors contributing to the reaction of the cell to stimulation, which can sometimes make it hard to determine the exact mechanisms involved in shaping its behavior. It is therefore a good idea to start out with a simple model consisting of just the soma. It was chosen for several reasons. Its nonstandard shape might lead to surprising behavior and has until now not been investigated with the channels used in this model. The sodium current reversal block, which is not well understood, occurs in this section. The soma also connects to all other parts and therefore directly influences them and can transfer action potentials from one neurite to the others.

6.1.1 Passive Behavior

Previously in this work, it was asserted that the potential within the soma equilibrate very quickly after an extracellular potential is applied. Since the membrane potential depends on the intracellular potential, this influences the formation of action potentials. it also affects few other things in the model, such as the question whether it is justified to connect the dendrites to the center of the soma. It is thus worth verifying whether the potential equalization is indeed fast compared to other processes.

In order to analyze the sphere without distortions, this model does not contain any channels (that includes the leakage channel and the internal calcium concentration mechanism). No ionic current can therefore pass between the inside and the outside of the cell. The soma retains its membrane capacitance and its intracellular conductance. While channels generally either don't react fast enough or, in the case of passive channels, don't have a high enough conductance to greatly influence the membrane potential at a small timescale, it is still prudent to eliminate all possible sources of distortion.

The standard time step used in the simulations for this thesis is 0.01 ms. This is generally acceptable for analyzing the spread of action potentials, for processes as short as potential equilibration this is close to the timescale of the effects we want to observe. Therefore, a finer time resolution of 0.01 μs was tried to observe the effect in detail. Later, we returned to the original time step length to see how it played out under usual simulation conditions.

Since 10 μm is a recurring electrode distance in this work, it is chosen for this task as well. The current is set to -0.01 mA, which is a plausible setting for stimulation at that distance (this will be tested in later experiments). The duration was set to a few ms, the exact value is not important since the effect to be observed takes place at the very beginning of the stimulation and at much smaller timescales. NEURON's GUI allows certain cell parameters such as membrane voltage, ion currents and many others to be recorded for each segment and to be displayed in charts if needed. In this experiment, the membrane voltage V_{m} and extracellular potential V_e for each segment was saved and the internal potential V_i calculated with the equation $V_e + V_m$. When the internal potential or equivalently, the membrane voltage stopped changing over time and all segments were at the same internal potential, the cell was equilibrated.

The time it took the system to equilibrate for the step size 1 ns[1] was ca 0.45 - 0.5 μs (see figure 6.1. For the step size 0.01 ms, the internal potential was equalized after 0.02 ms, with most of it happening during the initial 0.01 ms. This is much longer than it took for the first simulation. The reason is that this time step is too large for the differential equation solver to generate accurate results.

After 0.01 ms, the system has jumped from the resting state to nearly equipotentiality on the inside of the soma. It takes another 0.01 ms increment for it to fully settle (this is not visible in image B of chart 6.1 because it is a very small change). This discrepancy is not expected to have any consequences for the model since the end state is the same (see figure 6.1).

[1]This turned out to result in a smoother curve than 0.01 μs and was thus chosen instead.

Fellner (2017) reports that in his model[2] the time for equilibration even for a small step size was 1.5 - 2 μs, which is about three times as long as in our model. The cytoplasmic resistivity (300 $\Omega\ cm$) and the specific membrane capacitance 1 $\mu F/cm^2$ in his model were twice as high as in ours, therefore the simulation with a step size of 1 ns was run again with these two values changed . The resulting equilibration time was around 1.75 μs.

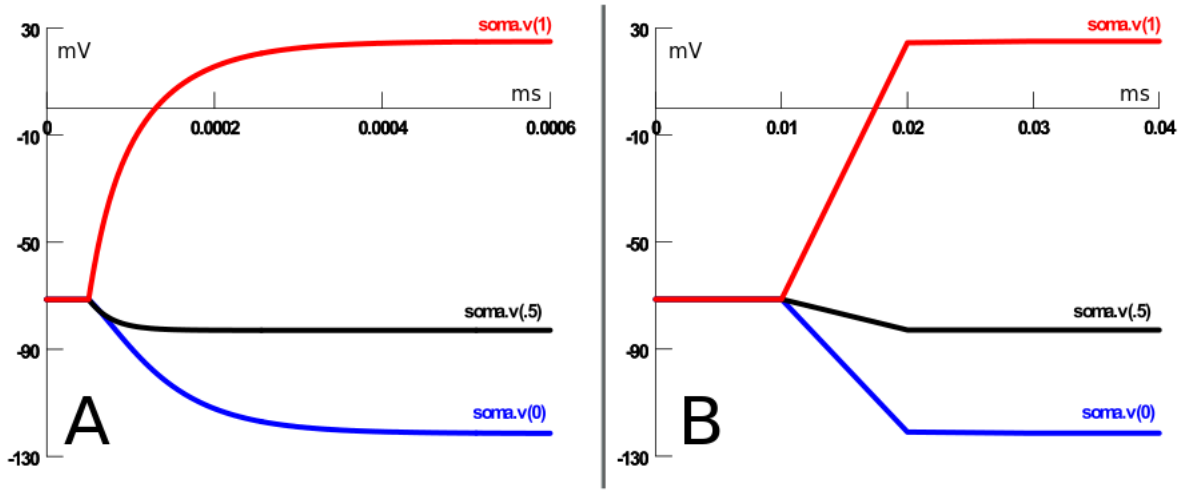

Figure 6.1: *Membrane Voltage over time curves for selected points in the soma. The numbers in parentheses indicate the arc length at which the curve is measured. 1 is at the pole closest to the electrode, 0 is at the pole farthest and 0.5 is in the segment in the center. The curves for all other segments look similar and lie in between the 1 and 0 traces. A) The step size here was 1 ns, with a stimulation start at 50 ns. B) Similar curves at a step size of 0.01 ms (as is usual during the experiments).*

To be able to better judge the extent of the hyper- and depolarized parts of the soma, it is interesting where on the soma the line between these two poles falls, i.e. in which segment the membrane voltage of the passive soma remains closest to the resting potential after the beginning of stimulation. Since the soma by default only has 21 segments, testing this with the original model would not yield a very detailed picture. For this experiment, the number of segments is therefore increased to 101. Several different electrode distances between 4 and 90.11 μm from the soma were tested and the arc position on the soma's axis that was closest to the resting potential recorded for each (see figure 6.4).

[2]Which has a comparable configuration, with a soma diameter of 20 μm, an electrode distance of 15 μm and a stimulus strength of -1 μA.

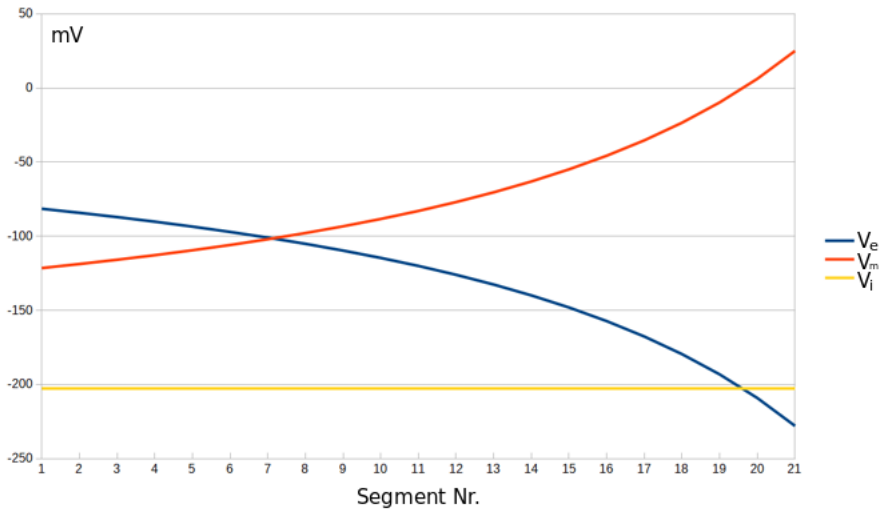

Figure 6.2: *V_e, V_m and the resulting V_i after equilibration for all segments. Segment 1 is at the pole far from the electrode and segment 21 is at the near pole. The internal potential is constant, which together with the potential differences of the external field results in a strong membrane potential gradient over the section. This chart displays voltages at 0.03 ms after stimulation start, using the larger timestep of 0.01 ms.*

This change over distance is due to the potential gradient being stronger closer to the electrode. If the soma is near the electrode, a larger percentage of the total potential drop over its length happens in the electrode-near part. The internal potential is constant over space and the average membrane potential always stays the same, which is true as long as no charge passes through the membrane. Due to the relation $V_\mathrm{m} = V_\mathrm{i} - V_\mathrm{e}$, this means that a higher percentage of the membrane potential rise over length will also occur in the part closer to the electrode. The result is a shift of the point where V_m is equal to the resting potential towards the electrode-near pole for smaller stimulation distances.

6.1.2 Active Behavior

Voltage Drift Correction

As in the model by Hu et al. (2009), the initial membrane voltage for the neuron was set to an uniform -70 mV. In practice, this led to a slight drift of the voltage from that original value towards one that was somewhat lower (In general somewhere between -71 and -75 mV), with the exact value depending on the neurites present. The reason is that the initial membrane potential set by the user in NEURON often doesn't not coincide

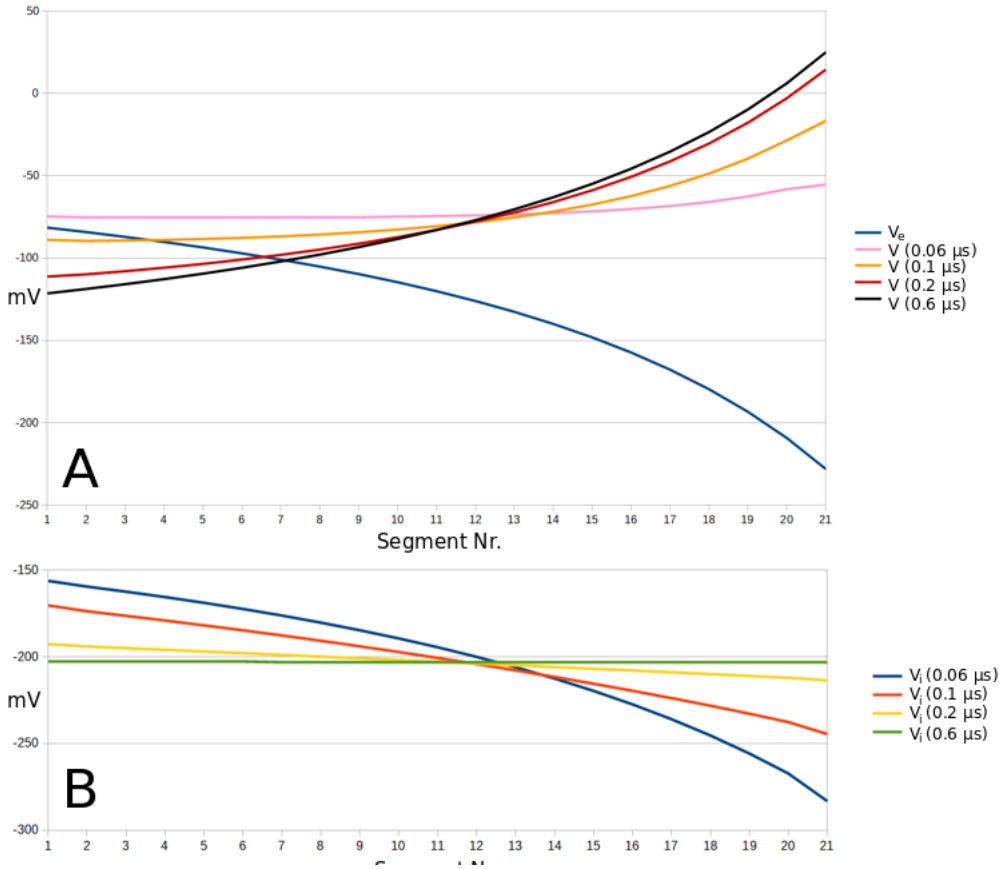

Figure 6.3: *Stimulation with a smaller timestep enables observation of the system during equalization. Image A) shows the (constant for all times) extracellular potential in blue and the adjusting membrane voltages at different times. The stimulating current was initiated at 0.06 μs. The membrane voltage adjusts over time starting from a constant value over the segments. B) Change of the internal potential over time towards equilibrium.*

with the steady state potential of the neuron, which among other factors leads to the aforementioned drift until the system has settled. In order to speed up this process, for each model the individual resting potential was determined by running a simulation without stimulation until it reached steady state. The resulting voltage was recorded and used as new initial value for all following simulations with that model.

Short Range Stimulation

The purpose of replacing the original soma with a spherical model was to enable stimulation closer to the soma than was previously possible. Therefore, in the next experiment, the electrode was set at a distance of 10 μm from the soma. The goal was to find out

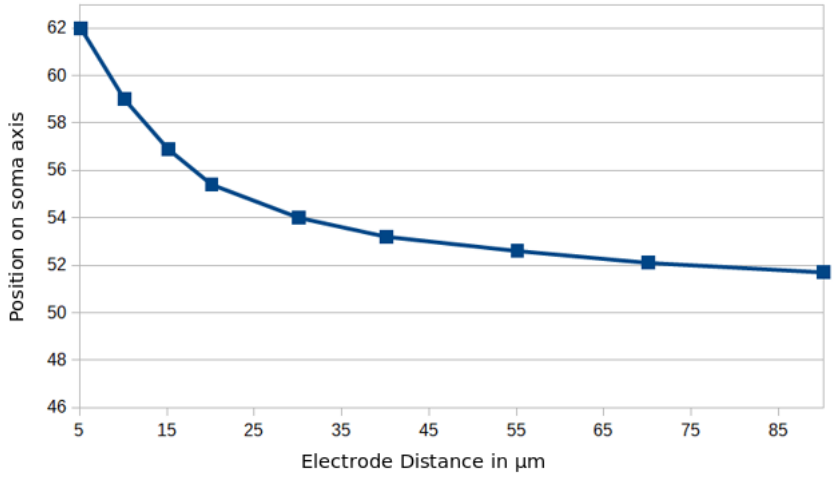

Figure 6.4: *The position along the soma's axis in percent (0 being at the electrode-far and 100 being at the electrode-near pole) where the membrane potential is around the resting potential. This is complementary to chart 6.2, where the second datapoint on this chart should correspond to the point in 6.2 where V_m is equal to the resting potential. Of course, this is not quite correct because the simulations were run with different numbers of segments but the general picture is similar.*

whether an action potential can be induced at that distance, what the upper and lower thresholds are (if any) and if an upper threshold can be detected, if the cause can be determined.

The lowest stimulation duration for which an action potential could be induced was 0.3 ms. This is a relatively long time, slender neurites can generally be excited with pulses of 0.1 ms and less. Starting with 0.3 ms, several stimulation intensities were investigated, and their upper and lower thresholds recorded (see figure 6.5). The figure documents the inability of the soma to become excited at lower stimulation times.

This leaves the question about the cause of the upper threshold. One candidate is sodium current reversal as proposed by Boinagrov et al. (2012). This seems plausible because at this stimulation distance the electrode-near pole is particularly close to the electrode. It might therefore have a high enough membrane potential to experience current reversal even at relatively low stimulation intensities.

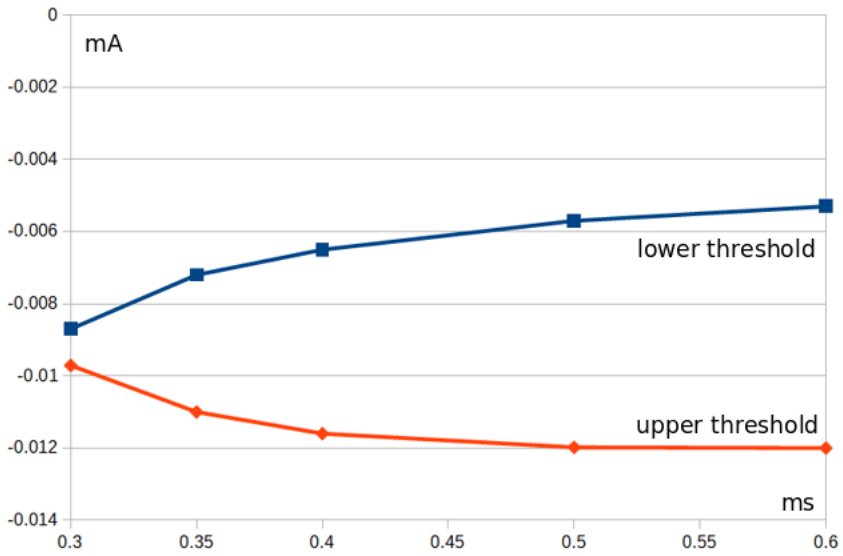

Figure 6.5: *Strength-Duration chart for a distance of 10 µm, with the duration on the x-axis and the stimulation current on the y-axis. The stimulation window widens as duration increases.*

NEURON allows for the recording of sodium membrane currents for each segment and each time step. If reversal is indeed responsible, net sodium currents out of the cell might be observable, either in individual segments or the soma as a whole. If the stimulation intensity is high but does not quite reach the reversal potential, the sodium current flowing into the cell might still be diminished. This could in turn mean reduce the soma's ability to form an action potential. Since this is still part of the same phenomenon that causes current reversal only in a milder form, the absence of sodium current outflow doesn't necessarily mean that the upper threshold has a completely unrelated cause.

In the last chapter, equation 6.2 for the total sodium conductivity across the membrane was introduced as

$$g_{\mathrm{Na}} = t_{adjust}\ \bar{g}_{\mathrm{Na}}\ m^3 h (V_m - V_{Na})$$

This shows the influence of the values of the gating factors m for activation and h for inactivation on the sodium current flow and therefore the formation of the action potenital. Both can have values from zero to one. Neuron allows these factors to be displayed during simulation, which can help in evaluating whether an action potential is inhibited due to low values of either (i.e. either activation of too few channels or inactivation of too many).

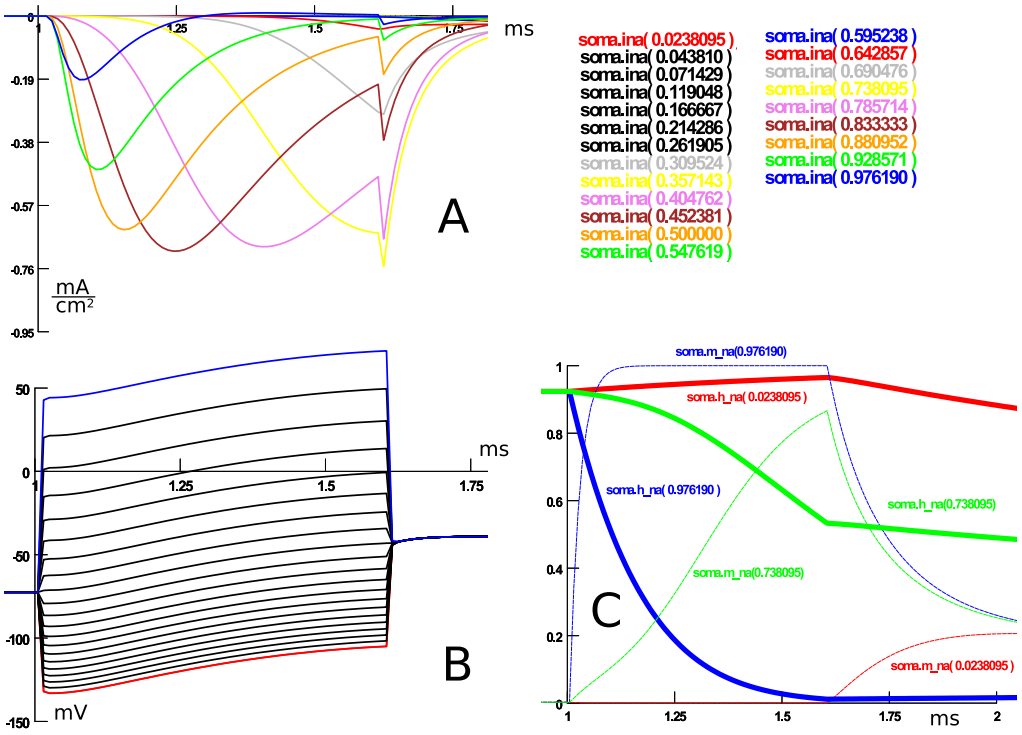

Figure 6.6: *Stimulation at 10 µm distance from the soma and with a stimulation time of 0.6 ms starting 1 ms after simulation start. The stimulation intensity is* -0.0121 *mA, which is just above the upper threshold. All x-axes have the dimension of time in ms. The x-axis is shifted so it starts out at* $t = 1$ *ms. A) Sodium currents for all different segments of the soma. The legend to the right starts with the segment furthest from the electrode and lists the one closest last. Only the traces of the 8 segments closest to the electrode can be distinguished well in this image. B) Membrane voltages for all segments. The blue trace belongs to the electrode-nearest segment, the red one to the farthest. C) Activating (thin lines) and inactivating (bold lines) factors over time for the electrode-nearest (blue), the electrode-farthest (red) and the sixth closest segment to the electrode (green).*

Figures 6.6, 6.7 and 6.8 give an impression of the processes in the cell during stimulation and shortly thereafter. After the stimulation begins, the segments rapidly adjust to their new membrane voltages, as happened in the passive sphere. The voltages then continue to rise as the sodium channels in segments on the positive pole of the soma (near the electrode) open. This is also visible in the gating diagrams, where the activation factors rise for the segments in the depolarized part. The hyperpolarized pole's channels do not activate.

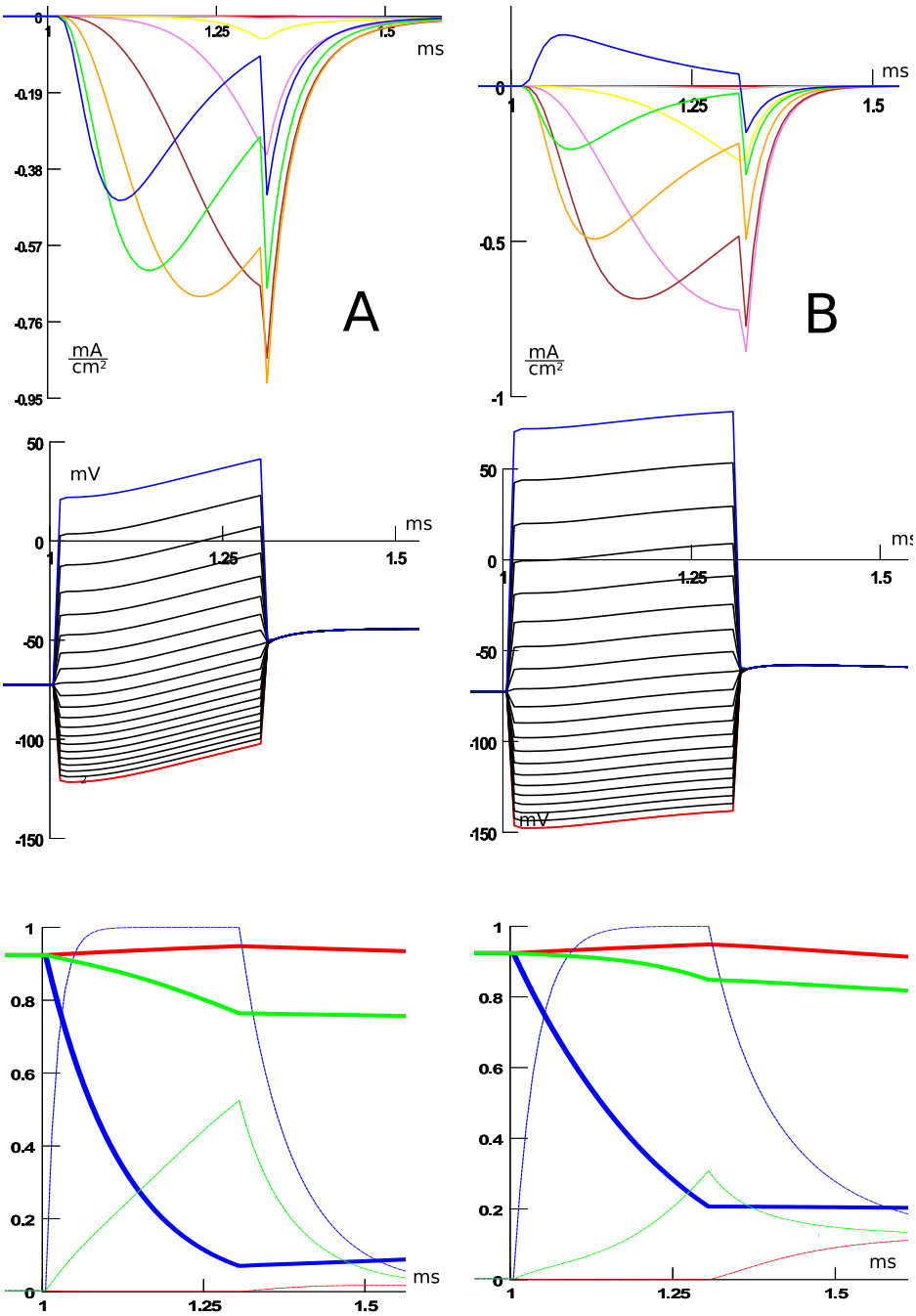

Figure 6.7: *Charts equivalent to figure 6.6 for a stimulation time of 0.3 ms. A) Stimulation at an intensity of -0.00972 mA, which is just above the upper threshold. B) Stimulation at a much stronger intensity of -0.015 mA to clearly show current reversal.*

This leads to increased currents in the segments concerned. The direction of the currents depends on the membrane potential. If it is lower than the Nernst potential, sodium moves into the cell, if it is higher, the opposite happens. The segments that experience significant

current flow show individually different behavior. The electrode-nearest segment shows an early activation and peak due to the higher voltage and therefore faster opening of the channels. Its peak is also lower, the reason for this is partially a faster drop of the inactivation factor, since the inactivation is not only time but also voltage dependent (the higher the voltage, the faster the inactivation). Another reason, especially in figure 6.6 is that the net positive charge streaming into the soma raises the membrane voltage in some segments near or above the Nernst potential (if one looks very closely, the current of the most depolarized segment changes from incoming to outgoing during the stimulation time). In case of strong stimulation (figure 6.7 B), the membrane voltage is high enough from the start to cause current reversal, which also decreases over time due to inactivation. If the stimulation intensity is increased further, more and more segments in the depolarized part will show current reversal until there is an outgoing net current for the whole soma. Going even further, it is possible to induce current reversal in each individual depolarized segment. Both cases require a large stimulation amplitude far above the upper threshold.

When the stimulating current is turned off, the membrane voltages collapse to a common value again, which is somewhat higher than the resting potential due to the inward current during stimulation (see for example figure 6.8, top). The activation factors of the previously depolarized regions fall again due to the decreasing membrane potential. For the hyperpolarized region, m rises now since after equilibration its membrane potential is now much higher than during the stimulation. If this happens in the stimulation window, the activation factors for all sections will rise simultaneously, causing an action potential. If the action potential happens during short stimulation, the channels on the formerly hyperpolarized side of the soma will experience most of the sodium influx since their inactivation factor has not decreased during stimulation (figure 6.8, mid). For long stimulations (longer than it takes for the action potential to form), their contribution is smaller since their membrane potential remains lower than in other sections during the action potential (which now occurs during stimulation), with a corresponding lower activation factor.

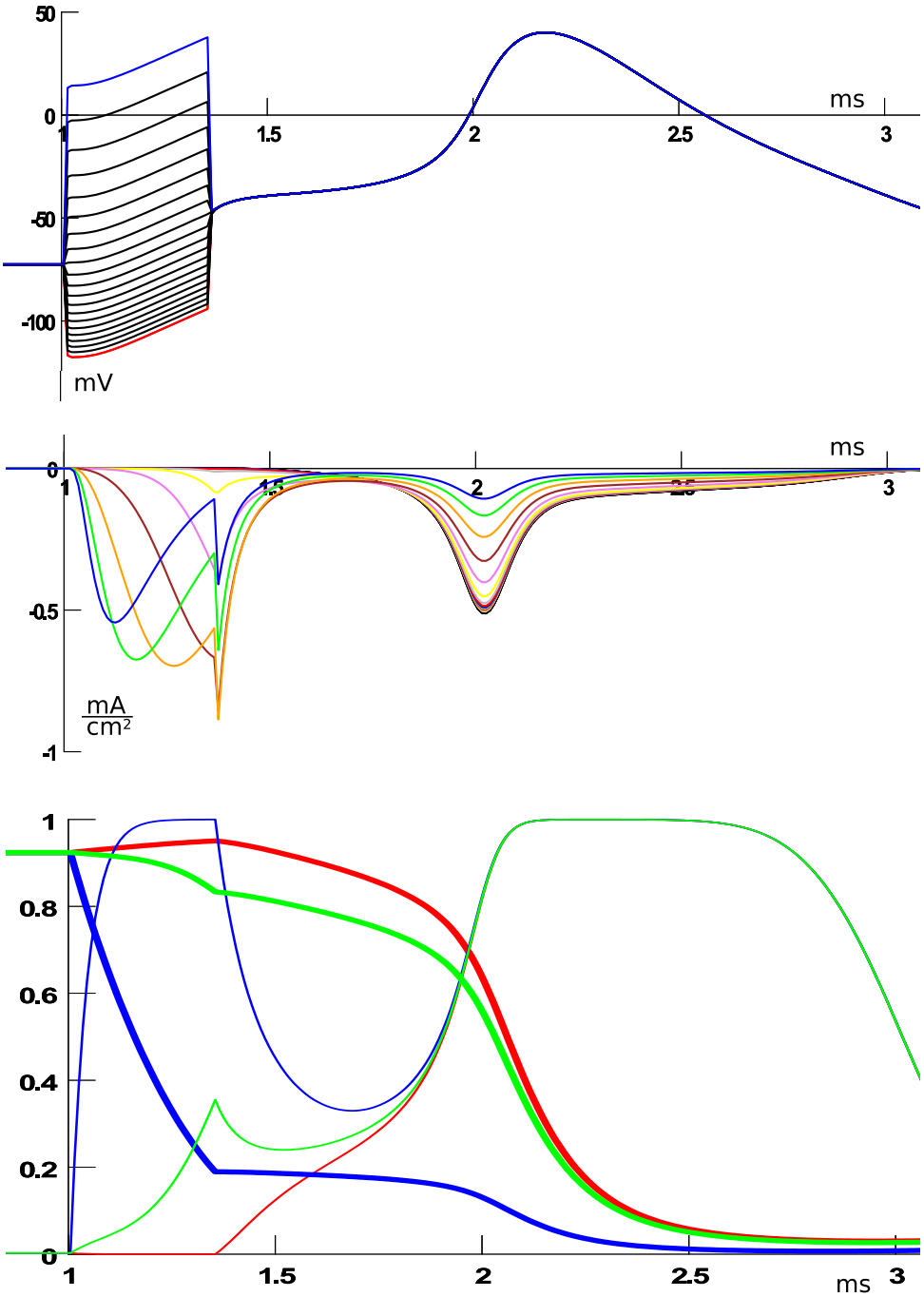

Figure 6.8: *Stimulation with a duration of 0.3 ms and an amplitude of 0.009 mA, inducing an action potential. Charts and legend similar to figure 6.6.*

In lower stimulation time ranges, none of the sections experience current reversal at or even somewhat above the upper threshold (figure 6.8, top). For longer durations, slight

sodium outflow can be measured in the later part of the stimulation time for the most depolarized segment. Even in this case, there is clearly a net current flowing into the cell (figure 6.6).

For this model, a net sodium current into the soma can therefore be ruled out as a cause for the upper threshold. For lower stimulation durations, even partial current reversal cannot be responsible. It is plausible that the decrease in ion inflow or even slight reversal of currents at higher stimulation times contributes to the inhibition of action potentials due to the reduced total charge that is present after the stimulation in such a case, but this is certainly not the only factor or even the main one for short stimulation durations.

Stimulation at a Distance

To better evaluate the influence of electrode position on the excitability of the soma, several stimulation distances were tried and the upper and lower threshold for each recorded. This might be important later on when experimenting with neurons consisting of multiple sections to determine whether an action potential can arise in the soma and whether the upper threshold effect is responsible for a block.

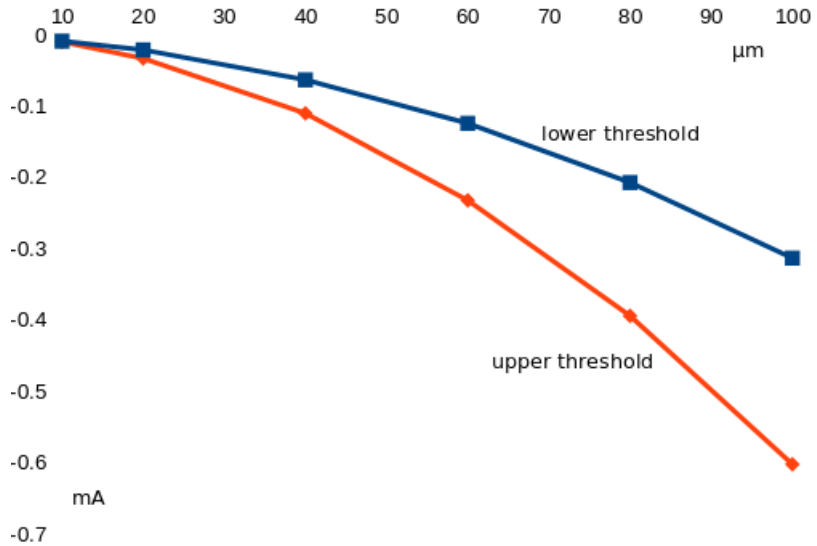

Figure 6.9: *Stimulation strength over electrode distance from the soma.*

While both thresholds go up with distance, the upper threshold rises faster than the lower one. This leads to a widening of the stimulation window for higher distances. The stimulation was performed at a duration of 0.3 ms for all cases for consistency.

6.2 Temperature Adjustment

As mentioned before, most of the ion channel mechanisms contain a temperature adjustment t_{adjust} which is multiplied with the term determining the maximum conductance for each ion channel type concerned. Using the example of a sodium channel, the resulting equation has the following shape.

$$g_{\mathrm{Na}} = t_{adjust}\ \bar{g}_{\mathrm{Na}}\ m^3 h(V_m - V_{Na})$$

This means that the effect of the temperature in this model is accounted for by a change in ion channel conductivity. The actual influence on ion channels is somewhat more complex than that. Importantly, it is affecting the gating variables as well. In some models it is added as a mulitplicative factor to the right sides of the rate equations. This is pictured here using the differential equation governing the sodium channel activation variable as an example

$$\frac{dm}{dt} = (\alpha_m(V_m)(1-m) - \beta_m(V_m)m)k$$

The parameter k is responsible for the temperature adjustment. It can be calculated in several ways, one possibility is to set $k = Q_{10}^{T_{mod}-T_0}$, with T_{mod} being the temperature during the simulation and T_0 the temperature the channels were recorded at in Celsius. The equation is structurally equivalent to equation 5.8 which is used for this model, but it is inserted at a different place in the Hodgkin-Huxley equations. The important thing is that k accounts for the change in the time it takes for the ion channels to react and activate or inactivate and does not simply act as a static change in the ion channel conductivity. The effect of adjustment to higher temperature for a model like this is accelerated gating, a shorter spike duration and faster propagation of the action potential. (Rattay, 1990) This might not be the case for the model used in this thesis. It is interesting what exactly the effect of temperature change is compared to the original 23 °C. For that purpose,

the simulation was done for both temperatures and the results compared. Measurements were taken for the soma to see the effects on this rather specific structure and once on the axon to see whether the propagation speed changes.

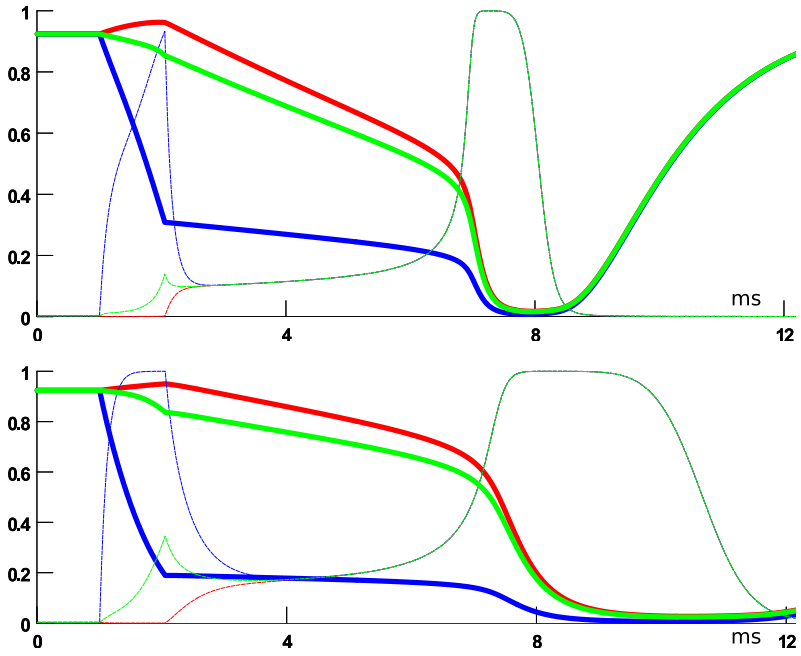

Figure 6.10: *Gating variable values for the soma during high temperature (top) and low temperature (bottom) stimulation.*

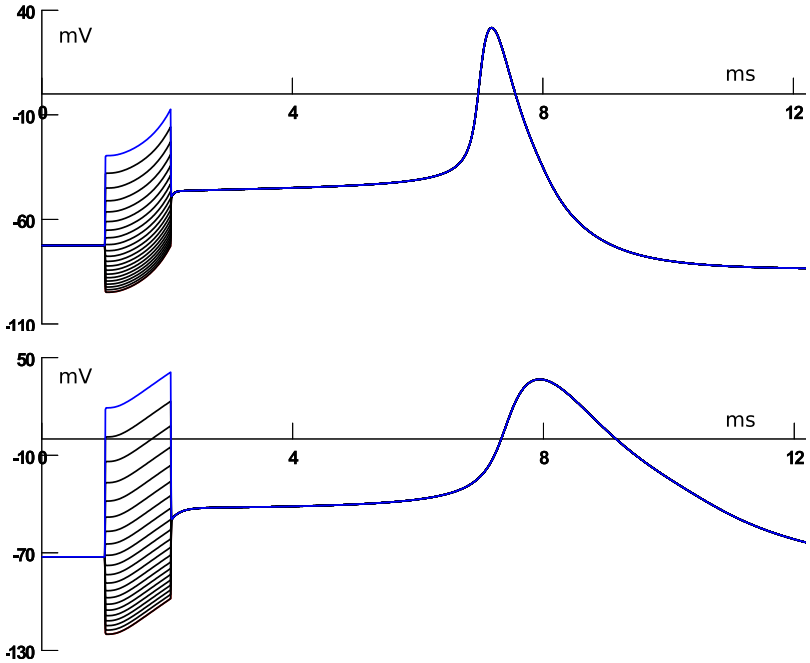

Figure 6.11: *Voltage values for the soma during high temperature (top) and low temperature (bottom) stimulation.*

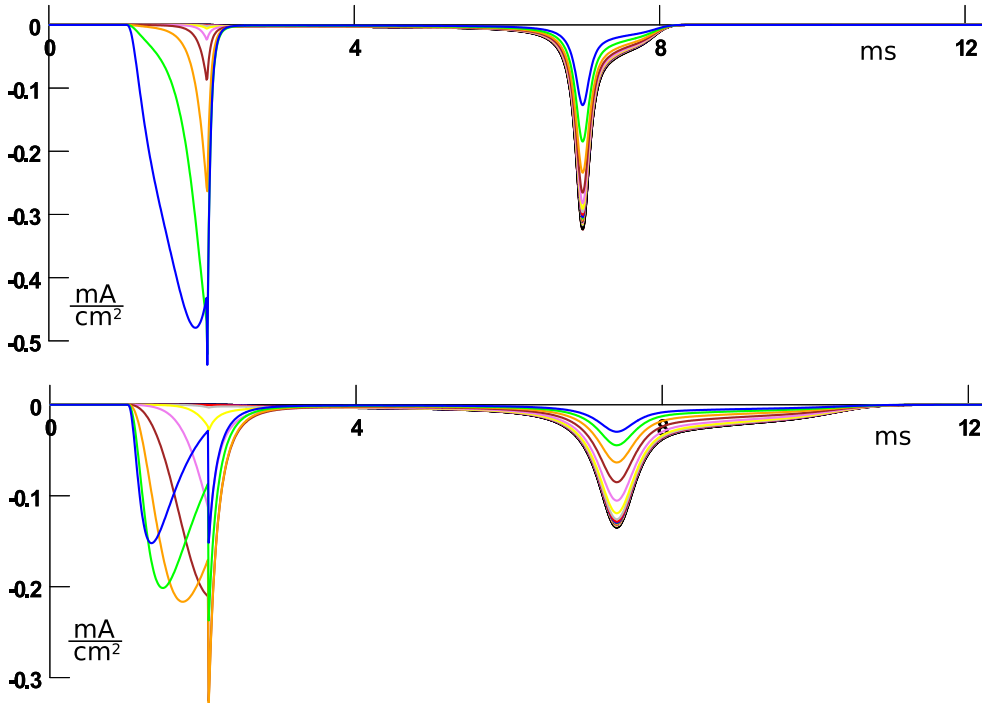

Figure 6.12: *Current flows for the soma during high temperature (top) and low temperature (bottom) stimulation.*

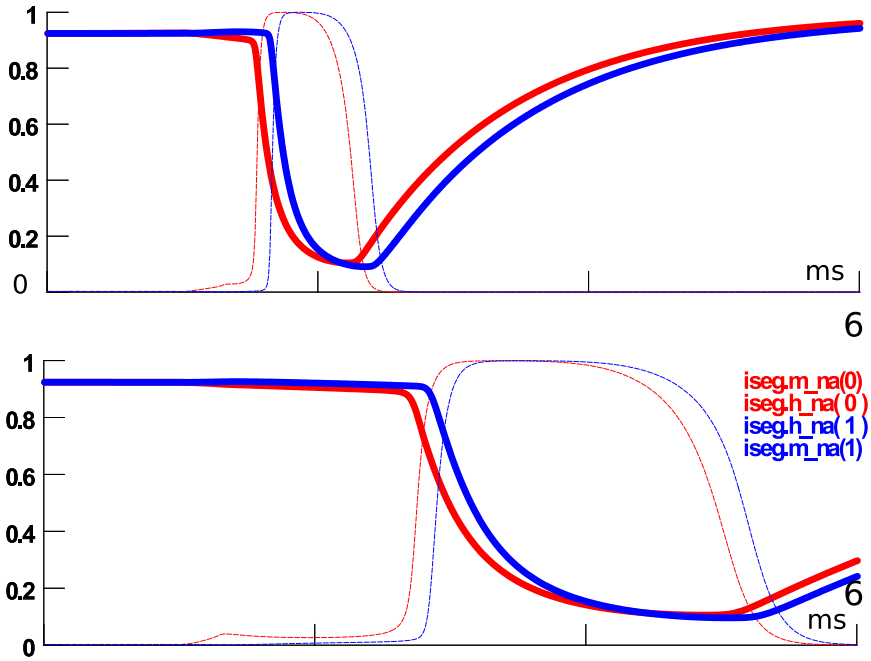

Figure 6.13: *Gating variable values, red at the beginning and blue at the end of the axon initial segment during high temperature (top) and low temperature (bottom) stimulation. The bold lines are the activation and the dashed lines the inactivation variables.*

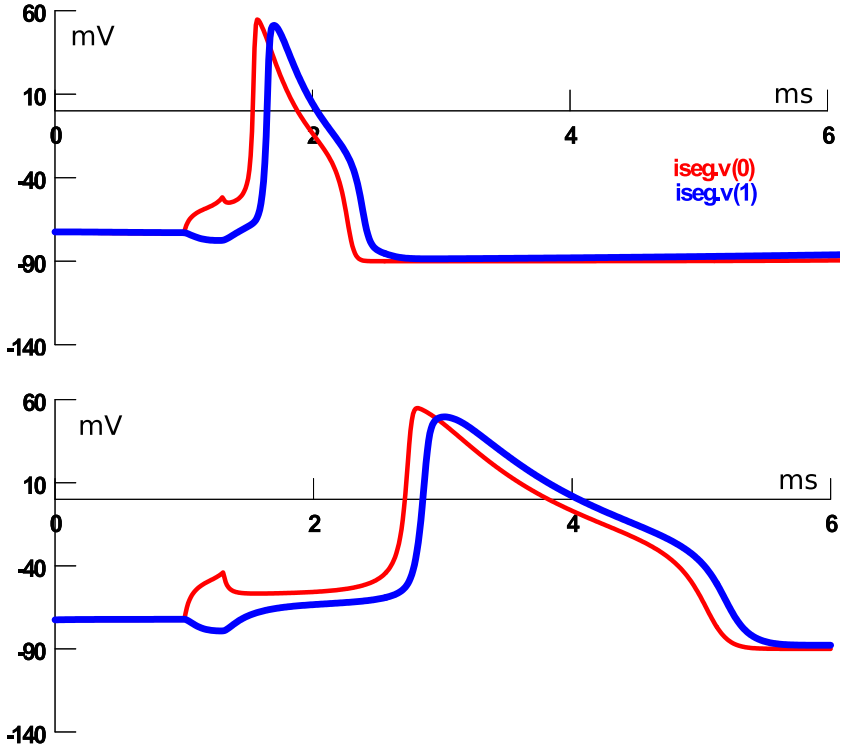

Figure 6.14: *Voltages, red at the beginning and blue at the end of the axon initial segment during high temperature (top) and low temperature (bottom) stimulation.*

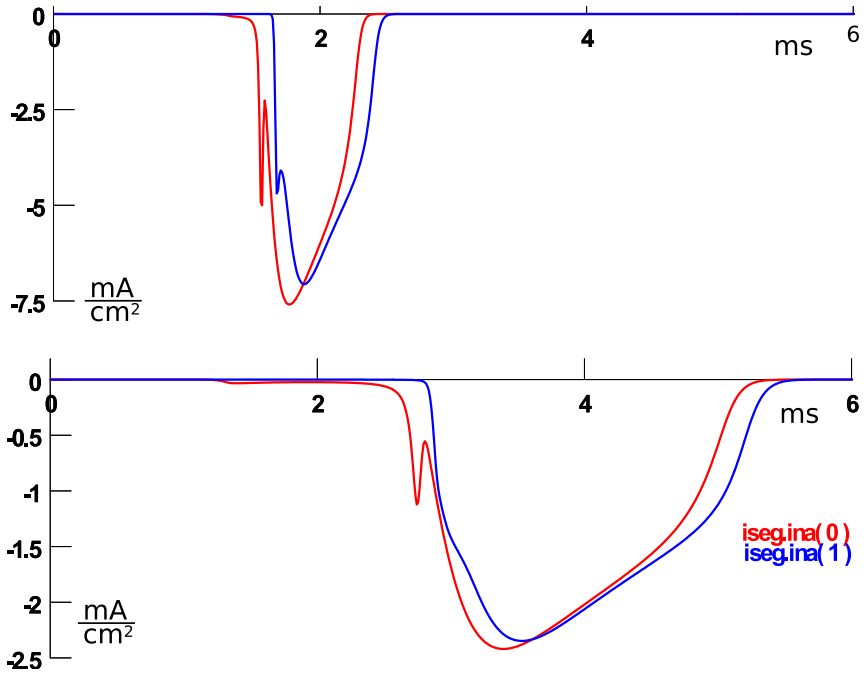

Figure 6.15: *Current flows, red at the beginning and blue at the end of the axon initial segment during high temperature (top) and low temperature (bottom) stimulation.*

The soma and axon were isolated from each other during the stimulation. The stimulation for the soma was performed at a distance of 10 μm and for the axon the electrode was placed 16 μm above the base of the hillock.

The stimulation duration for the soma is very long (1.05 ms) because at a low temperature, it could not be excited at all below that value. For the sake of comparison, this stimulation length is kept for the high temperature soma. The stimulation intensity used to create the charts was for the lower temperature -0.0095 mA and for the higher temperature -0.004558 mA. They were chosen so the resulting action potentials could be easily compared side by side. The lower threshold for room temperature was for that stimulation duration -0.0084 mA and the upper threshold -0.0099 mA and for body temperature it was -0.0045 mA and -0.0112 mA respectively.

The axon was easier to stimulate, with the usual 0.3 ms being sufficient to excite it. The charts were created at -0.0042 mA for the lower and -0.0028 mA for the higher temperature. These values also coincide with the lower thresholds for both, with the upper thresholds being -0.187 mA for room temperature and -0.08 mA for body temperature.

These facts and the side by side comparison of the different parameter charts allows a few conclusions about the effects of this model's way to adjust for temperature. For the soma, the gating variables react slower in the low temperature case even though the stimulation intensity is higher than for the soma at body temperature (figure 6.10). The same is true for the axon (figure 6.13). This means that the model is able to take the different activation and deactivation times for the channels into account, at least to some extent.

The action potential is also longer for the low temperature case and the currents lower, even though the stimulation intensity is higher (figures 6.11 and 6.14). In the axon, the propagation speed for the high temperature is slightly faster, which can be seen in the delay between the soma-near and soma-far action potential in the voltage diagrams. The neurites also have a lower threshold for body temperature.

These changes are consistent with the general way temperature adjustment should impact a model, which is a good sign. The question is still to what degree the resulting behavior is faithful to what would be found in nature for this channel type and this kind of neuron, which is rather harder to answer. For one, gating mechanisms in different or even the same channel types often don't react in a uniform way to temperature changes (Koch & Segev, 2003) and for another it is unclear to what extent the adjustment was empirically validated for higher temperatures.

6.3 Soma and Axon

The next step up in complexity from an active soma with channels is a soma with a connected axon. For this, the axon with properties as described in chapter four is chosen since it is straight and also otherwise simple enough that not too much unpredictable new behavior should be introduced at once.

Since it was a concern, the question whether action potentials could fail to backpropagate from the axon to the soma even during intracellular stimulation needed to be adressed. Tests for this were carried out for different positions and intensities inside of the axon. The only circumstance under which backpropagation failed was a long, sustained pulse (more than 5 ms), during which the first action potential arising could pass into the soma, but the second couldn't. The stimulation durations used in the simulations are much shorter than that so this won't be a concern. If an action potential fails to spread from the axon to the soma during the simulations and it seems likely that this backpropagation failure is one of the possible causes, the topic will be revisited.

In order to get a feel for how this system behaves under stimulation, the electrode was positioned 10 μm above the soma and moved at this height parallel to the axon's direction (see figure 6.16). One position does not quite fit into this pattern, this electrode was positioned 10 μm away from the soma, but on the side opposite to the axon. This turned out to yield exactly the same threshold values as stimulation directly above the soma and perpendicular to the axon, which is why these values were omitted from the diagram. For

each position indicated, stimulation was applied for a duration of 0.3 ms and the resulting upper and lower thresholds recorded (see figure 6.16).

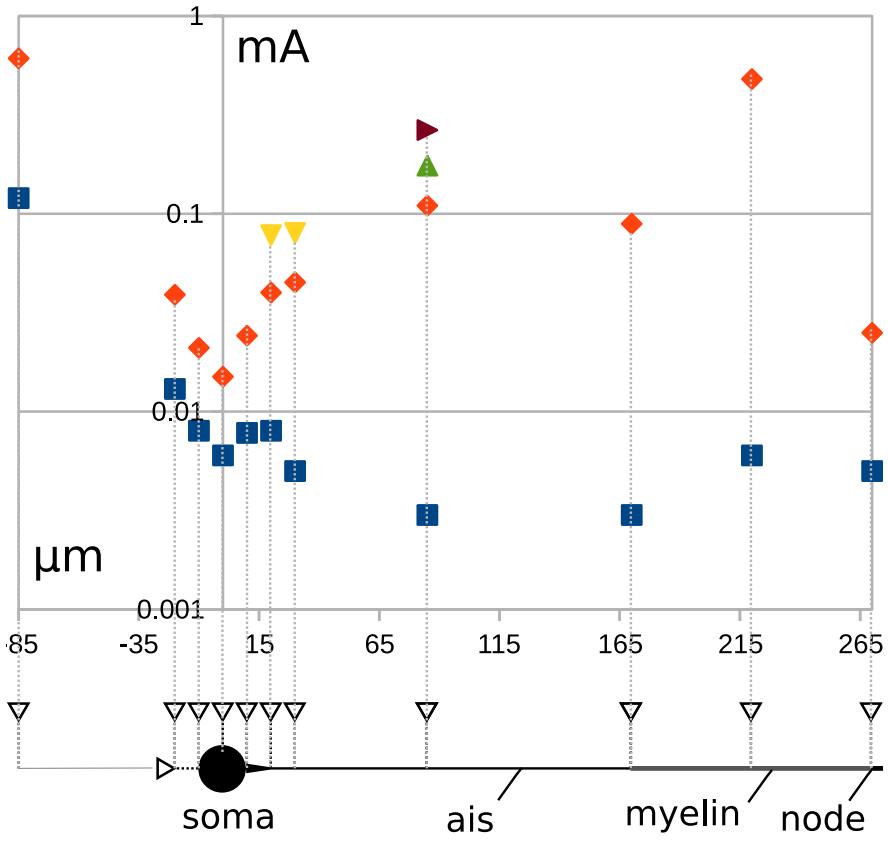

Figure 6.16: *Below: Sketch of the soma with axon, electrode positions are indicated by the black inverted triangles (the distance between electrode tips and neuron are not to scale). Top: chart with the lower (blue rectangles) and upper (salmon diamonds) thresholds for each electrode position. Sometimes the upper threshold is not unambiguous (the yellow inverted triangles indicate that the soma is no longer excitable above the values of the diamonds, but other parts of the cell are). The green and maroon triangles indicate that there is a second lower and upper threshold respectively. The graduation of the current axis is logarithmic and the stimulation cathodic.*

Several things of note could be observed. There was indeed an upper threshold for each position, but the way it came about out varied with location. They could be roughly be divided up into several groups.

Going from left to right on the chart, the first could be called the soma-leading group. They extend from the leftmost electrode to the one just above the right edge of the soma. What they have in common is that the action potential initiation only occurs after the end of the stimulation and is led by the soma (which does not mean that the action potential may not peak sooner in other segments, it just starts earlier in the soma). The action potential then spreads from there along the axon (see 6.17, top). Another characteristic is the relatively high lower and generally low upper threshold. At the upper threshold, no part of the neuron can be excited any more. These properties might be a consequence of the fact that the soma is the driving factor behind the generation of the action potential and if it cannot be excited, nothing will be. The gap between the thresholds is still larger than in the isolated soma model, which is owed to the influence of the axon. The higher upper threshold also means that there is a higher amount of current reversal in the soma within the stimulation window. The question is if this contributes to the upper threshold for these cases.

In order to investigate this, the sodium currents (figure 6.18), gating variables and membrane voltages at and above (figure 6.19, bottom) the upper threshold were looked into. The example used here is the electrode at x = 10 μm in figure 6.16, but the principle is the same for all electrodes to the left of it. The first interesting thing was the sodium current in the soma compartments. There was as expected more current out of the soma than when it was unconnected. Right at the beginning for a short time, there was even a net transmembrane current out of the soma (figure 6.18), which might be visible in the diagram displaying the voltages of the different soma compartments. An outward sodium current might cause a slight dip in the voltage for all segments, as is the case for the soma-only model. As can be seen in the top image of figure 6.20, this does not seem to be the case here. There must therefore be another process that is more than making up for the lost charge. If one removes all ion transport mechanisms from the model similar to what was done for the isolated soma and compares the results, it is possible to see whether another ion current is causing the slow rise at the onset.

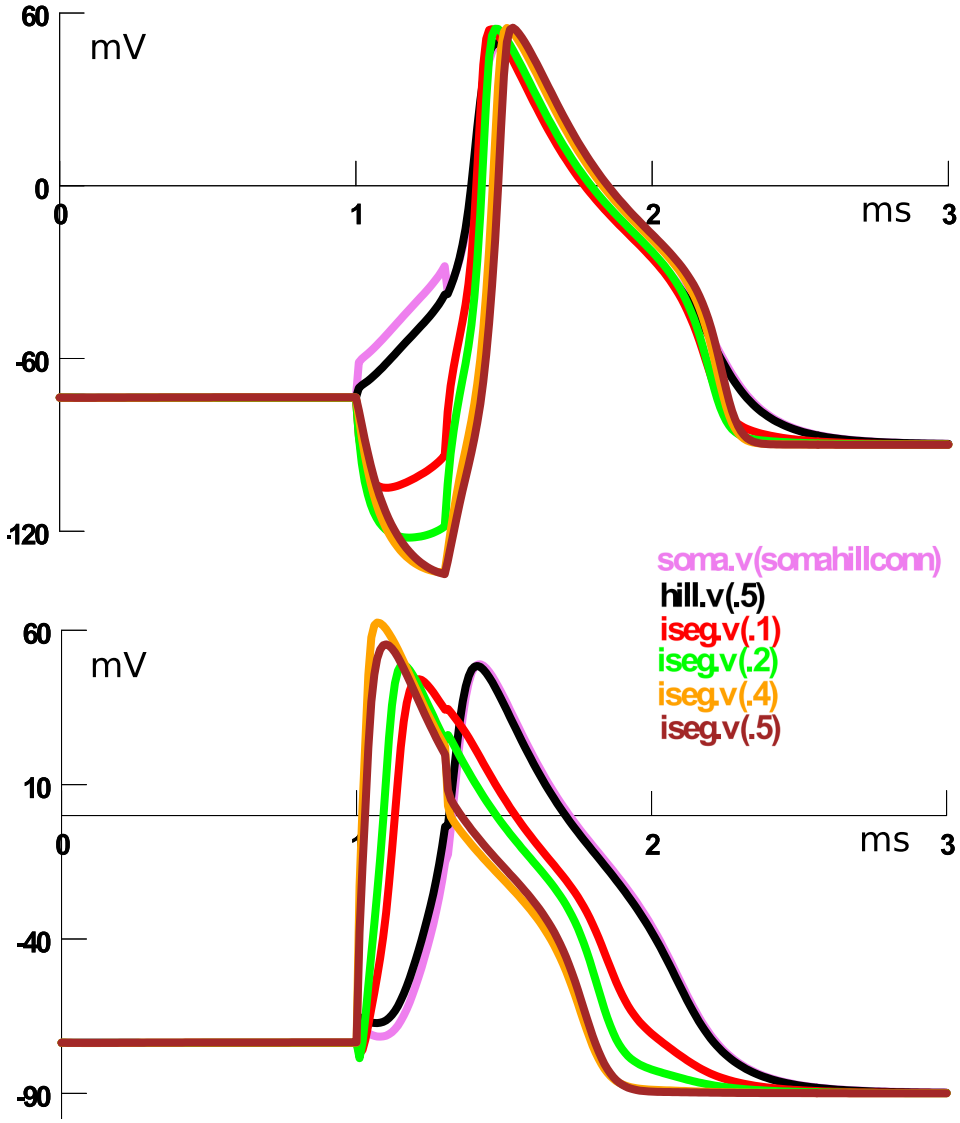

Figure 6.17: *Voltage charts for the soma segment connected to the axon (pink), the center of the hill and several AIS segments, with the numbers in parentheses signifying where on its arch length the voltage is measured. Position (.1) is close to the hill, (.5) is at half of its length. Top is an example for soma-leading stimulation (electrode position +10 µm in figure 6.16, at a stimulation strength of -0.015 mA), bottom is an example of axon-leading stimulation (electrode position at +85 µm, stimulation strength -0.02 mA).*

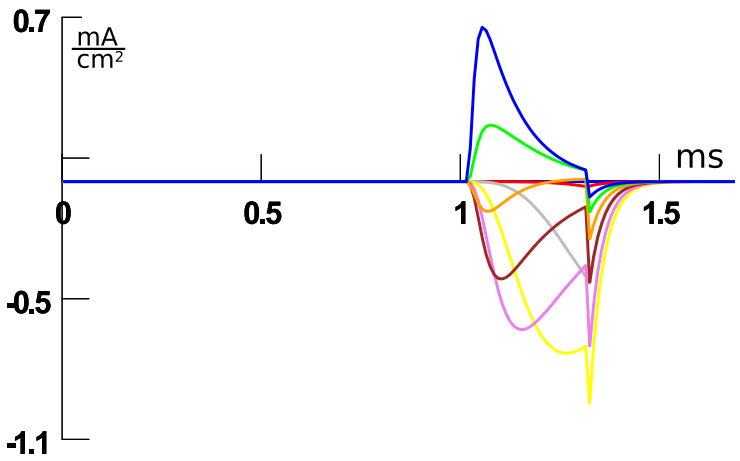

Figure 6.18: *Sodium current in different soma compartments, with the legend being the same as in figure 6.6. Stimulation start is as usual at t = 1 ms.*

It turns out that the chart with the ion channels looks very similar to the one without, i.e. most of the gain in membrane potential doesn't come from regular ion channel activity. Instead, another effect is at work which hasn't been looked into yet in this work. For large bodies such as the soma, intracellular charge equilibration takes place in a timeframe that is very short compared to the times channels need to transport charge. This is no longer true for thin neurites, whose dimensions restrict the intracellular movement of charges. Since this can easily be confused with or mask other effects such as transmembrane currents, it is a complicating factor for interpreting results and needs to be kept in mind.

The question is now what the consequences of the redistribution in the soma-axon system are. As in the isolated soma model, they move in order to equilibrate the internal potential differences, ie positive charge moves closer to the parts near the electrode. In figure 6.19, the effects on the soma and nearby neurites are shown. The soma and adjacent hill experience depolarisation, parts that are farther away increasing hyperpolarization. This might cause a surround block for sufficiently high intensities. In this situation, it helps explaining why the soma can be stimulated at higher intensities if it is connected to the axon. Positive charge flows into the soma during the stimulation, does not escape immediately afterwards and can thus contribute to the generation of an action potential.

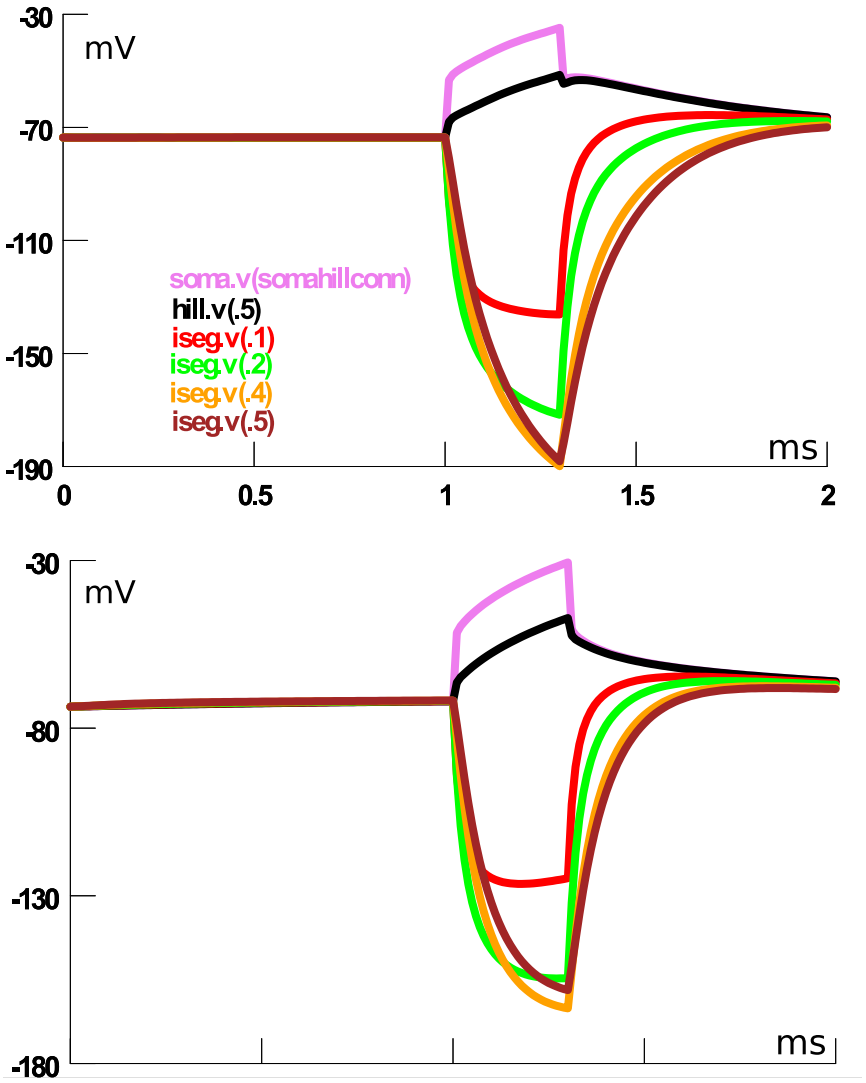

Figure 6.19: *Top: voltage chart for the axon-soma model with ion channels. Bottom: voltage chart for the the model without channels.*

While there are some sodium currents out of the cell at and above the threshold, the membrane potential rises nevertheless during stimulation and the action potential starts only afterwards.

If the stimulating electrode is placed further along the axon, the axon-leading group of excitement patterns can be observed (6.17, bottom). The soma doesn't play that much of a role in action potential formation any more. This means that an action potential can be generated elsewhere and even during stimulation. For stimulation positions closer to the soma, there are two upper thresholds, the lower of which signifies the point where the soma can no longer be stimulated (see figure 6.16). With the second upper threshold, no

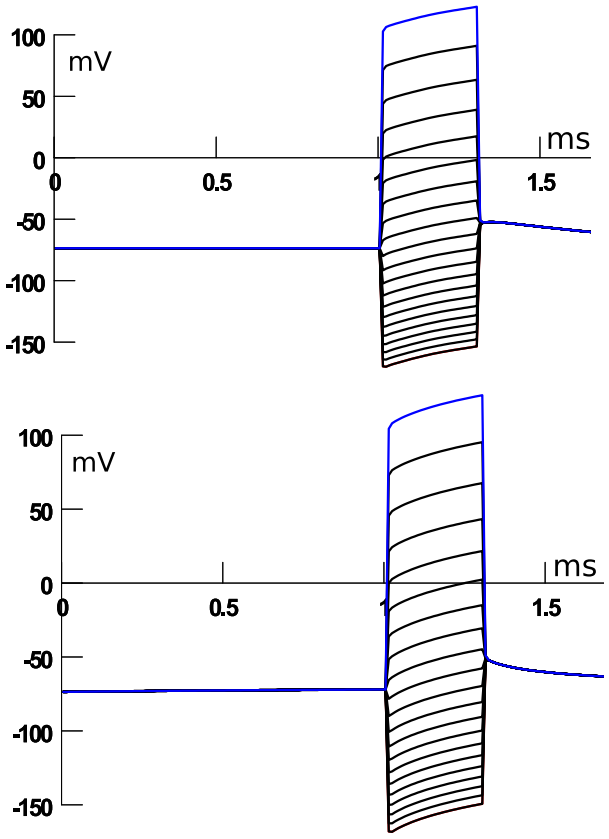

Figure 6.20: *The membrane voltages of the different soma compartments (the top line is again from the compartment closest to the electrode, with the others following in turn). Top is the chart for the soma-axon model with ion channel mechanisms, bottom is the same geometry without channels.*

action potentials are possible. It is not quite clear what causes this discrepancy. There is no current reversal in any part of the soma for this range, and it is questionable whether the surround block phenomenon is involved since other regions at the same distance from the electrode can still be excited.

At position 85, there are two stimulation windows separated by a gap. During the first window, the action potential seems to start in the axon near the electrode. In the second one, it seems to start in the AIS relatively close to the soma. Interestingly, it cannot propagate through the region near the electrode and so remains confined to the soma and soma-near axon.

When stimulated above a myelinated section, both upper and lower threshold increase. This seems to be due to the distance to excitable regions. The opposite is true for stimulation above a node. Both thresholds are low, and even strong stimulation cannot cause an action potential to form further away in the neuron.

6.4 Linear Neuron with three Sections

Adding a single linear dendrite is the next expansion of this model. The new neurite has a diameter of 5 μm, a length of 201 μm and is divided into 40 segments. The channel distribution is the same as in the dendrites of the pyramidal neuron and the electrode positions are the same as before. The results can be seen in chart 6.21.

When stimulated above the end or the middle of the dendrite, the action potential seems to start in the dendrite itself, but is quickly outpaced by excitation in the soma and especially the axon initial segment (figure 6.22). Between stimulation position -20 μm, and 0, the action potential seems to arise in the soma, as evidenced by the fact that the voltage starts rising there first and the fact that it only starts after stimulation ends. This corresponds to the soma-leading excitement pattern described for the previous model.

Another thing that is noticeable in figure 6.22 is the relatively high membrane voltage increase in the electrode-near dendrite even for small stimulation intensities. This was observed not just for this relatively thick dendrite but for thinner ones in other models as well.

A difference to the soma-axon model is the markedly higher upper threshold for the electrode position directly above the soma. A reason for this might be the larger increase of the soma's membrane potential for the same stimulation intensity in this model (see figure 6.23).

When investigating voltages and currents for electrode position 0, some interesting things can be observed. The fact that the soma membrane potential rise to a high value for the given stimulation intensity combined with the high upper threshold imply that near that

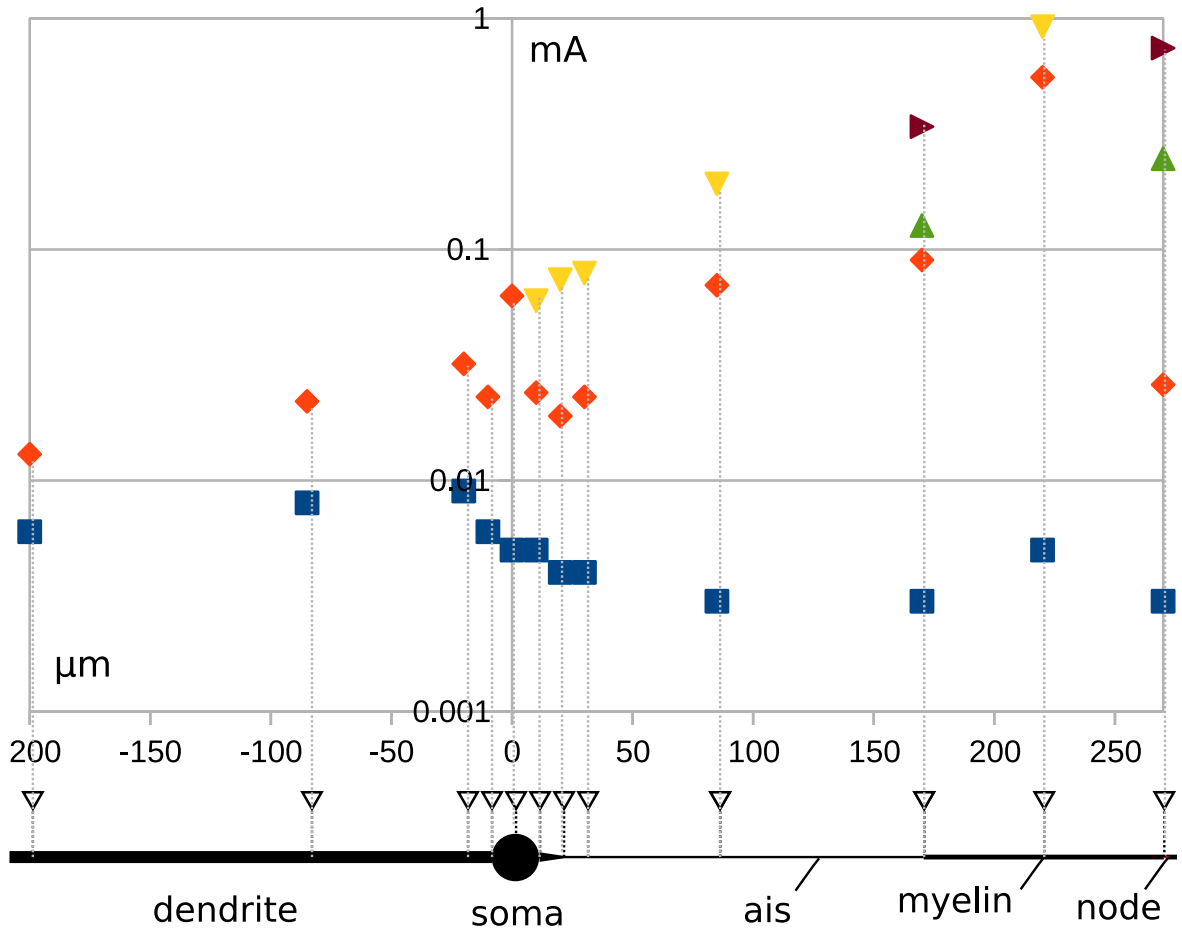

Figure 6.21: *Below: Sketch of the soma with axon and dendrite, electrode positions are indicated by the black inverted triangles. Top: chart with the lower (blue rectangles) and upper (salmon diamonds) thresholds for each electrode position. Sometimes the upper threshold is not unambiguous (the yellow inverted triangles indicate an upper threshold for part of the cell). The green and maroon triangles indicate that there is a second lower and upper threshold respectively. The graduation of the current axis is logarithmic and the stimulation cathodic.*

threshold a sodium current outflow of a large magnitude for some segments and possibly even a net current reversal for the whole soma might be observed. In figure 6.24, the relevant traces are displayed. It turns out that the whole soma experiences a very strong net current reversal (bottom chart). Nevertheless, not only can an action potential still be induced for that stimulation intensity (-0.06 mA), but it also seems to originate in the soma (top). To rephrase this point, a strong net current reversal in the soma for the entire stimulation duration is not sufficient to prevent it from forming an action potential, at

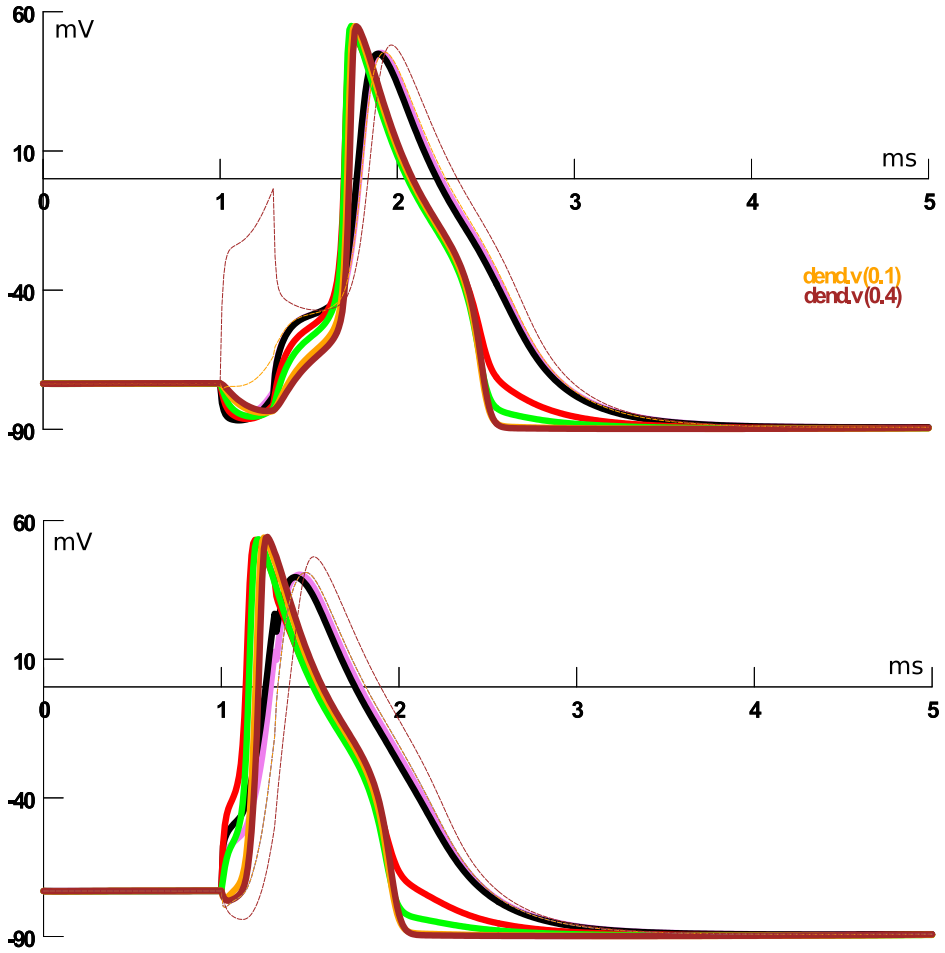

Figure 6.22: *Voltages for certain segments at electrode position -85 and intensity -0.006 mA (top) as well as position 30 and intensity -0.005 mA (bottom). Apart from the dendrite sections close to (thin orange) and further (thin brown) from the soma, the legend is the same as in figure 6.17. Importantly, the soma segment connected to the hill is pink, the center of the hill is black and the rest are various points on the axon initial segment.*

least under some circumstances. This is the most extreme such case encountered in all simulated configurations, it was chosen to illustrate that such a situation can arise.

Starting with an electrode position at 10 μm, the action potential forms in the axon during stimulation. The upper thresholds for the soma (salmon diamonds) are lower than in the model with only the axon. The general excitement pattern is also pretty similar to the axon-leading type in the soma-axon model, with the action potential again starting roughly at the region directly below the electrode and (slight) hyperpolarisation of regions

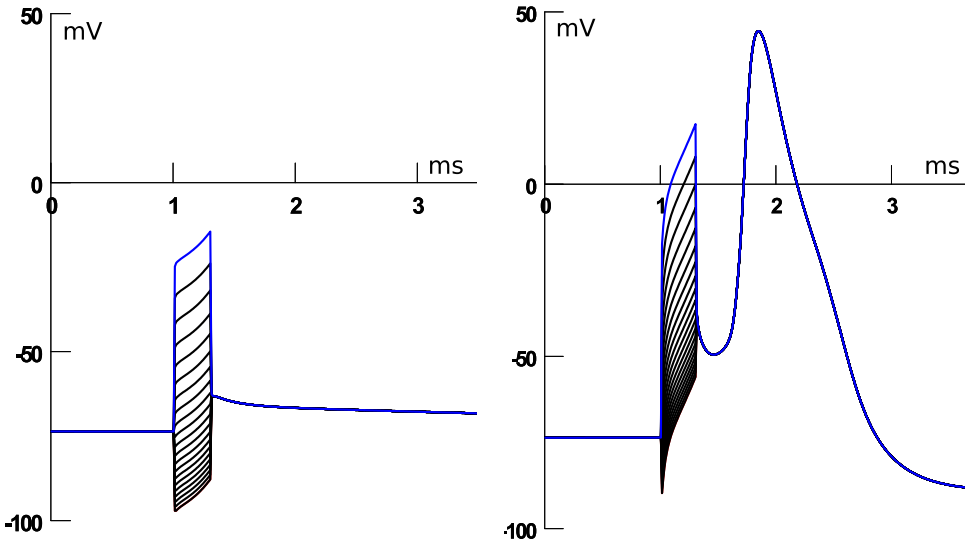

Figure 6.23: *Voltages for all soma segments for the soma-axon (left) and the dendrite-soma-axon model (right) at a stimulation intensity of -0.005 mA and at electrode position 0.*

a bit to the side. This is somewhat visible in figure 6.22, bottom, where two segments in the middle of the axon (thick orange and brown lines) show a slight dip after the start of the stimulation.

In this model there are more electrode positions for which there are either two lower and upper thresholds or where the soma stops being excitable before the axon (6.21). For all models simulated (including the ones described in the next section), these two cases are mutually exclusive for any single electrode position. Figure 6.21 sheds a bit of light on the situation in both stimulation windows. In the lower window, the action potential is initated in the axon, in the upper window it seems to start in the soma. Moreover, in figure 6.16, for position -85, the stimulation window is determined by the soma's excitability. In position 85, there is a second excitation window whose borders fit into the stimulation window in position -85.

This means that both the excitation sequence of the sections and the strength-distance relationship are consistent with the second window being caused by the excitability of the soma. It would also explain why no second window exists for cases in which the soma stops being excitable before the axon. In those situations, the soma seems to experience

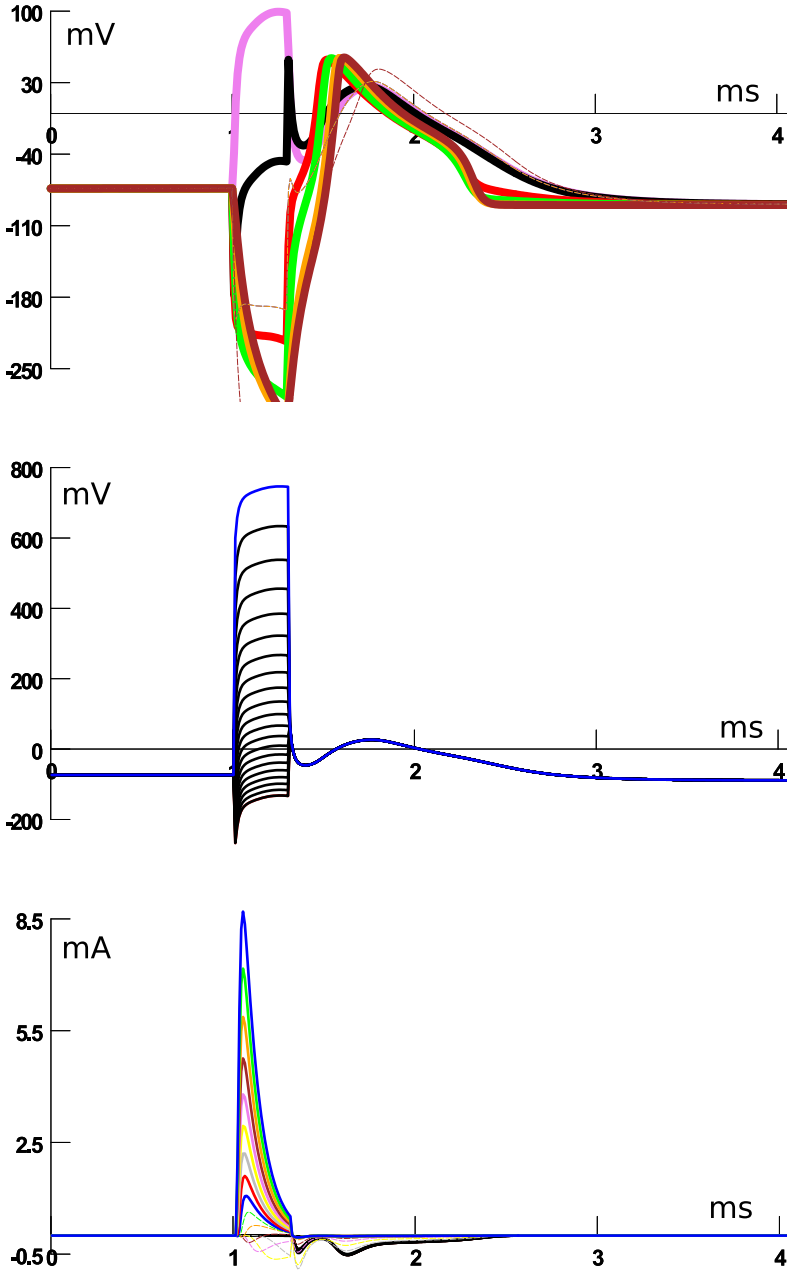

Figure 6.24: *Voltage and current traces for position 0 and stimulation strength -0.06 mA (near the upper threshold) in the single dendrite model. Top: Voltages in selected segments, the legends are the same as in figures 6.17 and 6.22. Middle: Voltages for segments of the soma, with the blue trace belonging to the electrode-nearest segment. Bottom: Sodium currents for the soma segments, legend according to figure 6.6.*

a block which cannot be lifted by applying more current. When two windows exist, it appears that the first upper threshold originates from a loss of excitability in the axon

with growing intensity (possibly due to the surround block phenomenon). This can be overcome by further increasing the current to a strength that allows excitation of the soma.

There are some things that this conjecture doesn't explain. Firstly, the stimulation window doesn't quite fit the strength-duration relation, which might be due to various interfering neurites. Secondly, there doesn't seem to be a clear reason for why either the two windows or the early soma block appear in the positions they are in or why that differs from model to model.

Adding the dendrite introduced a new neurite on which action potentials can be initiated. Much of its effect on the model appears to be indirect, though. The dendrite seems to help either in promoting excitability in the other sections (as in position 0) or in inhibiting it (in the positions somewhat to the right of 0).

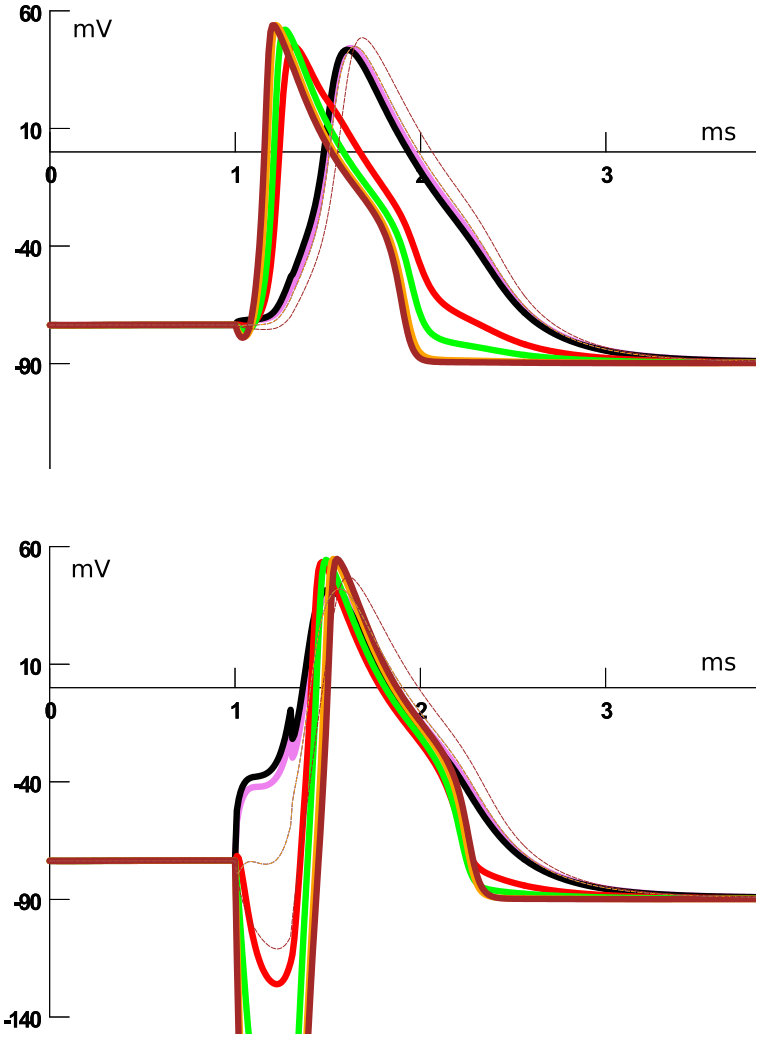

Figure 6.25: *Voltages for certain segments at electrode position 170 and intensity -0.008 mA (top) and intensity -0.13 mA (bottom). The top chart depicts the situation in the lower stimulation window (see figure 6.21), the bottom chart the situation in the upper window. The legend is the same as in figure 6.17.*

6.5 Pyramidal Neuron

An analogous stimulation regime was applied to the model of the traced pyramidal neuron. There are some differences, though. Specifically the distances of the electrodes to the apical dendrite are dependent on its curving path and are not directly comparable to the electrode distances to the straight dendrite of the last model. This means that care must be taken when comparing the results, especially for stimulation in the region in question.

In addition to the pyramidal neuron as originally traced, a two-dimensional version was also created. For this, the three-dimenstional neuron was projected on the plane perpendicular to the soma axis for electrode position 0. That way, while a lot of the original structure including all of the connections are preserved, small neurites cannot get too close to the electrode. This limits the potentially large impact that a coincidentally close dendrite can have on the excitation pattern.

The difference between this and the soma-axon model is the addition of traced dendrites. The electrodes remain in the same relative positions as in the last two models, which can be seen in figures 6.26 and 6.27. Only a small part of the neuron is shown in the figures, the distal parts of the apical dendrite and the axon were omitted for clarity's sake.

One of the most striking things about figure 6.26 is the region on the left side of the chart. In position -200, there is just one blue marker where the upper and lower threshold coincide at -0.003 mA. For the next two positions along the dendrite, it is impossible to induce an action potential at any intensity. This is not true for the two-dimensional model, where distinct upper and lower thresholds for all positions exist and are in the same order of magnitude as in the single dendrite model (again, caution has to be applied when drawing conclusions from this). The main difference between the two- and three-dimensional model is that in the former a greater distance (at least ca 20 μm) is forced between dendrites and the electrode. The number and distance of neurites close to the electrode (within 20 μm, which was chosen because it is about the closest that distal dendrites get to the electrode in the two-dimensional model) might help shed some light on the issue. For the position -200, one dendrite fits the bill, with a distance of roughly

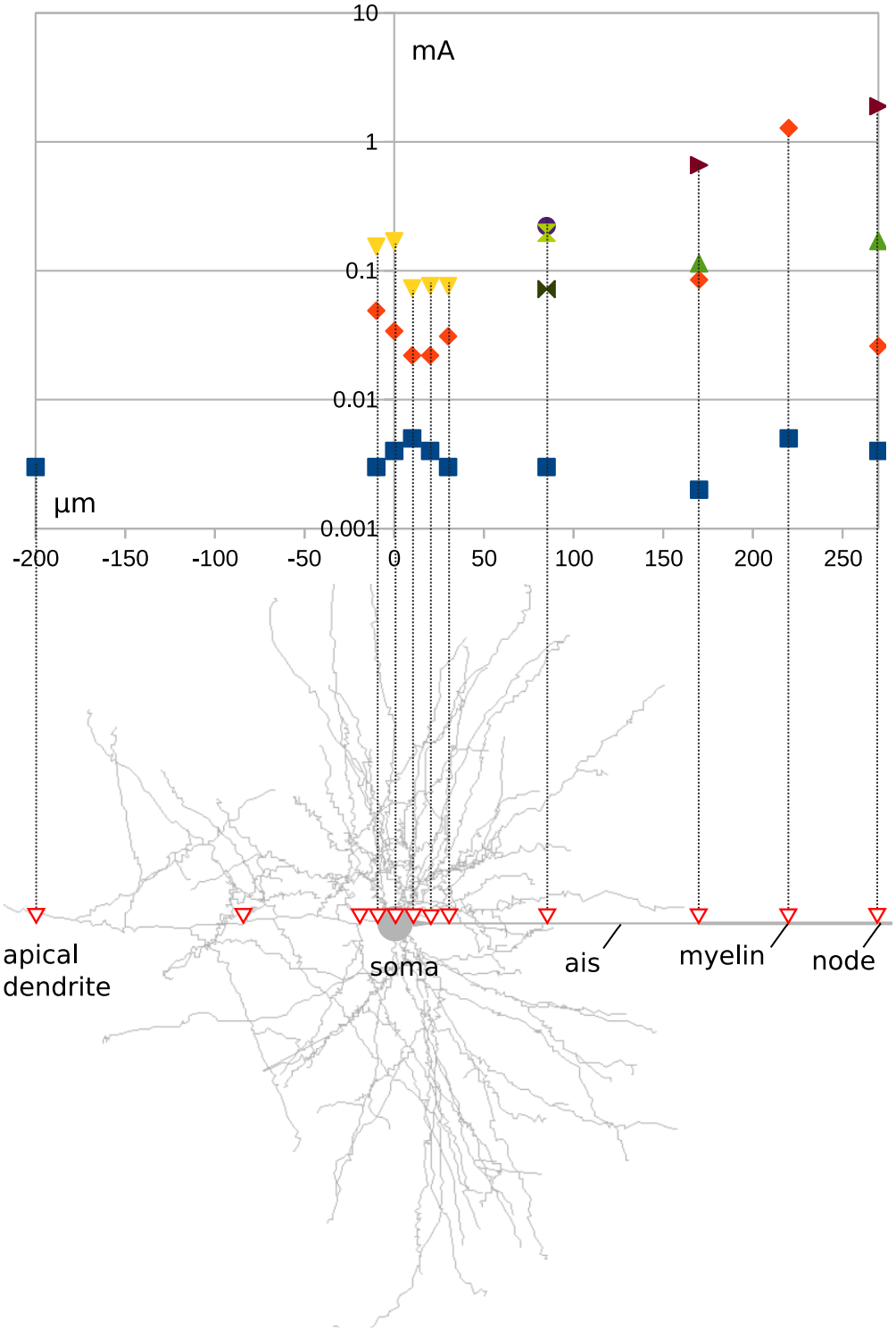

Figure 6.26: *Below: Sketch of part of the pyramidal neuron, seen from the side that the electrodes are on. The electrode positions are indicated by red inverted triangles. Top: Chart with various thresholds.*

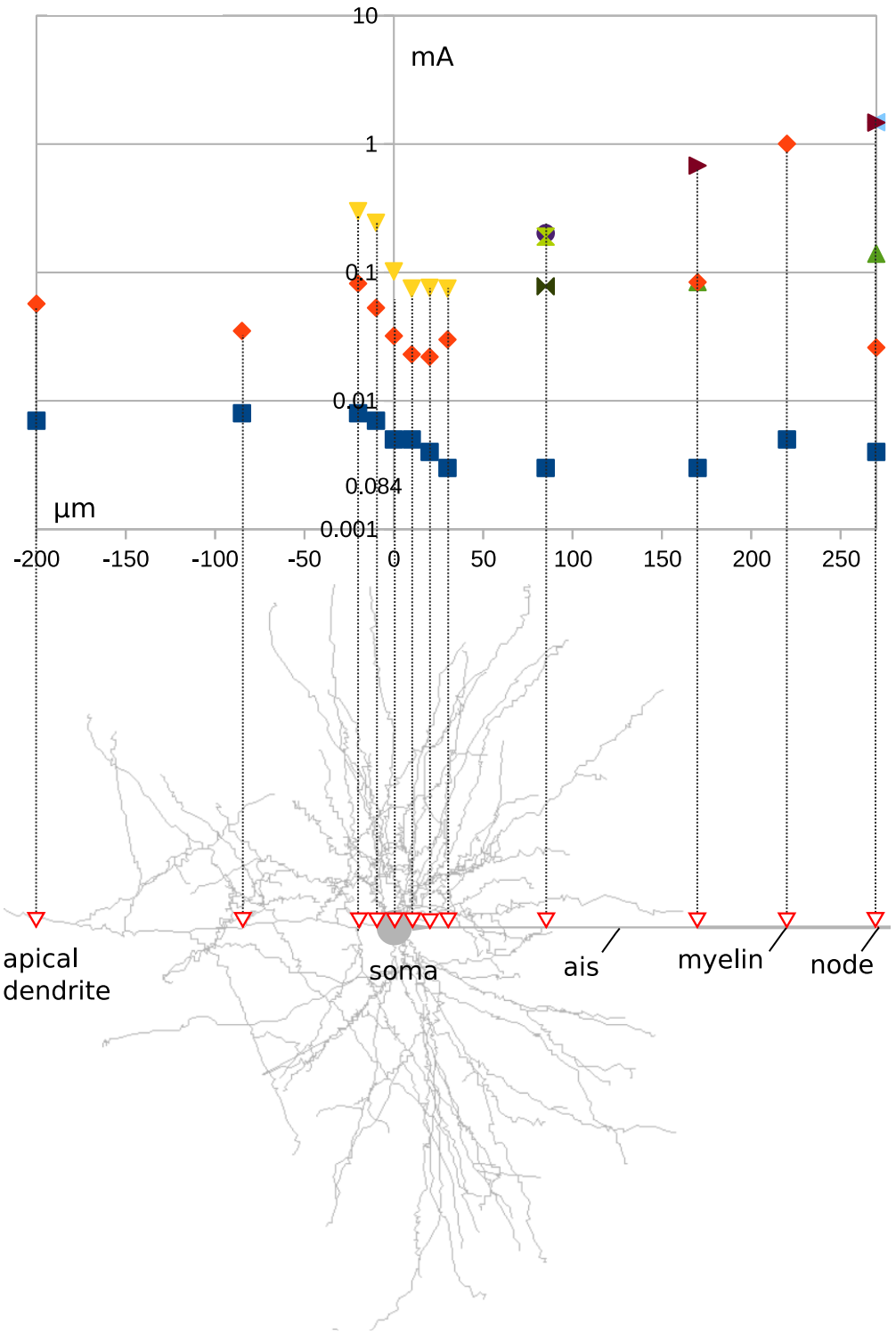

Figure 6.27: *Below: Sketch of part of the the two-dimensional projection of a pyramidal neuron. Again, electrodes are indicated with red triangles. Top: Chart with thresholds.*

11 μm. For -85, there are 10 dendrites nearby, the closest one at about 8 μm distance and most with over 10 μm. At -20, there were also 10, this time one of them was very close at

just 2.5 μm, with several others being under 10 μm away. For the sake of completeness it should be mentioned that this distance is calculated from the center of the segment as determined by the xtra mechanism, so the field determined by the mechanism differs significantly from the field that the neurite would actually experience at each point for electrode distances this small.

It would seem that nearby small dendrites have a large inhibiting impact on excitement as long as the electrode is close only to dendrites. When it approaches other sections (soma and axon), the excitability of these structures appears to overcome this effect. It is also possible that higher dendrite diameters near the soma (where the number of nearby dendrites is large and some distances comparable to the position -85 case) make a difference. Away from the soma and above the axon, there are also many dendrites nearby up to position 20 (afterwards they become significantly sparser and more distant), with the closest being 8 μm away at the position 10. While is possible that the difference in dendrite distribution contributes to the different behavior over soma and axon, there isn't much evidence for that. Near the soma but still above the apical dendrite (positions -10 and -20), exciting the neuron actually seems to be easier (the lower threshold has a smaller value) for the three-dimensional neuron than for the two-dimensional one.

Starting at position 10, the charts for both the flat and the three-dimensional neuron seem pretty similar. In position 85 for both cases, a new phenomenon appears, which is indicated with new markers in both charts. In addition to the markers introduced in figure 6.16, the charts for the pyramidal models use a green horizontal hourglass to signify a block from the middle of the axon initial segment to the distal end of the axon, a green vertical hourglass to mean an additional block starting at the beginning of the AIS and back to the soma and a purple circle to indicate that the region in between is experiencing a block as well. This is the first situation encountered in the simulations where the action potential stops propagating into the distal axon before it stops reaching/exciting the soma. It is not quite clear what causes it, this far along the soma there are relatively few (four) small dendrites nearby, which are all about 20 μm away for the three-dimensional model.

Altogether and somewhat unsurprisingly, introducing many curved and branching dendrites seems to mainly affect the thresholds/excitability near them and further from other structures. For these regions, stimulation close by small neurites seem to have a large damping effect on the formation of an action potential. Near other parts of the neuron such as the soma, this effect seems to lessen considerably.

7. Discussion

The questions this work set out to address was whether upper thresholds could be observed, whether there are differences in that regard in various models and what the causes of these blocks are.

In the section "Hypotheses and Predictions", the claim was made that for every configuration in which excitement is possible, there would also be an upper threshold. This turned out to be true for all models and all stimulation regimes (which involved different strengths, durations and electrode distances and always a single rectangular cathodic pulse). There were significant differences in the current needed to reach the upper thresholds, with variations between -3 μA (in position -200 of the three-dimensional pyramidal neuron) and 1.89 mA (position -270 in the same model). Some patterns found in different models will briefly be recapitulated and discussed here.

All models simulated had a soma with the same dimensions and channel densities in common. For the simple soma model, the lower threshold is with -8 μA higher and the upper threshold with -9.75 μA lower than in any other model. The stimulation window for electrode position 0 (directly above the soma) expands with an added axon and again if a dendrite is also present (both upwards and downwards, but for the most part the upper threshold rises). For both the two- and the three-dimensional pyramidal neuron models, the upper threshold is somewhere in between those of the soma-axon and the soma-axon-dendrite models.

At least for the models with simplified geometry, a large contribution to this behavior comes from intracellular potential equilibration and positive charge being redistributed to sections near the electrode (the soma in this case). For some of the cases investigated, this completely dwarfs the change in membrane potential due to sodium current, reversed or otherwise. This is a probable reason for why the earlier claim that net current reversal in the soma precludes the formation of an action potential turned out to be wrong.

As stated in the "Results" section, the influence of the dendrites on the model was mixed. They could either promote the formation of action potentials (stimulation near a single thick dendrite or the soma) or inhibit it (stimulation near the axon for the single dendrite model or near many small dendrites and far from soma and axon for the pyramidal model). The linear dendrite generally had a smaller stimulation window than the linear axon. Even if one of the slender dendrites in the pyramidal model was close to the electrode, it was never the case that an action potential started there. At best (if soma or axon were nearby), they acted supportive towards excitement in other sections (as evidenced by the sometimes larger stimulation windows near the axon in the three-dimensional pyramidal neuron).

The claim made in the "Hypotheses" section that a linear dendrite would be easier to stimulate than the soma should be revisited in the light of these findings. It seems to hold when comparing the thresholds of a single linear dendrite stimulated near its distal end (6.21 to the thresholds of an isolated soma stimulated from the same distance (-8.1 and 20 μA). In all other cases, (e.g. small or curved dendrites, connected soma etc.) it seems to either be the other way around or more complicated with no clear answer.

The assertion that the axon was the easiest neurite to stimulate held true. It both contributed to an easier excitability of the soma and had itself a comparably wide stimulation window. It also turned out to be correct that for comparable distances from both, an action potential was initiated in the axon rather than the soma.

The remaining question is what the cause of the upper thresholds in each situation was. The model that was easiest to analyze in that regard was the single soma. It could be shown that for the stimulation time and distance typically used in the simulations no current reversal could be shown in any segment (and especially no net current reversal for the whole soma). It was also demonstrated that the reason for the upper threshold was due to a failure of the values of the activating gating variables to increase after stimulation. This is not a satisfying answer because it still tells us nothing about the reason why this is the case.

The picture for more complicated neurons is even less clear. For the soma, even a strong net current reversal didn't always stop an action potential and as in the single soma model, a membrane voltage above the threshold after stimulation did not reliably result in excitation. It is therefore hard to tell exactly what the factors are that cause the upper threshold.

For slender neurites, depolarization in electrode-near parts and hyperpolarization for further away regions could be observed and is also visible in some of the figures provided (e.g. 6.17 and 6.22). Whether this leads to anodal surround block and if so, whether that is the cause of the upper thresholds is a more complicated question. It certainly seemed to be the case that the de- and hyperpolarization got more extreme with increasing current and in some cases (e.g. the one depicted in 6.25), the region in question stopped generating action potentials. This same case however also demonstrates that action potentials generated elsewhere might still be capable of penetrating the hyperpolarized region, which demonstrates that the surround block effect depends on the membrane kinetics, too.

Given these considerations, it could not be determined from the data gathered what the exact causes of the upper thresholds are in the models. The most that can be said with any certainty is that (total) current reversal is not responsible in the single soma case for the standard stimulation conditions.

Before the advent of very small microelectrodes, stimulation of neurons mostly took place from relatively far away and using electrodes with large dimensions that could not be modeled as point-shaped current sources. Since this has changed, it is important to find suitable models for close range stimulation with (nearly) point-shaped electrodes. The goal is to be able to predict the behavior of neurons under stimulation and as a consequence to identify good stimulation regimes to achieve the desired effects during stimulation in vivo. This work was meant to provide a contribution to a better understanding of such stimulation configurations. While there are still many uncertainties, it could be shown that there is a high variance in outcomes for small distance stimulation depending on which neurites are nearby.

Even though care was taken to create a sufficiently accurate model, there are still some limitations. One of the issues that was adressed but not quite answered satisfactorily is the question about the reliability of the temperature adjustment. Another question is how well a spherical soma works as a model for the elongated irregular shape of a real pyramidal soma, especially for stimulation in close quarters where the differences should be particularly pronounced. The calculation of the stimulating field for a point at the center of each segment instead of the actual surface likely still has some influence on the results, even though pains were taken to minimize the impact.

7.1 Outlook

There are several ways in which the model and results presented in this thesis might be built upon.

One thing that stood out when analyzing the results of the pyramidal neuron model is that the behavior of the dendrites (especially thin and curved ones) under stimulation and the causes for it were hard to understand. This hampered the interpretation of the results and it would therefore be interesting to analyze the neurites under different conditions, starting with single linear fibres and working up to the complexity of a whole neuron. It is possible that hyperpolarization is the main reason for the inability to excite the dendrites in some configurations. It could therefore be useful to test stimulation with anodic pulses as well, in which case it should be possible to find at least a lower threshold.

Another avenue would be to use different pyramidal neuron tracings and ion channel distributions to see where the commonalities are and which parameter changes the results are especially sensitive to.

As mentioned before, there is some discrepancy between the calculated and actual distances to the electrode. For very close stimulation distances to the soma, the center of a segment might be relatively far from the equipotential surfaces that its mantle lies on. It should be possible to correct for this in NEURON.

Finally, it would be good to have external validation for the model, either by a different simulation approach or by a study involving real neurons.

References

Action potential. (n.d.). https://en.wikipedia.org/wiki/Action_potential. (Accessed: 2017-11-09)

Bareket, L., Barriga-Rivera, A., Zapf, M. P., Lovell, N. H., & Suaning, G. J. (2017). Progress in artificial vision through suprachoroidal retinal implants. *Journal of Neural Engineering*, *14*(4), 045002.

Barriga-Rivera, A., Guo, T., Yang, C.-Y., Al Abed, A., Dokos, S., Lovell, N. H., ... Suaning, G. J. (2017). High-amplitude electrical stimulation can reduce elicited neuronal activity in visual prosthesis. *Scientific Reports*, *7*.

Blackwell, K. (2014). *Computational neuroscience*. Elsevier Science & Technology Books. Retrieved from https://books.google.at/books?id=vTLqngEACAAJ

Boinagrov, D., Loudin, J., & Palanker, D. (2010). Strength–duration relationship for extracellular neural stimulation: numerical and analytical models. *Journal of neurophysiology*, *104*(4), 2236–2248.

Boinagrov, D., & Palanker, D. (2014). Reply to rattay. *Journal of neurophysiology*, *112*(10), 2666–2666.

Boinagrov, D., Pangratz-Fuehrer, S., Goetz, G., & Palanker, D. (2014). Selectivity of direct and network-mediated stimulation of the retinal ganglion cells with epi-, sub-and intraretinal electrodes. *Journal of neural engineering*, *11*(2), 026008.

Boinagrov, D., Pangratz-Fuehrer, S., Suh, B., Mathieson, K., Naik, N., & Palanker, D. (2012). Upper threshold of extracellular neural stimulation. *Journal of neurophysiology*, *108*(12), 3233–3238.

Borchers, S., Himmelbach, M., Logothetis, N., & Karnath, H.-O. (2012). Direct electrical stimulation of human cortex—the gold standard for mapping brain functions? *Nature Reviews Neuroscience*, *13*(1), 63–70.

Budvytyte, R., Gonzalez-Perez, A., Mosgaard, L. D., Nissen, S., & Heimburg, T. (2015). Penetration of action potentials during collision in the medial giant axon of invertebrates. *Biophysical Journal*, *108*(2), 207a.

Carnevale, N. T. (2005). *Extracellular stimulation and recording.* `https://www.neuron.yale.edu/phpBB/viewtopic.php?f=28&t=168`. (Accessed: 2017-11-17)

Chronaxie. (n.d.). `https://en.wikipedia.org/wiki/Chronaxie`. (Accessed: 2017-11-16)

Chuang, A. T., Margo, C. E., & Greenberg, P. B. (2014). Retinal implants: a systematic review. *British Journal of Ophthalmology*. Retrieved from `http://bjo.bmj.com/content/early/2014/01/08/bjophthalmol-2013-303708` doi: 10.1136/bjophthalmol-2013-303708

Cioni, B. (2007). Motor cortex stimulation for parkinson's disease. *Operative Neuromodulation*, 233–238.

Curcio, C. A., Sloan, K. R., Kalina, R. E., & Hendrickson, A. E. (1990). Human photoreceptor topography. *Journal of comparative neurology*, *292*(4), 497–523.

Destexhe, A., Babloyantz, A., & Sejnowski, T. J. (1993). Ionic mechanisms for intrinsic slow oscillations in thalamic relay neurons. *Biophysical journal*, *65*(4), 1538–1552.

Destexhe, A., & Huguenard, J. R. (2007). Modeling voltage-dependent channels.

Eiber, C. D., Lovell, N. H., & Suaning, G. J. (2013). Attaining higher resolution visual prosthetics: a review of the factors and limitations. *Journal of neural engineering*, *10*(1), 011002.

Fellner, A. (2017). *Modelling block of excitation of a retinal ganglion cell stimulated with microelectrodes using python and neuron* (Unpublished master's thesis). Vienna University of Technology.

Fischl, B., & Dale, A. M. (2000). Measuring the thickness of the human cerebral cortex from magnetic resonance images. *Proceedings of the National Academy of Sciences*, *97*(20), 11050–11055.

Fohlmeister, J., & Miller, R. (1997). Impulse encoding mechanisms of ganglion cells in the tiger salamander retina. *Journal of neurophysiology*, *78*(4), 1935–1947.

Fontaine, D., Hamani, C., & Lozano, A. (2009). Efficacy and safety of motor cortex stimulation for chronic neuropathic pain: critical review of the literature. *Journal of neurosurgery*, *110*(2), 251–256.

Hamill, O., Huguenard, J., & Prince, D. (1991). Patch-clamp studies of voltage-gated currents in identified neurons of the rat cerebral cortex. *Cerebral Cortex*, *1*(1), 48–61.

Hines, M. (1993). Neuron—a program for simulation of nerve equations. *Neural systems: Analysis and modeling*, *127*, 136.

Hodgkin, A. L., & Huxley, A. F. (1952). Propagation of electrical signals along giant nerve fibres. *Proceedings of the Royal Society of London. Series B, Biological Sciences*, 177–183.

Hu, W., Tian, C., Li, T., Yang, M., Hou, H., & Shu, Y. (2009). Distinct contributions of nav1. 6 and nav1. 2 in action potential initiation and backpropagation. *Nature neuroscience*, *12*(8), 996–1002.

Huguenard, J. R., Hamill, O. P., & Prince, D. A. (1988). Developmental changes in na+ conductances in rat neocortical neurons: appearance of a slowly inactivating component. *Journal of Neurophysiology*, *59*(3), 778–795.

Johnson, M. D., Lim, H. H., Netoff, T. I., Connolly, A. T., Johnson, N., Roy, A., ... others (2013). Neuromodulation for brain disorders: challenges and opportunities. *IEEE Transactions on Biomedical Engineering*, *60*(3), 610–624.

Kaniusas, E. (2012). *Biomedical signals and sensors i*. Springer.

Koch, C., & Segev, I. (2003). *Methods in neuronal modeling: From ions to networks*. MIT Press. Retrieved from `https://books.google.at/books?id=iphrpwAACAAJ`

Lewis, P. M., Ackland, H. M., Lowery, A. J., & Rosenfeld, J. V. (2015). Restoration of vision in blind individuals using bionic devices: a review with a focus on cortical visual prostheses. *Brain research*, *1595*, 51–73.

Lewis, P. M., Ayton, L. N., Guymer, R. H., Lowery, A. J., Blamey, P. J., Allen, P. J., ... Rosenfeld, J. V. (2016). Advances in implantable bionic devices for blindness: a review. *ANZ journal of surgery*, *86*(9), 654–659.

Lipski, J. (1981). Antidromic activation of neurones as an analytic tool in the study of the central nervous system. *Journal of neuroscience methods*, *4*(1), 1–32.

Lynch, J. C. (n.d.). *The cerebral cortex.* `https://clinicalgate.com/the-cerebral-cortex-2/`. (Accessed: 2017-11-09)

Mainen, Z. F., Joerges, J., Huguenard, J. R., & Sejnowski, T. J. (1995). A model of spike initiation in neocortical pyramidal neurons. *Neuron*, *15*(6), 1427–1439.

McNeal, D. R. (1976). Analysis of a model for excitation of myelinated nerve. *IEEE Transactions on Biomedical Engineering*(4), 329–337.

Noachtar, S., & Rémi, J. (2009). The role of eeg in epilepsy: a critical review. *Epilepsy & Behavior*, *15*(1), 22–33.

Norman, R. A., & Fernandez, E. (n.d.). *Introduction to visual prostheses.* `http://webvision.med.utah.edu/book/part-xv-prosthetics/introduction-to-visual-prostheses-by-eduardo-fernandez-and-richard-normann/`. (Accessed: 2017-11-07)

Normann, R. A., & Fernandez, E. (2016). Clinical applications of penetrating neural interfaces and utah electrode array technologies. *Journal of neural engineering*, *13*(6), 061003.

Normann, R. A., Maynard, E. M., Rousche, P. J., & Warren, D. J. (1999). A neural interface for a cortical vision prosthesis. *Vision research*, *39*(15), 2577–2587.

Purves, D., Augustine, G. J., Fitzpatrick, D., Hall, W. C., LaMantia, A., McNamara, J. O., & Williams, S. M. (2004). *Neuroscience*. Sinauer.

Ranck, J. B. (1975). Which elements are excited in electrical stimulation of mammalian central nervous system: a review. *Brain research*, *98*(3), 417–440.

Rasche, D., & Tronnier, V. M. (2016). Clinical significance of invasive motor cortex stimulation for trigeminal facial neuropathic pain syndromes. *Neurosurgery*, *79*(5), 655–666.

Rattay, F. (1986). Analysis of models for external stimulation of axons. *IEEE transactions on biomedical engineering*(10), 974–977.

Rattay, F. (1990). *Electrical nerve stimulation: Theory, experiments and applications.* Springer Vienna.

Rattay, F. (1999). The basic mechanism for the electrical stimulation of the nervous system. *Neuroscience*, *89*(2), 335–346.

Rattay, F. (2014). On the upper threshold phenomenon of extracellular neural stimulation. *Journal of neurophysiology*, *112*(10), 2664–2665.

Rattay, F., Greenberg, R. J., & Resatz, S. (2003). Neuron modeling. In E. F. Warren & P. G. LoPresti (Eds.), *Handbook of neuroprosthetic methods.* CRC Press LLC.

Rattay, F., Paredes, L., & Leao, R. (2012). Strength–duration relationship for intra- versus extracellular stimulation with microelectrodes. *Neuroscience*, *214*, 1–13.

Rattay, F., & Resatz, S. (2004). Effective electrode configuration for selective stimulation with inner eye prostheses. *IEEE transactions on biomedical engineering*, *51*(9), 1659–1664.

Reuveni, I., Friedman, A., Amitai, Y., & Gutnick, M. (1993). Stepwise repolarization from ca2+ plateaus in neocortical pyramidal cells: evidence for nonhomogeneous distribution of hva ca2+ channels in dendrites. *Journal of Neuroscience*, *13*(11), 4609–4621.

Risher, C., Üstünkaya, T., Alvarado, J., & Eroglu, C. (2014, 09). Rapid golgi analysis method for efficient and unbiased classification of dendritic spines. , *9*, e107591.

Ruiz, M. (n.d.). *Cell membrane.* `https://en.wikipedia.org/wiki/Cell_membrane`. (Accessed: 2017-11-09)

Rush, A. M., Dib-Hajj, S. D., & Waxman, S. G. (2005). Electrophysiological properties of two axonal sodium channels, nav1. 2 and nav1. 6, expressed in mouse spinal sensory neurones. *The Journal of physiology*, *564*(3), 803–815.

Seifter, J., Sloane, D., & Ratner, A. (2005). *Concepts in medical physiology*. Lippincott Williams & Wilkins.

Shah, B., Stevens, E., Pinnock, R., Dixon, A., & Lee, K. (2001). Developmental expression of the novel voltage-gated sodium channel auxiliary subunit β3, in rat cns. *The Journal of physiology*, *534*(3), 763–776.

Spruston, N. (2008). Pyramidal neurons: dendritic structure and synaptic integration. *Nature Reviews Neuroscience*, *9*(3), 206–221.

Tasaki, I. (1949). Collision of two nerve impulses in the nerve fibre. *Biochimica et biophysica acta*, *3*, 494–497.

Watson, A. B. (2014). A formula for human retinal ganglion cell receptive field density as a function of visual field location. *Journal of Vision*, *14*(7), 15–15.

Werginz, P., & Rattay, F. (2015). Past, present, future: a review on visual prostheses. *Minerva medica*, *106*(1), 65–77.